NASA Contractor Report 165681

Fatigue Degradation in Compressively Loaded Composite Laminates

R.L. RAMKUMAR

NORTHROP CORPORATION
HAWTHORNE, CA 90250

CONTRACT NAS1-15956
APRIL 1981

National Aeronautics and
Space Administration

Langley Research Center
Hampton, Virginia 23665

DISCLAIMER NOTICE

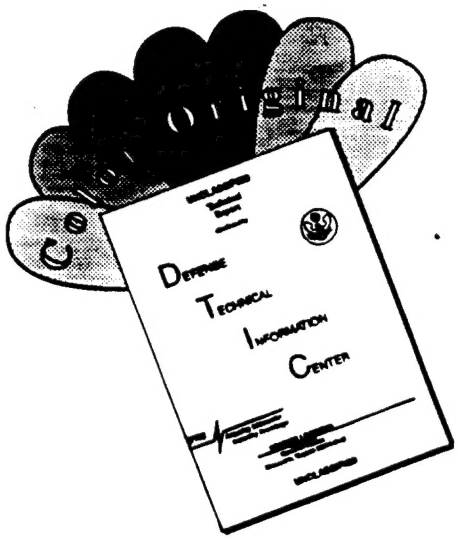

THIS DOCUMENT IS BEST QUALITY AVAILABLE. THE COPY FURNISHED TO DTIC CONTAINED A SIGNIFICANT NUMBER OF COLOR PAGES WHICH DO NOT REPRODUCE LEGIBLY ON BLACK AND WHITE MICROFICHE.

NASA Contractor Report 165681

Fatigue Degradation in Compressively Loaded Composite Laminates

R.L. RAMKUMAR

NORTHROP CORPORATION
HAWTHORNE, CA 90250

CONTRACT NAS1-15956
APRIL 1981

National Aeronautics and
Space Administration

Langley Research Center
Hampton, Virginia 23665

ACKNOWLEDGEMENT

The author thanks: Mr. W. R. Sturrock for his assistance in acquiring a microfocus X-ray unit and in ensuring its safe operation when mounted near the test machine in the laboratory; Mr. D. T. Mih and Mr. R. Allen for their assistance with controlled laser-drilling of holes in the test specimens: Ms. Ann Fourcher and Ms. Donna Salee for fabricating the test panels; Mr. N. P. Barrett and his colleagues for machining the test panels and specimens: Mr. Steve Sandor, Jr. for his assistance with DIB-enhanced radiography; Mr. John Bock for conducting the various tests; Ms. Rocio Cordero for her assistance with tables and figures; Ms. B. P. Parish for her diligent typing efforts; and Dr. R. M. Verette for his help during the program period.

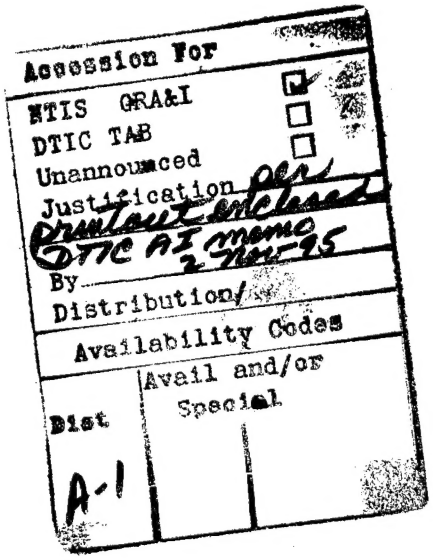

*MSG DI4 DROLS PROCESSING-LAST INPUT IGNORED

*MSG DI4 DROLS PROCESSING - LAST INPUT IGNORED

-- 1 OF 2
-- ***DTIC DOES NOT HAVE THIS ITEM***
-- 1 - AD NUMBER: D432545
-- 6 - UNCLASSIFIED TITLE: FATIGUE DEGRADATION IN COMPRESSIVELY LOADED
-- COMPOSITE LAMINATES,
--10 - PERSONAL AUTHORS: RAMKUMAR,R. L. ;
--11 - REPORT DATE: APR , 1981
--12 - PAGINATION: 150P
--14 - REPORT NUMBER: NOR-81-79
--15 - CONTRACT NUMBER: NAS1-15956
--18 - MONITOR ACRONYM: NASA
--19 - MONITOR SERIES: CR-165681
--20 - REPORT CLASSIFICATION: UNCLASSIFIED
--22 - LIMITATIONS (ALPHA): APPROVED FOR PUBLIC RELEASE; DISTRIBUTION
-- UNLIMITED. AVAILABILITY: NATIONAL TECHNICAL INFORMATION SERVICE,
-- SPRINGFIELD, VA. 22161. NASA-CR-165681.

33- / [redacted]

-- END Y FOR NEXT ACCESSION END

Alt-Z FOR HELP3 ANSI 3 HDX 3 3 LOG CLOSED 3 PRINT OFF 3 PARITY

1. Report No.	2. Government Accession No.	3. Recipient's Catalog No.
NASA CR-165681		

4. Title and Subtitle	5. Report Date
Fatigue Degradation in Compressively Loaded Composite Laminates	April 1981
	6. Performing Organization Code
7. Author(s)	8. Performing Organization Report No.
R. L. Ramkumar	NOR 81-79
	10. Work Unit No.
9. Performing Organization Name and Address Northrop Corporation Aircraft Division One Northrop Avenue Hawthorne, California 90250	11. Contract or Grant No. NAS1-15956
	13. Type of Report and Period Covered Contractor Report
12. Sponsoring Agency Name and Address National Aeronautics and Space Administration Washington, D.C. 20546	14. Sponsoring Agency Code

15. Supplementary Notes

Langley Technical Monitor: John D. Whitcomb
Final Report

16. Abstract

This report describes an experimental program conducted to assess the effect of imbedded delaminations on the compression fatigue behavior of quasi-isotropic, T300/5208, graphite/epoxy laminates. Teflon imbedments were introduced during panel layup to create delaminations. Test specimens were 64-ply thick, and had 3.81 cm square test sections that were unconstrained laterally during compression testing. Static and constant amplitude ($R=10$, $\omega = 10$ Hz) fatigue tests were conducted. S-N data and half-life residual strength data were obtained.

During static compression loading, the maximum deflection of the buckled delaminated region was recorded. Under compression fatigue, growth of the imbedded delamination was identified as the predominant failure mode in most of the test cases. Specimens that exhibited other failures had a single low stiffness ply above the Teflon imbedment. Delamination growth during fatigue was monitored using DIB-enhanced radiography. In specimens with buried delaminations, the dye-penetrant (DIB) was introduced into the delaminated region through a minute laser-drilled hole, using a hypodermic needle. A low-kV, microfocus, X-ray unit was mounted near the test equipment to efficiently record the cyclic growth of buried delaminations on Polaroid film.

17. Key Words (Suggested by Author(s))	18. Distribution Statement
Composites Delamination Growth DIB-Enhanced Radiography Compressive Loading, Fatigue Degradation	Unclassified - Unlimited

19. Security Classif. (of this report)	20. Security Classif. (of this page)	21. No. of Pages	22. Price*
Unclassified	Unclassified	150	

For sale by the National Technical Information Service, Springfield, Virginia 22161

TABLE OF CONTENTS

SECTION 1

INTRODUCTION

Limited success has been recorded in the literature pertaining to the development of an analytical understanding of the compression fatigue behavior of composites. The problem becomes more involved when the composite material contains discontinuities due to process- or service- induced flaws. Process-induced flaws are identified through nondestructive inspection (NDI) techniques employed for quality control, and a negligible amount ($< 1\%$ by volume) of microvoids is almost always detected in composites. These are declared 'harmless' and tolerable as long as they are located within the matrix material. But, if these flaws exist over a considerable area at the fiber-matrix interface, or at the interfacial surface between any two adjacent plies, they could have deleterious effects on the compression behavior of the laminate. During the service life of the laminated composite, say as an aircraft structural component, similar damage can be introduced by the operating environment. Low velocity impact situations, for example, could precipitate considerable interlaminar damage with no visible evidence on the impacted surface (Refs. 1, 2. and 3). An analytical prediction of the effect of such a flaw on the compression fatigue behavior of composites is very complicated, and is generally reduced to an empirical forecast based on generated experimental data. There is, therefore, a need to develop a basic understanding of the various failure modes that initiate and grow during cyclic compressive loading of flawed laminated composites.

Compression fatigue behavior of laminated structural components is affected by many factors that have negligible effects under tensile loading. This is attributable to local or global instabilities that are induced in these laminates by a compressive load. A long and slender member, for example, exhibits an Euler buckling phenomenon in compression, which is a global instability. Local instability is induced by the presence of delaminations or by the disbonding of the fiber-matrix interface.

Compressive loads generally cause a delaminated region to buckle, especially if the delamination is located near the free surface. This local instability may in turn, precipitate laminate failure through an unstable growth of the delamination during static or fatigue loading. The other local instability, referred to earlier, is caused by a disbond between the fiber and the matrix in any layer. If this disbond exists over a length that is sufficient to induce Euler buckling of the fibers in the compression layer, fiber microbuckling results. Any additional load causes the post-buckled strain in the fiber to increase rapidly, eventually precipitating fiber failure.

In this study, specimen gross (Euler) buckling, local buckling of a delaminated region, and fiber microbuckling were identified as compression-critical failure modes of interest. Emphasis was laid on the compression fatigue behavior of T300/5208 graphite/epoxy laminates in the presence of imbedded delaminations. Test specimen geometry was chosen to preclude the occurrence of global instability. This was achieved by selecting a thick (64-ply), quasi-isotropic layup for the test laminate, and by restricting the unsupported test length to be 6.35 cm. Destructive inspection of selected test specimens was employed to investigate the occurrence of fiber microbuckling, if any. While the growth of imbedded delaminations under various compression fatigue loading conditions was monitored during testing, the possible occurrence of specimen gross buckling was also interrogated. This program isolated the effect of delaminations on the compression fatigue behavior of laminates as the primary topic of interest. This problem has been investigated by others, both experimentally and analytically, with limited reported success (see References 4 to 15).

The objective of this study was achieved through an experimental program. Test specimens were fabricated with Teflon imbedments to simulate delaminations. Two types of delaminations were considered: (1) A rectangular delamination that extended across the entire width of the specimen at a chosen interface, and was hypothesized to induce a self-similar one dimensional (1-D) growth of the flaw along the interfacial surface; and (2) A circular delamination that was buried within the test specimen at a chosen interface, and was hypothesized to cause a two dimensional

(2-D) growth of the flaw in its interfacial plane. The flaw locations were chosen to be near one of the free surfaces to simulate a low velocity impact damage. One location was directly below the surface ply, between plies 1 and 2. The other location was chosen to be between plies 4 and 5. Three stacking sequences of a quasi-isotropic, T300/5208 graphite/epoxy laminate, with the surface ply fiber orientation in the laminate changed from 0° to 45° to 90°, were tested. The effect of the imbedded flaw type and location on the static compressive strength was measured initially. As the quasi-static load was increased slowly, the out-of-plane deflection of the thinner delaminated region was recorded using a dial indicator, until failure. Failure was defined to have occurred when the imbedded delamination propagated to the tab boundary. Based on static compression test results, constant amplitude compression fatigue tests were conducted at R=10 and ω= 10 Hertz. R is the ratio of the minimum to the maximum fatigue load, and ω is the cyclic load frequency. S-N data were generated for tested combinations of laminates and delaminations. Again, fatigue failure was defined to have occurred when the delamination propagated to the tab boundary. Limited half life residual strength data were also generated. During fatigue the growth of imbedded delaminations was selectively monitored via enhanced radiography. A low kV-rated, microfocus X-ray sytem was stationed adjacent to the test machine to eliminate the need for intermittent removal of test specimens from the machine for inspection. Details of the experimental program are presented in Section 2, and the generated results are discussed in Section 3. The achievements of the program and recommendations for future studies are presented in Section 4.

Use of commercial products or names of manufacturers in this report does not constitute official endorsement of such products or manufacturers, either expressed or implied, by the National Aeronautics and Space Administration.

SECTION 2

DETAILS OF THE EXPERIMENTAL PROGRAM

The experimental program discussed in this section attempted to identify the dominant mechanisms of compression fatigue degradation in T300/5208 graphite/epoxy laminates with imbedded interlaminar flaws. The various details of the experimental program are discussed in the following subsections.

2.1 Test Material

All the test specimens were fabricated from T300/5208 graphite/epoxy prepreg tapes. This material was purchased to comply with Lockheed specification C-22-1379/144. The resin content of the material was 35% by volume, and its areal density was 144 gm/m^2. Quality control (QC) tests were performed on the acquired material to ensure its compliance with the specifications. Table 1 presents a summary of the prepreg QC test results. The physical properties from four batches of the acquired material met the specifications. Table 2 presents a summary of the mechanical properties obtained from tests on $[0]_{16T}$ T300/5208 laminates. Though the scatter is relatively large, the properties are still within the acceptable range. The QC test results from Tables 1 and 2 are also in good agreement with the vendor QC test data presented in Table 3. Consequently, the acquired material was declared adequate for the test program.

2.2 Test Laminates

Three different stacking sequences of a quasi-isotropic layup were tested in the program. The outer ply fiber orientation was chosen to be 0° in one laminate, 45° in the second laminate, and 90° in the third laminate. The test laminates were chosen to be 64-ply thick, with the following configurations:

Laminate A: $[0/45/90/-45]_{8s}$

Laminate B: $[45/90/-45/0]_{8s}$

Laminate C: $[90/45/0/-45]_{8s}$

2.3 Test Panel Fabrication

Four panels were fabricated according to Figures 1, 2 and 3. One panel of laminate A was fabricated per Figure 1, and another panel of the same layup was fabricated per Figure 2. One panel each of laminates B and C was fabricated per Figure 3. During layup, flaws of predetermined sizes were imbedded between two chosen plies. A delamination was created by inserting two layers of 0.009 cm (.0035 in) - thick Teflon at one of two locations. Location 1 was below the first ply, that is between plies 1 and 2. Location 4 was below the fourth ply, that is between plies 4 and 5 (see Figure 1).

The panel layup was surrounded by the arrangement shown in Figure 4 prior to entering the autoclave. The use of a bleeder ply below the panel layup, immediately above the tool surface, allowed "breathing" from both the top and the bottom surfaces, and retained ply uniformity and symmetry in the cured laminate. The following cure cycle was imposed on the arrangement in Figure 4:

1. Apply full vacuum
2. Heat to 275°F ± at 2-4°F per minute.
3. Dwell at 275°F ± for 45 minutes (starting @ 265°F).
4. Apply 100 ±5 psi, venting vacuum at 20 psi.
5. Heat to 355 ±5 F at 2-4 F per minute.
6. Cure at 355 ± F for 120 +10, -0 minutes.
7. Cool to 170°F under pressure.

2.4 Quality Control of Fabricated Test Panels

Initially a laminate A panel was fabricated per Figure 1. The acceptability of the cured laminate was evaluated via ultrasonic through transmission. Lead tapes were bonded to the corners of the panel to obtain the proper settings (decibel level, gate frequency, etc.) for the C-scan record. A portion of this record, indicating the presence of some anomalies, is shown in Figure 5. To interrogate this further, a radiographic record of the panel was also obtained. Figure 6 presents a contact photographic print

of the radiograph corresponding to the area of panel shown in Figure 5. The radiograph in Figure 6 confirms the presence of defects at the locations identified in the C-scan record of Figure 5, though only an experienced radiologist can identify these defects to be microvoids.

Subsequently, a 1.27 cm square specimen was machined off the panel corresponding to a location of excess material, labelled "Extra" in Figure 1. Two edges of this specimen, parallel and perpendicular to the 0° fiber direction (Figure 1), were chosen to correspond to a location in the panel where the C-scan record indicated the presence of anomalies. If "X" and "Y" are chosen to be axes along the 0° and 90° fiber directions, "Z" would denote an axis in the thickness direction of the laminate. Two faces of the machined specimen, corresponding to "XZ" and "YZ" planes containing the chosen edges, were examined under a microscope. Figure 7 presents a photomicrograph of the "XZ" face of the specimen at 16x magnification A random distribution of negligibly small microvoids at various thickness locations is observed. A photomicrographic record of the "YZ" face of the specimen is presented in Figure 8, indicating the presence of similar microvoids. An enlarged view (50x magnification) of a portion of this face is shown in Figure 9. Even though most of the microvoids are located at interlaminar boundaries, causing concern regarding their effect on the compression behavior of the specimens, their sizes appear to be too small to be of any significance. Figure 9 also indicates the presence of some "harmless" resin pockets.

In conclusion, an examination of the C-scan, X-ray and photomicrographic records confirmed the presence of a random distribution of a small number of microvoids in the test panel. A few resin pockets were also present in the panel. No major flaw - a delamination of any significant size was detected. Therefore, although the small number of microvoids and a few resin pockets resulted in a "bad" C-scan, the volume content of the microvoids was small enough ($\ll 1\%$) to declare the test panel acceptable. A similar inspection technique was employed for the other three test panels also (see Figure 10).

2.5 Type of Flaw and Flaw Location

A delamination can cause a significant loss in the compression

strength of a laminate (Ref. 3), and may be process or service-induced. Process-induced delamination is precipitated during fabrication due to entrapped moisture or humid environment in the clean room. Low velocity impact of a cured laminate by a hard object is a plausible service situation, during the lifetime of the laminated component, that precipitates delaminations (Ref. 1). Assuming a delamination to be the most critical flaw under compressive loading, it was introduced in the test panels, during the layup operation, using non-adhering Teflon inserts (see Figures 1, 2, and 3).

Two types of imbedded delaminations were considered in this program. In the first category, the delamination was 1.27 cm(0.5 in.) long, centered between tabs, and extended across the entire width of the test specimen (Figures 1 and 2). The second type of delamination was 1.27 cm (0.5 in.) in diameter, centered within the test section. The first (1-D) type of flaw was expected to grow in a one-dimensional manner, along the delaminated interface. Such growth can be predicted using a simplified, one-dimensional analysis (Ref. 15). The second (2-D) type of flaw is representative of an impact-induced delamination, and an analytical prediction of its growth is a difficult task. A few laminate A specimens in the reported test program had 1-D flaws imbedded in them. Most of the specimens tested in this program had a 2-D flaw imbedded in them.

The location of the flaw is an important parameter affecting the compressive strength and fatigue lifetime of the test laminate. A low velocity impact situation precipitates delaminations near the free surface away from the impacted face, as shown in ultrasonic C-, B- and 3D-scans (Ref. 1 and 2). Based on this evidence, delaminations were imbedded at two locations near the surface ply in the test program (see Figures 1, 2 and 3). The first location (location 1) was below the surface ply, or between plies 1 and 2 (Fig. 1). The second location (location 4) was below the fourth ply, or between plies 4 and 5.

2.6 Test Specimen Design

The test specimen geometry chosen for this program is shown in Figure 11, along with tab details. During testing, stability-related compression fatigue degradation may be induced by : (a) local buckling and subsequent post-buckling of the delaminated region (1 or 4 plies) causing the delamination to propagate; (b) fiber microbuckling culminating in fiber failure; and (c) Euler buckling of the test specimen in the unsupported test section. In this program, the primary objective was to induce compression fatigue degradation predominately via (a), and to selectively monitor during and after testing, any contribution due to (b) or (c). The 15.24 cm (6 in.) long, 3.81 cm (1.5 in.) wide specimen geometry in Figure 11 was chosen to meet this objective. The specimen had a 3.81 cm (1.5 in.) square test section that was laterally unconstrained during testing. The free surfaces of the test section permitted uninhibited growth of delaminations imbedded near the surface ply. The test length was chosen to be small (3.81 cm between tabs) and the laminates were chosen to be thick (0.81 cm) to make the Euler buckling stress exceed the virgin compressive strength of the unflawed test specimen. The unsupported bevelled tab regions were accounted for in this computation.

2.7 Specimen Preparation

During the layup of the panels in Figures 1, 2 and 3, Mylar drawings of the full-scale panels were prepared. The planform locations of the various flaws were marked in these drawings, and 1.27 cm diameter holes punched out wherever the 2-D flaws were to be imbedded during layup. This ensured the proper positioning of the 2-D flaws in the test panel. C-scan records of the cured laminates were compared with Mylar drawings to ensure that the Teflon inserts remained at the imbedded locations. Then, the fabricated panels were block-machined and tabbed. Tab details are given in Figure 11. Tabbed blocks were then sawed to yield test specimens with imbedded flaws located at the center of the test section. Specimen ends were finally ground to be flat and parallel. This ensured alignment of the applied load, most of which was introduced through direct

bearing on the flat ends. Prepared specimens were identified for easy reference. An example is given below.

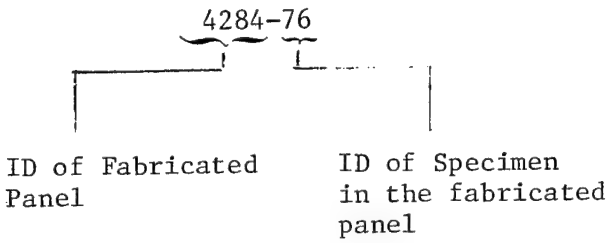

Examination of the specimens prepared from the initially fabricated, laminate A panel revealed a special problem. Some of the specimens with an imbedded delamination just below the surface ply exhibited matrix cracks between fibers in the delaminated region. Two explanations are forwarded as possible reasons for this undesirable damage. First, when a laminate is cured in an autoclave under pressure, resin flows thrcugh a porous Armalon glass cloth placed over the layup. After curing, the panel is removed from the autoclave, and the glass cloth is peeled off the panel surface. Due to the presence of resin in its pores, the glass cloth adheres to the surface of the panel fairly well, and if the surface ply of the layup is "separated" from the rest of the plies at certain locations, peeling off the glass cloth could conceivably pull out the surface ply at these locations. A second, and more probable, situation under which the mentioned damage could have occurred is during the tabbing operation. A group of specimens was initially block-machined from the test panel prior to tabbing. The test sections of the specimens in the blocked-machined panel are then covered by an adhesive tape to prevent the flow of adhesive onto the test sections during the tab cure cycle. After tabbing was completed, the adhesive tape was peeled off the test section, across the width of the specimen, causing the allowable transverse tension strain limit to be exceeded in the surface 0^{o} ply at imbedment locations. This caused the pull-out of the surface ply at locations where Teflon inserts were placed to simulate delaminations.

Two specimens manifested a total pull-out of the surface ply at the delamination location. In a few other specimens, fine cracks between fibers in the delaminated ply were observed. Damaged specimens were rejected, and the tabbing procedure was modified to eliminate similar damage in subsequent test specimens.

2.8 Type of Loading

The various test specimens were subjected to static compression or constant amplitude compression fatigue loading. During fatigue testing, the algebraic minimum-to-maximum fatigue load ratio (R) was maintained at ten. The maximum compressive stress during fatigue was chosen to be a fraction, S, of the static compressive strength for each test case. Fatigue loading was introduced at a 10 Hertz frequency (ω).

2.9 Tests Conducted Under the Program

Table 4 defines the various tests conducted on laminate A specimens, and Table 5 defines the tests conducted on laminates B and C. A total of 185 specimens were built, of which 50 were tested in static compression, 115 were tested in compression fatigue (R = 10; ω= 10 Hertz), and 20 were delivered to the funding government agency.

Laminate A specimens were tested in the virgin state, with a 1-D delamination below the surface ply, with a 2-D delamination below the surface ply, and with a 2-D delamination between plies 4 and 5 (Table 4). Static compressive strengths were obtained for every flaw situation. S-N curves were generated for the three delamination cases, and half-life residual strengths were obtained for specimens with 2-D delaminations at two locations. In the fatigue life tests used to generate S-N curves, specimens that complete a million cycles without failing constitute a "run-out". Failure, in this report, refers to the state when an imbedded delamination propagates to the tab region.

Specimens from laminates B and C were tested in the virgin state and with 2-D delaminations at two locations (Table 5). Static compressive strengths and S-N curves were generated for all the test cases.

2.10 Static Test Measurements

During static testing strain gage readings were obtained from locations shown in Figure 12. Two back-to-back gages were centrally located in unflawed specimens, and their readings obtained at regular load intervals. When the two gages indicate almost the same reading, the end loads are properly aligned and bending effects are negligible. If the specimen buckles between grip fixtures, the resulting bending motion introduces tensile and compressive stresses in the outer and inner plies, respectively, as manifested by a widening difference between the two gage readings.

In specimens with a centrally imbedded delamination near the surface ply, back-to-back gages were located 0.64 cm (0.25 in.) from the tab edge in three out of five static test specimens to monitor gross specimen buckling between test grips (Figure 12). In the other two static test specimens, a third gage was located at the center of the test section, on the surface closer to the delamination (Figure 12). The third gage will indicate the same reading as the back-to-back gages when the delaminated set of (1 or 4) plies does not suffer local buckling. When the third gage starts indicating lower compressive strains, local buckling has occurred. When the delaminated region suffers large out-of-plane deflections in the post-buckled state, the third gage will indicate tensile strains. In addition to the use of the third gage, a 0.00254 cm (0.001 inch) per division dial indicator was employed to periodically read the maximum out-of-plane deflection at the center of the buckled delaminated region (on the side closer to the flaw).

Local buckling was thus monitored during static compression tests on flawed specimens through a dial indicator, sometimes assisted by a third strain gage. Specimen gross buckling between test grips, if any, was monitored through back-to-back gages until the imbedded flaw propagated toward the tab location. As the imbedded delamination propagates, the buckled state of the plies above it induces tensile strains in the outer ply, resulting in a growing difference between the back-to-back gage readings. This should not be interpreted to be an indication of gross specimen buckling between test grips.

Back-to-back strain gages located near the tabs in Figure 12 were also used in the residual strength tests on the half-life laminate A specimens

(Table 4). Again, these readings can be used to ensure load alignment and to monitor gross specimen buckling only if the imbedded delamination propagated very little over half its lifetime.

2.11 Compression Fatigue Measurements

Compression fatigue tests, at R = 10 and ω= 10 Hertz, were conducted on 75 laminate A specimens and 20 specimens each of laminates B and C (Tables 4 and 5). The objectives of this task were to: (1) obtain S-N data for the various combinations of test laminates and delaminations; (2) obtain residual strength vs. N data for laminate A specimens for two locations of a 2-D delamination; (3) monitor the growth of the imbedded flaw during fatigue; and (4) monitor the occurrence of gross specimen buckling between test grips and fiber microbuckling, if any. The first objective was met by choosing S values based on appropriate static compressive strengths. S_3, S_4 and S_5 in Table 4, for example, were based on the average static strength corresponding to test series 2. Residual strength data on laminate A specimens were obtained after fatigue loading the specimens for approximately half their average lifetime at the chosen S value. The growth of imbedded delaminations was monitored during testing using visual inspection and DIB-enhanced radiography described in Section 2.12. Radiographic monitoring of delamination growth was restricted to two out of five specimens in each fatigue test case. The remaining three were visually inspected with the aid of a fiber optic light source. Occurrence of gross specimen buckling, if any, was established through back-to-back strain gage data corresponding to static tests. Fiber microbuckling, if any, was interrogated through photomicrographic techniques after the tests were completed.

2.12 Monitoring Delamination Growth Using Enhanced Radiography

Radio-opaque dye-penetrants of high atomic numbers have been used by others to monitor the growth of delamination initiating from the free surface of an open hole or from the free edges of a test specimen. In these situations, the penetrant is brushed over the free surface, and it seeps into every opening that it encounters. This technique was adopted for tests on laminate A specimens with a 1-D flaw below the surface ply. Cyclic compression loading was stopped after a few cycles, a small compression load was retained on the specimen, the dye-penetrant injected into the delaminated region from a free edge, and a radiograph of the specimen obtained.

The dye "followed" the delamination boundary during fatigue, and its radio-opaque characteristic enhanced monitoring the growth of the delamination. The test set-up used in the program is shown in Figure 13. A close-up of the test area is presented in Figure 14. DI-iodo butane (DIB) was chosen to be the radio-opaque dye-penetrant. The employed radiographic technique is rendered very efficient by the microfocus X-ray source that is mounted near the specimen. This equipment precludes the need to remove the specimen from the test fixture every time a nondestructive inspection (NDI) is required. Details on the microfocus X-ray source are given in Section 2.13.

While monitoring of 1-D delamination growth was accomplished using procedures employed by others, monitoring of buried, 2-D delamination growth presented a challenge. Successful use of enhanced radiography required the introduction of DIB into the delaminated region. This was accomplished in this program by drilling a very small hole (approximately 0.01 cm in diameter), using a laser beam, from the nearer free surface to the delaminated interface (see section 2.14). The hole was considered too small in size to cause undesirable post-buckling response of the delaminated region (Ref. 16). DIB was then injected into the delaminated region, through the laser-drilled hole, using a hypodermic needle, just before the radiographic record was obtained. This procedure has never before been employed in the literature, and was successfully demonstrated in this program. Cyclic loading was interrupted a few times during the fatigue life of the test specimen, DIB injected into the delamination region , an enhanced radiograph obtained on Polaroid film, and cyclic loading resumed. The specimen remained in the test fixture until failure was observed.

From each sequence of radiographs, the change in the 1-D or 2-D delamination size with the number of fatigue load cycles (N) was obtained. If the scatter in the data was not large, a plot of delamination size versus N for each S value could be used to compute the effect of S on the rate of growth of the imbedded delamination.

2.13 Microfocus X-ray System

The X-ray system used in this program was a Magnaflux Microfocus MXK-100M Portable X-Ray System (see Fig. 13), designed primarily for applications requiring extremely fine resolution, direct enlargements up to 36 times, utility in inspection areas inaccesible to conventional X-ray tubes, and for use on structures where the X-ray film cannot be placed directly in

contact with the area of the part under examination. It presents a degree of detail and resolution in X-ray pictures never before possible.

One of the limitations of radiographic testing in the past has been the relative lack of definition or detail on the X-ray film. This loss of resolution in the image is partly due to the source of the radiation being too vague and unconcentrated. The problem is compounded when the tube must be placed close to the film plane, resulting in a loss of resolution in the film image.

The Magnaflux MX-10-50 microfocus tube produces an extremely fine point of radiation by use of variable voltage biasing of the radiating beam. Whereas in conventional tubes a spot of .4mm is considered adequate, the new microfocus tube spot can be reduced to .05mm. Such a minute spot allows the tube to be brought much closer to the film plane retaining an astounding degree of resolution.

The low kV range in which the equipment can be operated enables one to meet radiation safety requirements simply by using lead-lined vinyl sheets around the test frame (see Fig. 13). This enhances the use of the X-ray system in a testing laboratory environment, and eliminates the need to remove the specimen from the test fixture for periodic NDI to monitor fatigue growth of imbedded delaminations.

In the reported program, radiographs were obtained on Polaroid type 52 film. The microfocus X-ray system was operated at 32 kV and 0.18 m amp of current. An exposure time of 3 minutes was used in obtaining the presented radiographs.

2.14 Laser-Drilled Holes

Laser-drilled holes were introduced in a few test specimens to monitor the fatigue growth of imbedded, 2-D delaminations. A solid state laser using a cylindrical YAG (yttrium-aluminum garnet) rod source and neodymium as the laser medium, was employed. A preliminary study was conducted to determine the laser exposure required to drill holes to various depths in a graphite/epoxy specimen. In this study, a long specimen was subjected to the incidence of a 6-Watt laser beam many different times at different locations along its length. Each exposure occurred over a 1.27 cm (0.5 in.) width, and was automated to be achieved by pushing the control button once. After the various locations were subjected to different

numbers of exposures, the specimen was cut along the length at the mid-width of the exposed region. The cut cross-section was then examined under a scanning electron microscope (SEM) to measure the depth of laser penetration at each test location. Figure 15 presents the variation in the measured depth of laser penetration with the number of 6 -Watt exposures. Although Figure 15 data were obtained for woven AS/3501-6 material, the laser depth/exposure relationship was assumed to be valid for the T300/5208 tape material used in the program. While penetration to the delaminated interface was a mandatory requirement, a slight additional penetration of the plies below the Teflon inserts would not have caused any undesirable results. Consequently, five and twenty exposures of the 6-Watt laser source were used to drill holes at least one and four plies deep, respectively. The laser-drilled holes were approximately 0.01 cm in diameter. A hypodermic needle was used to inject DIB through these holes to the delaminated region.

2.15 Experimental Procedure

Static compression tests on unflawed specimens (test series 1) were conducted initially. Back-to-back strain gage data were supplemented by out-of-plane deflection measurements using a dial indicator. These tests established that gross buckling between test grips was insignificant in unflawed specimens up to failure. A small out-of-plane deflection was measured at large loads, and was predominantly the Poisson strain in the thicknesss direction. Very near the failure load, interlaminar delaminations initiated and eventually precipitated specimen failure, as manifested by increasing out-of-plane deflection measurements.

Subsequent to static compression tests on unflawed specimens, static compression tests on flawed specimens were conducted (test series 2, 6 and 13 for laminate A, and test series 6 and 13 for laminates B and C). Failure was defined as the propagation of the imbedded delamination to the tab boundary. These tests determined the effect of imbedded flaws on the static compressive strength, and produced data that were required for conducting fatigue life tests and half-life residual strength tests. Back-to-back strain gages located near the tabs (Figure 12) indicated the absence of any signifcant bending effects due to gross specimen

buckling between test grips until failure. Observed gage readings were valid because the imbedded flaw grew to failure in a catastrophic manner, and hence the effect of buckling of the delaminated region did not influence the strain readings near the tabs until failure. The maximum out-of-plane deflection at the center of the delaminated region was measured using a dial indicator. In a few cases, the strain variation at this location was also recorded. These data defined the extent of post-buckling deformation in the delaminated region at failure. They will be useful in assessing the validity of future analyses that attempt to quantify such a behavior.

Compression fatigue life tests on flawed specimens (test series 3, 4, 5, 7, 9, 11, 14, 16, and 18 for laminate A, and test series 7, 8, 14, and 15 for laminates B and C) were carried out after the static tests were conducted. All the fatigue tests were conducted at R = 10 and ω = 10 Hertz. Based on the measured average static strength, the maximum compressive fatigue load (or the S value) was chosen for each delamination situation, to induce fatigue failure within a predetermined range of fatigue cycles (see Tables 4 and 5). The results were then cast in the form of S-N curves. Also, the growth of an imbedded delamination during fatigue was monitored using DIB-enhanced radiography. These records were analyzed to yield delamination growth rates as a function of S for each test case. It must be reiterated that fatigue life was defined as the number of cycles required for an imbedded flaw in the specimen to propagate to the tab boundary. Unlike the static test results, most of the imbedded delaminations grew in a stable manner under compression fatigue until failure. From the S-N data and the delamination size versus N data, a relationship between the residual strength and the delamination size at any N could be obtained for a given delamination situation in a laminate.

Subsequent to the completion of fatigue life tests, half-life residual strength tests on laminate A specimens (test series 8, 10, 12, 15, 17 and 19 in Table 5) were conducted. For example, specimens in test series 8 were cycled at S_7 (the S value used for the fatigue life test series 7) for approximately $N_{f_7}/2$ cycles, where N_{f_7} is the average fatigue life for specimens in series 7. These specimens were then failed in static

compression, and the residual strengths recorded. The flaw size prior to residual strength testing was recorded in two out of five specimens in each test case , using enhanced radiography.

The results obtained from the various tasks are presented and discussed in the following section.

SECTION 3

DISCUSSION OF RESULTS

3.1 Static Compression Tests on Unflawed Laminates

Results from static compression tests on unflawed specimens are presented in Table 6. It is seen that laminate A specimens, with a 0^{o} ply on the surface, exhibit the maximum strength and stiffness. Laminate B, with a 45^{o} surface ply, ranks second, and laminate C, with a 90^{o} surface ply, exhibits the least strength and stiffness. Five specimens of each layup were tested, and the scatter in the presented data seems to be moderate. During these tests, the out-of-plane deflection of the specimen was monitored using a dial indicator. Improper load alignment, if any, was manifested as bending effects, and monitored through back-to-back strain gage readings and dial indicator readings. When this was detected, the load was removed, specimen grip fixtures and the loading arrangement adjusted for alignment, and the test restarted. Care was exercised in this program to grind the specimen ends to be flat and parallel, within a narrow tolerance range, to ensure proper load introduction. Consequently, the dial indicator detected no bending effects. Since imbedded flaws affected the strain gage and dial indicator readings in subsequent tests, results from tests on unflawed specimens were used to demonstrate lack of specimen gross buckling between supports.

Tested specimens were examined to identify the failure modes. Failure was declared to have been precipitated when a significant unloading was indicated. In every test case, this was accompanied by a fairly loud "popping" sound, characteristic of a delamination. It must be reiterated that all the test specimens were unsupported laterally during static and fatigue tests. The absence of lateral constraints, commonly used in conventional compression tests, permitted precipitation of failure-inducing delaminations.

The predominant failure mode in the $[0/45/90/-45]_{8s}$ (laminate A) specimens was observed to be a delamination between the surface 0° ply and the adjacent 45° ply. This was verified by inspecting failed specimen cross sections under a microscope at 50X magnification. In a few specimens, the delamination between plies 1 and 2 crossed over to a delamination between plies 3 and 4 (90/-45 interface) or between plies 4 and 5 (-45/0 interface) near the tab region.

The predominant failure mode in $[45/90/-45/0]_{8S}$ (laminate B) specimens was observed to be a delamination between plies 4 and 5, at the 0/45 interface. In one specimen (4255-5), a surface ply delamination (at the 45/90 interface) crossed over to the interface between plies 4 and 5 in one corner. The variability in the failure surfaces in replicates was probably a result of a coupling between tab effects and specimen end geometry.

In the unflawed $[90/45/0/-45]_{8S}$ (laminate C) specimens, the predominant failure mode was a delamination between plies 4 and 5 (-45/90 interface) that penetrated into the tab region. In specimen 4282-1, a delamination between plies 2 and 3 (45/0 interface) crossed over to the -45/90 interface, two plies below, near the tab region. This was observed at two diametrically opposite corners of the test cross-section. The delamination between plies 4 and 5 went into the tab region, as in the other specimens.

3.2 Static Compression Tests on Laminate A Specimens With A 1-D Delamination Below the Surface Ply

Five laminate A specimens, with 1.27 cm long delaminations below the surface ply, extending across the entire width, were tested in static compression. Table 7 presents the obtained results. Except for specimen 4238-10, only a moderate scatter in the strength and failure strain data is observed. Two of the five specimens were gaged to read strain data at the center of the delaminated region, and the maximum out-of-plane deflection at the same location was measured in every case using a dial indicator. Failure occurred in each case through an unstable propagation of the imbedded delamination to the tab boundary. A 41% loss in the compression strength of the unflawed specimen was induced by the imbedded 1-D delamination below the surface ply. It must be noted that failure

of the delaminated specimen did not correspond to its maximum load-carrying capacity. The average compression failure stress for these specimens was 304 MPa, and the corresponding value for the applied strain was 6923 μcm/cm. The maximum out-of-plane deflection of the thinner delaminated region and the tension strain at that location were linearly extrapolated to be 0.006 cm and 1747 μcm/cm, respectively. At failure, initially used dial indicators suffered an impulsive load from the surface ply that rendered them inoperable. Consequently, during subsequent tests, the dial indicator was removed at approximately 90% of the failure load. This was also extended to later tests with 2-D delaminations below the surface ply.

An examination of the failed specimens revealed cracks oriented in the 0° direction, in the matrix of the delaminated surface ply. This matrix splitting between fibers was induced by the exceedance of the ultimate transverse tension strain value in the surface 0° ply. It is believed to have happened due to the Poisson effect prior to buckling or during the large post-buckled deflection.

3.3 Static Compression Tests on Laminate A Specimens With 2-D Delamination Below the Surface Ply

Results from these tests are presented in Table 8. Failure in each specimen was induced by the catastrophic growth of the imbedded delamination to the tab region. In doing so, the surface 0° ply with a circular delaminated region, suffered a large transverse deflection locally that induced a transverse tensile strain in excess of the failure value. This occurred at points where the tangents to the initial flaw geometry were in the fiber (0°) direction. Consequently, matrix splitting between fibers occurred in the surface ply at these locations and biased the manner in which the imbedded delamination grew. The initially circular delaminated region, therefore, appeared rectangular at failure, the length extending between tab edges, and the width equal to the diameter (1.27 cm) of the imbedded delamination. Additional matrix cracks between fibers were also observed in some specimens within this region.

From Table 8 it is noted that a 31% loss in the compression strength of the unflawed specimen was induced by the imbedded 2-D delamination

below the surface ply. Again, failure in the delaminated specimen did not correspond to its maximum load-carrying capability. Compressive stress and strain values at failure were 358 MPa and 8052 μcm/cm, respectively. These values are larger than those for a 1-D delamination (section 3.2), and are expected to be so due to the increased boundary constraint of the buried delamination. The maximum transverse deflection at the center of the delaminated region and the tensile strain at that location, at failure, were 0.0432 cm and 10,140 μcm/cm, respectively.

3.4 Static Compression Tests on Laminate A Specimens With 2-D Delamination Between Plies 4 and 5

Results from these tests are presented in Table 9. Two of the failed specimens (4284-74, 75) exhibited failures similar to specimens with a circular delamination below the surface ply. That is, the initially circular delamination propagated to the tab region in an unstable manner, bounded by 0° matrix cracks originating from either diametrical end of the imbedded delamination. In the remaining three specimens, the imbedded delamination catastrophically spread over the entire test section, separating the top 4 plies from the rest of the laminate. This was also accompanied by a few matrix cracks between fibers in the failed region.

A 34% loss in the compression strength of the unflawed specimen was induced by the imbedded 2-D delamination between plies 4 and 5. It must be noted that failure in the delaminated specimen did not correspond to its maximum load-carrying capacity.

The average applied compressive stress and strain values at failure are 341 MPa and 7715 μcm/cm, respectively (Table 9). These values are lower than those for specimens with the same flaw located below the surface ply (see section 3.3). The increased bending stiffness of the four-ply delaminated region in spite of a lower modulus, is a probable explanation for this. A rigorous interlaminar stress analysis and a reliable delamination failure criterion are required to investigate this analytically. The maximum transverse deflection of the delaminated region and the tension strain at that location, at failure, were 0.0212 cm and 2132 μ cm/cm, respectively. These are lower than the corresponding values for the flaw location below the surface ply (section 3.3), and were expected

to be so due to the increased bending stiffness of the four-ply region.

3.5 Static Compression Tests on Laminate B Specimens With 2-D Delamination Below the Surface Ply

Test results for this case are presented in Table 10. The average values of the applied compressive stress and strain, at failure, are 518 MPa and 12,768 μcm/cm, respectively. Comparing these results with those corresponding to unflawed laminate B specimens (Table 6), it is seen that the introduction of the 1.27 cm diameter delamination below the surface ply had no deleterious effect on the laminate strength. Actually, failure initiated in flawed specimens at a stress level that is (4%) larger than the value for unflawed specimens. The small difference is attributed to scatter in the data.

An examination of the failed specimens revealed delamination between plies 4 and 5 (0/45 interface) in most of the specimens. In one specimen (4255-10) failure occured between plies 59 and 60 also, in a symmetric manner. In specimen 4255-12, the back surface ply delaminated along the 90/45 interface. It is recalled that similar failures were observed in the unflawed specimens (Section 3.1).

3.6 Static Compression Tests on Laminate B Specimens With 2-D Delamination Between Plies 4 and 5

Results from these tests are presented in Table 11. A 20% loss in the compression strength of the unflawed specimen was induced by the 2-D delamination between plies 4 and 5. The average compressive failure stress (401 MPa) and strain (9991 μcm/cm) values are much lower than those corresponding to the flaw location below the surface (see section 3.5). Also, the maximum out-of-plane deflection of the delaminated region, at failure, is much smaller than the value corresponding to the flaw location below the surface ply. The failed specimens exhibited many interlaminar delaminations. It is surmised that the unstable propagation of the imbedded delamination instigated the precipitation of other delaminations in that transient phase. Some of the specimens were broken into two pieces. This could have happened through the failure of thin delaminated groups of plies in the post-buckled state. Consequently, all the specimens exhibited a "broomed" out edge view.

3.7 Static Compression Tests on Laminate C Specimens With 2-D Delamination Below the Surface Ply

Results for this case are presented in Table 12. Comparing these with Table 6, it is seen that the failure stress was not affected by the presence of the flaw, and was actually 18% larger than the unflawed specimen strength. No explanation is available for this difference. An examination of the failed specimens exhibits failures similar to the unflawed specimens.

3.8 Static Compression Tests on Laminate C Specimens With 2-D Delamination Between Plies 4 and 5

Results from five of these tests are presented in Table 13. Comparison with Table 6 reveals a 19% strength loss due to the presence of the delamination between plies 4 and 5. The difference in the failure stresses for the two flaw locations (Tables 12 and 13) is very large (31%). As seen in the other laminates, the transverse deflection of the delaminated region is lesser for the deeper location of the delamination. An examination of the failed specimens revealed propagation to the tab region of the imbedded delamination, over the entire test section area. During this unstable failure phenomenon, other delaminations were also precipitated, leading to a "brooming" out effect.

3.9 Summary of Static Compression Test Results

A summary of all the static compression test results (sections 3.1 to 3.8) is presented in Table 14. The following conclusions are made based on the summarized results:

(1) The unflawed strength of $[0/45/90/-45]_{8S}$ (laminate A) specimens is affected deleteriously by 1-D and 2-D delaminations. A 1-D delamination below the surface ply induces a 41% strength loss. A 2-D delamination below the surface ply induces a 31% strength loss, and a 2-D delamination between plies 4 and 5 induces a 34% strength loss. As the 2-D delamination location is moved from location 1 to location 4, failure occurs at a lower applied stress value and is accompanied by a smaller transverse deflection of the delaminated region.

(2) When a 1-D or 2-D delamination is located just below the surface (0°) ply in laminate A specimens, the post-buckled large transverse deflection of the delaminated ply induces matrix cracks between fibers. Even if the imbedded delamination has an initial circular geometry, precipitation of matrix cracks at the flaw boundary causes the circular delamination to propagate over a projected rectangular area.

(3) The unflawed strength of $[45/90/-45/0]_{8S}$ (laminate B) and $[90/45/0/-45]_{8S}$ (laminate C) specimens is unaffected by locating a 2-D delamination below the surface ply. The low bending stiffness of the surface ply in the delaminated region is believed to be the reason for this observation. Consequently failure was not initiated at the imbedded delamination location in either laminate.

(4) A 20% strength loss was measured in laminate B specimens with 2-D delaminations between plies 4 and 5. In laminate C specimens, the same delamination induced a 19% strength loss.

(5) When the 2-D delamination was moved from location 1 to location 4, a smaller transverse deflection of the buckled region accompanied a larger strength loss in laminates B and C, too.

(6) Failure initiates and propagates in an unstable manner under static compressive loading. No stable delamination growth was observed.

3.10 Compression Fatigue Life Tests on Laminate A Specimens With 1-D Delamination Between Plies 1 and 2

Constant amplitude compression fatigue tests were conducted at the completion of static tests, at R=10 and at ω= 10 Hertz. For laminate A specimens with 1-D delaminations below the surface (0°) ply, the maximum compressive stress during cyclic loading was chosen to be a fraction, S, of the static failure load (Table 14). Three values of S were chosen for test series 3, 4 and 5 in Table 4, to cause failure after desired numbers of cycles. A larger S will induce failure after fewer cycles of loading, N. An attempt was made to select S values to adequately define the S-N behavior of the flawed laminate. Failure was defined as the propa-

gation of the imbedded delamination to the tab boundary, and was determined through enhanced radiography and visual inspection.

Table 15 presents the compression fatigue life data (S-N data) for laminate A specimens with 1-D delamination below the surface ply. These S-N data are plotted in Figure 16. The figure indicates minimal scatter in the data. Two of five tests in each series were monitored using DIB-enhanced radiography to observe the growth of the imbedded delamination. Figures 17 to 25 present examples of delamination growth records. The delamination boundaries in Figures 17, 19 and 21 are traced over and presented in Figures 18, 20 and 22, respectively. The 3.81 cm square test section and a small portion of the tab region are shown in the figures. Figure 24 presents radiographs at 1.8x magnification, while the others are full-scale radiographs.

In all the figures it can be observed that matrix cracks between fibers develop in the delaminated surface ply near failure. These are seen as fine shaded lines in the loading (0°) direction. These cracks complicate the use of damage size versus N curves in developing analytical models. Another observation of interest is the manner in which the imbedded delamination grows. A 1-D delamination growth assumes the width-wise linear boundaries to propagate in a self-similar manner toward the tabs. It is evident from Figures 17 to 25 that this assumption is not valid for the chosen specimen dimensions. Free edge effects are significant, and matrix cracks between fibers in the post-buckled delamination ply bias the flaw growth further. It is recommended that future tests of this type be conducted on narrower ($\sim$2.54 cm wide) specimens with a larger test section between tabs.

3.11 Compression Fatigue Life Tests on Laminate A Specimens With 2-D Delamination Between Plies 1 and 2

Compression fatigue life data for laminate A specimens with 2-D delaminations below the surface ply are presented in Table 16. These results are plotted as an S-N curve in Figure 26. Considerable scatter was observed in the data corresponding to S=0.55 (test series 11). Subsequently, two extra specimens were tested at S=0.55, and the additional

data fell within the scatter band established by the earlier tests.

Figures 27 to 31 present sample radiographic records for delamination growth histories at the various S values (test series 7, 9, and 11). With the exception of one, all the monitored specimens manifested identical failure growth patterns. Except for specimen 4284-66 (Figure 31), matrix cracks between fibers in the delaminated surface (0°) ply caused the imbedded flaw to propagate toward the tab over a rectangular planform area bounded by these cracks. In specimen 4284-66, this occurred suddenly over half the test section area when N reached the failure value.

3.12 Compression Fatigue Life Tests on Laminate A Specimens With 2-D Delamination Between Plies 4 and 5

Compression fatigue life data for Laminate A specimens with 2-D delaminations between plies 4 and 5 are presented in Table 17 and plotted as an S-N curve in Figure 32. A significant amount of scatter is observed in these data. Figures 33 to 36 present sequences of radiographic records that indicate delamination growth with cycles of loading. It is seen, in all these figures, that failure is precipitated suddenly in an unstable manner, as was observed during static testing. This is different from the stable flaw growth observed in specimens when the delamination was located below the surface ply (section 3.11). It is also noted that, at failure, matrix cracks between fibers in the surface (0°) ply are precipitated. In a few specimens, these were accompanied by similar matrix cracks between fibers in the second (45°) ply.

3.13 Summary of Laminate A Fatigue Life Data

The S-N data for laminate A specimens with 1-D delaminations at location 1 and 2-D delaminations at locations 1 and 4 are summarized in Figure 37. Results from sections 3.10, 3.11 and 3.12 are superimposed in this figure for relative evaluation. When the delamination is moved from location 1 to location 4, the threshold value of S at which "run-out" occurs increases. And, for the considered flaw sizes, a 1-D delamination at location 1 results in a lower threshold S value compared to a 2-D delamination at the same location.

3.14 Compression Fatigue Life Tests on Laminate B Specimens With 2-D Delamination Between Plies 1 and 2

Compression fatigue life test data for laminate B specimens with 2-D delaminations below the surface (45°) ply are presented in Table 18 and plotted as an S-N curve in Figure 38. Only a small amount of scatter is observed in the data.

Figures 39 to 42 present sample radiographic records showing the growth in the imbedded delamination with fatigue cycles for two S values. As was seen in laminate A specimens with the same flaw size and location, a stable growth of the flaw is observed, and it is accompanied by matrix cracks between fibers in the delaminated surface (45°) ply.

3.15 Compresion Fatigue Life Tests on Laminate B Specimens With 2-D Delamination Between Plies 4 and 5

Compression fatigue life test data for laminate B specimens with 2-D delaminations between plies 4 and 5 are presented in Table 19. The data exhibit a moderate amount of scatter. These are plotted in the form of an S-N curve in Figure 43.

Sample radiographic records of the delamination growth with N are presented in Figures 44, 45 and 46. In every case, the damage did not grow until failure. At failure, the imbedded delamination propagated in an unstable manner to the tab region, accompanied by matrix cracks in the surface (45°) ply. This is similar to what was observed in laminate A specimens with the same flaw type and location. A different failure was observed in specimen 4256-35. In this case, a delamination was precipitated near the tab boundary, close to the back surface, and away from the imbedded flaw location.

3.16 Summary of Laminate B Fatigue Life Data

S-N curves for laminate B specimens, with 2-D delaminations at locations 1 and 4, are compared in Figure 47. The results are taken from sections 3.14 and 3.15. It is seen that the threshold S value is higher for location 4. A similar observation was made on laminate A S-N data in section 3.13 (Figure 37).

3.17 Compression Fatigue Life Tests on Laminate C Specimens With 2-D Delamination Between Plies 1 and 2

S-N data for laminate C specimens with a 2-D delamination below the surface (90°) ply are presented in Table 20, and plotted as Figure 48. The data exhibit a moderate amount of scatter. Figures 49 and 50 present sample radiographic records indicating the growth of the imbedded delamination with N. No growth is observed until failure. And, at failure, only one specimen indicated probable propagation of the imbedded delamination to the tab region (Figure 50). The other specimens delaminated near the tab at failure, with accompanying matrix cracks between fibers in the surface (90°) ply near the tab boundary. The failure-inducing delamination did not propagate from the imbedded flaw location. This indifference of fatigue failure to the delamination below the surface (90°) ply was observed in most of the test specimens, and is believed to be due to the low bending stiffness of the delaminated 90° ply.

3.18 Compression Fatigue Life Tests on Laminate C Specimens With 2-D Delamination Between Plies 4 and 5

S-N data for laminate C specimens with a 2-D delamination between plies 4 and 5 are presented in Table 21, and plotted as Figure 51. Moderate scatter is observed in the presented data. Figures 52 and 53 present sample radiographic records of delamination growth with N. No significant damage growth was observed until failure, which occurred suddenly as it did in laminates A and with 2-D delaminations between plies 4 and 5. In specimen 4282-29 (Figure 52), the imbedded delamination propagated to the tab region, accompanied by matrix cracks between fibers in the surface (90°) ply and the second (45°) ply. In specimen 4282-38 (Figure 53), failure was precipitated by a delamination near the tab that did not seem to merge with the imbedded delamination.

3.19 Summary of Laminate C Fatigue Life Data

S-N curves for laminate C specimens, with 2-D delaminations at locations 1 and 4, are extracted from section 3.17 and 3.18 and plotted as Figure 54. As already observed in laminates A and B, the threshold S value is higher for location 4.

3.20 Half-Life Residual Strength Tests on Laminate A Specimens With Imbedded 2-D Delaminations

Half-life residual strength tests were conducted in the reported study to estimate half-life fatigue degradation in delaminated specimens. It is recalled that, under static compression loading, a 2-D delamination below the surface ply did not grow or reduce the unflawed static compression strength of laminates B and C (see section 3.9). On the other hand, laminate A specimens with 2-D delamination at locations 1 or 4 exhibited delamination growth and a strength loss of approximately 30% under static compression loading. Consequently, only laminate A ($[0/45/90/-45]_{8S}$) specimens with imbedded 2-D delaminations at locations 1 and 4 were chosen for half-life residual tests.

In Table 4, these are identified as test series 8, 10 and 12 for a 2-D delamination imbedded below the surface ply, and as test series 15, 17 and 19 for a 2-D delamination located between plies 4 and 5. In conducting these tests, the specimens were initially subjected to compression fatigue loading (R=10; ω = 10 Hz) at the S value corresponding to the fatigue life test series in Table 4. For example, specimens tested under series 8 were initially fatigued at S_7 = 0.66 for 1000 cycles at R = 10; ω = 10 Hertz, and then tested for residual strength. Cyclic loading was imposed for approximately half the average lifetime of the preceding fatigue life test series. At the completion of half-life cyclic loading, selected specimens were radiographed, using DIB for enhancement, to record the half-life growth of the imbedded delamination. Subsequently, the specimens were failed in static compression to determine the half-life residual strength.

A static strength loss of 30% reduces the static strength of the delaminated specimen to 70% of the unflawed specimen strength. If this delaminated specimen is subjected to compression fatigue at an S value of 0.7, the maximum cyclic compressive stress is only half the strength of the unflawed specimen. Consequently, apart from the measured delamination growth, negligible degradation is expected otherwise in the fatigued specimen. And, the half-life residual strength is expected to be the static strength of an unfatigued, laminate A specimen with an imbedded flaw corresponding to the half-life delamination size.

Table 22 presents half-life residual strength data for laminate A specimens with 2-D delaminations below the surface (0°ply). These data are superimposed over the S-N data, generated through test series 7, 9 and 11, in Figure 26. It is noted that two specimens suffered fatigue failure (4284-53, 60) before they could be cycled to approximately half the average lifetime of the preceding test series. Figures 55, 56 and 57 present radiographs of selected specimens from test series 8, 10 and 12, respectively, after they were fatigued to the noted number of cycles. It is seen that varying extents of growth in the imbedded delamination were realized for some of the specimens. Caution must, therefore be exercised in interpreting the corresponding residual strength data.

From the residual strength data in Figure 26, it is inferred that specimens that survived 1000 cycles at S=0.66 retained their static strength to within $\pm$5%. Consequently, some specimens were cycled to a smaller number of cycles to avoid fatigue failure (see Table 22). Specimen 4284-53 suffered fatigue failure after 680 cycles at S=0.66. Specimen 4284-59 suffered a 10% loss in the static strength after 500 cycles at S=0.66. This specimen was cycled only to 500 cycles because considerable delamination growth was observed within that time. This is reflected in the larger (10%) strength loss. Specimens that sustained 5000 cycles of loading at S=0.58 suffered strength losses ranging from 9% to 19%. One specimen suffered fatigue failure after 700 cycles at S=0.58, and another suffered a 15% loss in static strength after 2800 cycles at S=0.58. Similar results for specimens fatigued at S=0.55 are given in Table 22 and plotted in Figure 26.

Table 23 presents half-life residual strength data for laminate A specimens with 2-D delaminations between plies 4 and 5. Figures 58, 59 and 60 present radiographs of selected specimens from test series 15, 17 and 19, respectively, after they were fatigued to approximately half their lifetimes. The data in Table 23 are superimposed over the corresponding S-N data, generated through test series 14, 16 and 18, in Figure 32. Only one specimen suffered fatigue failure after 550 cycles at S=0.77. Compared to the previous case (Table 22, Figure 26), half-life residual strength data for this case exhibit very little scatter. Also, a smaller

percentage reduction in the static strength was realized during these residual strength tests. A 3% to 18% loss was realized in specimens fatigued for 1000 cycles at S=0.77, a 3% to 9% loss in specimens fatigued for 7500 cycles at S=0.72, and 0% to 15% loss in specimens fatigued for 100,000 cycles at S=0.66. It is believed that differing extents of delamination growth after the same number of fatigue cycles induce different percentage reductions in the static strength. Unfortunately, only a few of these test specimens had laser-drilled holes in the delaminated region that enabled recording of half-life delamination size using DIB-enhanced radiography. Consequently, the half-life damage sizes of many specimens were not recorded.

3.21 Ultimate Strength Tests

In the fatigue life tests and the half-life residual strength tests, failure was assumed to have occurred when an imbedded delamination propagated to the tab boundary. At this failure load level, the specimen need not necessarily lose all its load-carrying capacity. To determine the excess strength left in the specimens after this initial failure, ultimate static strength tests were conducted on fatigue life and half-life residual strength test specimens. The load was increased in a quasi-static manner, and two failure load levels were recorded. The lower value corresponded to an initial delamination failure, accompanied by a loud "popping" sound The higher value corresponded to ultimate failure, beyond which no additional load can be sustained by the specimen. Tables 22 and 23 present ultimate strength data on half-life residual strength test specimens. It is seen that the ultimate strengths are considerably ($\sim$ 50%) larger than the stresses corresponding to delamination failure. Table 24 presents similar ultimate strength data on fatigue life test specimens. Laminate B specimens seem to carry minimal additional load beyond delamination failure.

3.22 Post-Test Inspection of Test Specimens For Fiber Microbuckling

Specimens used in the fatigue life tests and half-life residual strength tests were inspected, at the completion of the tests, under a microscope to

observe fiber microbuckling, if any. At a magnification factor of 50, no fiber microbuckling was visible. Subsequently, selected photomicrographs were obtained to verify the visual observation. Figures 61 to 67 present selected photographs and photomicrographs. It is seen from these pictures that no fiber microbuckling was precipitated during the conducted tests. Figure 67 magnifies a very small portion of one edge (XZ cross section) of a test specimen by a factor of 200 to reinforce the same conclusion.

SECTION 4

CONCLUSIONS AND RECOMMENDATIONS

4.1 Conclusions

An experimental program was conducted to assess the effect of imbedded delaminations on the compression fatigue behavior of quasi-isotropic, T300/5208 graphite/epoxy laminates. Specimen gross buckling between tabs, local buckling of the delaminated region, and fiber microbuckling were identified as instability-initiating, failure-inducing failure modes of interest. A 64-ply laminate layup and a 3.81 cm square test section were chosen to preclude specimen gross buckling. Post-test inspection of the specimens revealed the absence of any fiber microbuckling. Consequently, the predominant failure mode was the growth of the imbedded delaminations. When the delaminations reached the tab region, failure was assumed to have occurred. Ultimate strength tests quantified the excess load-carrying capacity of the specimens beyond delamination failure.

Two types of delamination were considered in the program. One extended across the entire width of the specimen and was 1.27 cm long. It was called a 1-D delamination because it was expected to grow in a self-similar manner along the delaminated interface. The other type was 1.27 cm in diameter, and was located at the planform center of the test specimen. This buried delamination was called a 2-D flaw, assuming its growth in its plane to be two-dimensional. Delaminations were introduced during fabrication through Teflon imbedments. Imbedded delaminations were located near the surface ply to simulate low velocity impact damage. One location was just below the surface ply, and the other one was between plies 4 and 5. Three stacking sequences of a quasi-isotropic laminate were tested, each layup having a different surface ply fiber orientation. The surface plies had a 0°, 45° or 90° fiber orientation.

DIB-enhanced radiography was employed in the program to monitor delamination growth. The use of this technique is restricted to situations where the dye can be applied to the surface from which delaminations initiate and

grow; namely, free edge delaminations and delaminations originating from a cut-out. Buried delamination growths have hitherto been monitored via ultrasonic techniques that require periodic removal of the specimen from the test fixture, and are time-consuming. In the reported program minute laser-drilled holes were introduced in the thin delaminated region, in specimens with buried 2-D flaws. DIB was then introduced through these holes to the delaminated region, and radiographs obtained subsequently, to monitor the growth in the buried delamination. When the flaw was located below the surface ply, matrix cracks did initiate from this hole as they did from other locations, too. But, no measurable deleterious effect of the laser-drilled hole on the fatigue life or the half-life residual strength was observed. It can therefore be concluded that a very efficient procedure has been developed in this program to monitor the growth of imbedded delaminations via enhanced radiography.

Static compression tests on unflawed quasi-isotropic specimens exhibited increasing strengths as the surface ply changed from 90° to 45° to 0°. Failure was induced by the precipitation of delaminations in the laterally unsupported test specimens. Back-to-back strain gage data from these tests also indicated the absence of any significant bending (gross buckling) effects due to the laterally unsupported test section.

Static compression tests on laminate A ($[0/45/-90/-45]_{8S}$), laminate B ($[45/90/-45/0]_{8S}$) and laminate C ($[90/45/0/-45]_{8S}$) specimens with imbedded delaminations revealed some interesting results. Laminate A specimens with 1-D delaminations at location 1 or 2-D delaminations at locations 1 or 4, suffered a strength loss due to the unstable propagation of the flaw to the tab region. The unflawed laminate A strength in static compression was reduced by 41% through the introduction of a 1-D flaw at location 1, 31% by a 2-D delamination at location 4. These reductions correspond to the initial flaw sizes mentioned earlier.

Static compression tests on laminates B and C, with a 2-D delamination below the surface ply, indicated no deleterious effect of the flaw on the unflawed laminate strength. Actually a small increase, attributable to scatter, in the measured average strength was recorded. The imbedded flaw did not grow, and did not seem to have any influence on delaminations

that were precipitated at failure at locations other than the initial flaw location. The low modulus and bending stiffness of the delaminated ply are believed to be the cause of this response.

Static compression tests on laminate B specimens with a 2-D delamination between plies 4 and 5 (location 4) recorded a 20% loss in the unflawed laminate strength. Similar tests on laminate C specimens with the same flaw resulted in a 19% loss in the unflawed laminate strength. Failure was precipitated, in either case, by an unstable propagation of the imbedded delamination to the tab region.

During the static tests, the maximum lateral deflection of the buckled delaminated region was measured. As the flaw location was changed from location 1 to location 4, the lateral deflection at failure decreased. In laminate A specimens, with a 1-D or 2-D delamination below the surface ply, matrix splitting between fibers in the surface ply occurred in the delaminated region. These cracks biased the direction of growth of the imbedded delaminations, especially the buried (2-D) circular flaws. Similar matrix cracks between fibers were also observed in failed specimens of all three layups that contained an initial 2-D delamination at location 4. Consequently, caution must be exercised in the use of presented data in developing or validating an analysis that can predict the observed response. Static compression tests manifested an unstable growth of the imbedded delaminations to failure, except for the two mentioned cases.

Constant amplitude compression fatigue tests on flawed specimens generated S-N curves and delamination growth data. These tests were conducted at R = 10 and ω= 10 Hertz, and delamination growth was monitored visually and via DIB-enhanced radiography. S-N data for laminate A specimens revealed a higher threshold S value as the initial flaw was changed from a 1-D delamination at location 1 to a 2-D delamination at location 1. A further increase was observed when the 2-D delamination was imbedded at location 4. S-N curves for laminates B and C, with 2-D delaminations at locations 1 or 4, exhibited a similar behavior. A higher threshold S value increases the fatigue lifetime of the specimen at an S value between $S_{threshold}$ and one.

Fatigue life tests on laminates A and B, with a delamination below the surface ply, exhibited stable flaw growth with N, the number of fatigue load cycles. The large lateral deflections of the buckled ply also caused matrix splitting between fibers in the delaminated region. It is interesting that a laminate B specimen with a 2-D delamination below the surface ply exhibits stable flaw growth during fatigue when the same flaw demonstrates no influence during static compression loading. Compression fatigue tests on laminate C specimens with a 2-D flaw below the surface ply, resulted in no growth of the imbedded flaw. The low modulus and bending stiffness of the 90°ply in the delaminated region is believed to be the cause of this response.

Fatigue life tests on specimens of all three layups, with 2-D delaminations at location 4, revealed negligible growth in the imbedded delamination until failure. At failure, the flaw spread to the tab region in an unstable manner, similar to the static response.

Half-life residual strength tests on laminate A specimens, with 2-D delaminations at locations 1 or 4, yielded strengths that were representative of the observed or recorded flaw growth. For a larger delamination growth at half-life, a larger strength loss was recorded.

Ultimate strength tests were also carried out at the end of the program to assess the maximum load-carrying capacity of the test specimens. As expected, all the specimens carried additional loads beyond fatigue failure, defined as the propagation of the imbedded delamination to the tab region.

4.2 Recommendations

Based on the conclusions mentioned above, it is recommended that tests on specimens with 1-D delamination be repeated on narrower and longer specimens for reliable data generation. Delaminations should be chosen to be at least two plies below the surface. A simple analysis, similar to that in Reference 15, also needs to be developed to predict the observed results. A validated analysis may then be used to understand and quantify the effect of delaminations on the compression fatigue behavior of laminates, without resort to an extensive experimental program. A similar analysis for the more realistic 2-D delamination growth is more involved, and could be attempted after successfully understanding 1-D delamination growth.

SECTION 5

REFERENCES

1. Ramkumar, R. L., "Composite Impact Damage Susceptibility," Naval Air Development Center Report NADC-790-68-60. Northrop Corporation, January 1981.
2. Bhatia, N. M.,"Impact Damage Tolerance of Thick Graphite/Epoxy Laminates," Naval Air Development Center Report No. NADC-79038-60, January 1979.
3. Ramkumar, R. L., "Environmental Effects on Composite Damage Criticality," Naval Air Development Center Contract N62269-79-C-0259. Northrop Corporation, June 1981.
4. Chatterjee, S. N., Hashin, Z. and Pipes, R. B., "Definition and Modeling of Critical Flaws in Graphite Fiber Reinforced Resin Matrix Composite Materials," NADC-77278-30, August 1979.
5. Ratwani, M. M. and Kan, H. P., "Compression Fatigue Analysis of Fiber Composites," NADC-78049-60, September 1979.
6. Byers, B. A., "Behavior of Damaged Graphite/Epoxy Laminates Under Compression Loading," NASA-CR-159293, August 1980.
7. Brussat, T. R., Chiu, S. T., and Mostovoy, S., "Fracture Mechanics For Structural Adhesive Bonds, Phases I and II," Report AFML-TR-77-163, Parts I and II, 1978.
8. Wilkins, D. J., Eisenmann, J. R., Camin, R. A., Margolis, W. S., and Benson, R. A., "Characterizing Delamination Growth in Graphite/ Epoxy," Presented at the ASTM Conference on Damage in Composite Material, Bal Harbor, Florida, November 1980.
9. Saff, C. R., "Compression Fatigue Life Prediction Methodology for Composite Structures-Literature Survey," Naval Air Development Center Report No. NADC-78203-60, June 1980.
10. Wang, S. S. "Delamination Crack Growth in Unidirectional Fiber-Reinforced Composites Under Static and Cylic Loading," ASTM STP 674, Composite Materials: Testing and Design (Fifth Conference),1979.

11. Reifsnider, K. L., Henneke, E. G. and Stinchcomb, W. W., "Delamination in Quasi-Isotropic Graphite-Epoxy Laminates", ASTM STP 617, Composite Materials: Testing and Design (Fourth Conference), 1977.
12. Ramkumar, R. L., Kulkarni, S. V. and Pipes, R. B., "Definition and Modeling of Critical Flaws in Graphite Fiber Reinforced Epoxy Resin Matrix Composite Materials", Naval Air Development Center Report No. NADC-76228-30, January 1978.
13. Wang, S. S. and Mandrell, J. F., "Analysis of Delamination in Unidirectional and Crossplied Fiber-Composites Containing Surface Cracks", NASA CR-135248, May 1977.
14. Chai, M. Babcock, C. D. and Knauss, W. G., "On the Failure of Laminated Plates by Delamination Buckling", Report No. 80-16, California Institute of Technology, July 1980.
15. Whitcomb, J. D., "Analysis of Instability-Related Delamination Growth", Proceedings of the Mechanics of Composites Review, Bergamo Center, Ohio, October 1980.
16. Tirosh, J., "On the Tensile and Compressive Strength of Solids Weakened (Strengthened) by an Inhomogeneity", Journal of Applied Mechanics, September 1977.

TABLE 1. SUMMARY OF T300/5208 PREPREG DATA (QC TESTS AT NORTHROP)*

LOT ID.	AVERAGE RESIN CONTENT (% BY WT)	AVERAGE AREAL FIBER WT. (gm/m^2)	AVERAGE % VOLA-TILES	AVERAGE GEL TIME (min)	TACK
ACL 4223	35.3	151.6	.23	18.4	Acceptable
ACL 4224	35.9	143.7	.23	17.0	Acceptable
ACL 4225	32.4	151.9	.28	17.2	Acceptable
ACL 4226	34.9	151.4	.20	17.3	Acceptable
SPEC. REQUIRE-MENTS**	34 ± 3	144 ± 5	3.0 (max.)	—	Acceptable

*Northrop Specification No. NAI-1371 for test procedures.

**Lockheed Specification No. C-22-1379/114 for T300/5208 material quality.

TABLE 2. SUMMARY OF T300/5208 LAMINATE DATA (QC TESTS AT NORTHROP)*

LOT ID.	RESIN CONTENT (% BY WT)	SPECIFIC GRAVITY	FIBER VOL %	VOID CONTENT	$\sigma^{tu}(90^o)$ (MPa) **	$\varepsilon^{tu}(90^o)$ (μcm/cm) **	$E(90^o)$ (GPa) **	$\sigma^{tu}(0^o)$ (MPa) †	$E(0^o)$ (GPa) †	$\tau^{ult}(0^o)$ (MPa) ††
ACL 4223	29.9	1.57	62.7	0	61.7	7680	8.20	1793	148.9	127.3
ACL 4224	29.1	1.59	64.0	0	63.8	7950	8.14	1661	132.2	129.6
ACL 4225	24.5	1.61	69.1	0	68.7	7727	9.17	1762	131.2	135.4
ACL 4226	24.4	1.61	69.6	0	56.3	6113	9.35	1692	126.2	132.6
SPEC. REQUIREMENTS	—	1.54-1.60	60-68	—	44.8 (min.)	4000 (min.)	9.65 (min.)	1448 (min.)	124.1 (min.)	89.6 (min.)

*Results were obtained from $[0]_{16}$ laminate tests

**Transverse Tension Tests. The material is acceptable even though E(90) does not meet specification requirements because, σ^{tu} (90) and ε^{tu} (90) exceed required minimum values by a large margin.

†Longitudinal Flexure Tests - ††Short Beam Shear Tests

TABLE 3. AVERAGE VENDOR (NARMCO) DATA ON T300/5208

Resin Content (by weight)	35% (uncured)
Areal Fiber Weight	144 gm/m^2
Volatile Content	0.3%
Flow	14/12%
Gel Time	22'47"
Tack	Acceptable
Specific Gravity	1.59
Fiber Volume	67%
Cured Ply Thickness	0.012954cm (.0051 in.) -8 ply 0.013208cm (.0052 in.) -16 ply
Longitudinal (0^{O}) Flexural Strength (RT)	2004 MPa (291 ksi)
Longitudinal (0^{O}) Flexural Modulus (RT)	136.7 GPa (19.83 Msi)
0^{O} Tensile Strength (RT)	1458 MPa (211.5 ksi)
0^{O} Tensile Modulus (RT)	146 GPa (21.2 Msi)
0^{O} Flex. Strength ($180^{O}F$)	1924 MPa (279 ksi)
0^{O} Flex. Modulus ($180^{O}F$)	131.1 GPa (19.02 Msi)
Short Beam Shear Strength (RT)	147.1 MPa (21.34 ksi)
Short Beam Shear Strength ($180^{O}F$)	130.0 MPa (18.85 ksi)

TABLE 4. TESTS CONDUCTED ON LAMINATE A[++]

Test Series ID	Delamination Type	Flaw Location ID	Compressive Load Type	S (R=10; ω=10 Hz)	No. of Fatigue Cycles, N	No. of Specimens
1	None	--	Static	1.0	0.25	5 + 2*
2	1-D	1	Static	1.0	0.25	5 + 2*
3	1-D	1	Fatigue	0.60	$3<\log N_{f_3}<4$**	5
4	1-D	1	Fatigue	0.47	$4<\log N_{f_4}<5$	5
5	1-D	1	Fatigue	0.45	$5<\log N_{f_5}<6$	5
6	2-D	1	Static	1.0	1	5 + 2*
7	2-D	1	Fatigue	0.66	$3<\log N_{f_7}<4$	5
8	2-D	1	Fatigue	0.66	$N_{f_7}/2$; RS+	5
9	2-D	1	Fatigue	0.58	$4<\log N_{f_9}<5$	5
10	2-D	1	Fatigue	0.58	$N_{f_9}/2$; RS	5
11	2-D	1	Fatigue	0.55	$5<\log N_{f_{11}}<6$	5
12	2-D	1	Fatigue	0.55	$N_{f_{11}}/2$; RS	5
13	2-D	4	Static	1.0	1	5 + 2*
14	2-D	4	Fatigue	0.77	$3<\log N_{f_{14}}<4$	5
15	2-D	4	Fatigue	0.77	$N_{f_{14}}/2$; RS	5
16	2-D	4	Fatigue	0.72	$4<\log N_{f_{16}}<5$	5
17	2-D	4	Fatigue	0.72	$N_{f_{16}}/2$; RS	5
18	2-D	4	Fatigue	0.66	$5<\log N_{f_{18}}<6$	5
19	2-D	4	Fatigue	0.66	$N_{f_{18}}/2$; RS	5
					Total	103

* Two specimens to be delivered to the funding government agency.

** N_{f_i} denote the number of cycles for fatigue failure at S_i

\+ These are half-life residual strength (RS) tests

++ $[0/45/90/-45]_{8s}$ layup.

TABLE 5. TESTS CONDUCTED ON LAMINATES B AND C[+]

Test Series ID	Delamination Type	Flaw Location ID	Compressive Load Type	S (R=10; ω=10 Hz)	No. of Fatigue Cycles, N	No. of Specimens
1	None	--	Static	1.0	0.25	5 + 2*
6	2-D	1	Static	1.0	0.25	5 + 2
7	2-D	1	Fatigue	S_7[††]	$3<\log N_{f_7}^{**}<4$	5
8	2-D	1	Fatigue	S_8	$4<\log N_{f_8}<5.5$	5
13	2-D	4	Static	1.0	1	5 + 2
14	2-D	4	Fatigue	0.77	$3<\log N_{f_{14}}< 4$	5
15	2-D	4	Fatigue	0.77	$4<\log N_{f_{15}}< 5.5$	5
					TOTAL	41

*Two specimens to be delivered to the funding government agency.

**N_{f_i} denote the number of cycles for fatigue failure at S_i.

+ $[45/90/-45/0]_{8s}$ and $[90/45/0/-45]_{8s}$ layups, respectively.

††For laminate B, $S_7 = 0.61$, $S_8 = 0.54$, $S_{14} = 0.66$, and $S_{15} = 0.61$

For laminate C, $S_7 = 0.62$, $S_8 = 0.49$, $S_{14} = 0.75$, and $S_{15} = 0.67$

TABLE 6. STATIC COMPRESSION TEST RESULTS ON UNFLAWED SPECIMENS

Laminate Type	Specimen ID	Failure Stress (MPa)	Failure Strain (μcm/cm)	Compression Modulus (GPa)
A	4238-1	-486.9	-11,295	45.62
	-2	-543.1	-13,036	45.55
	-3	-523.9	-12,591	44.66
	-4	-492.6	-11,759	44.90
	-5	-550.7	-13,489	44.75
	Average	-519.4	-12,434	45.10
B	4255-1	-458.2	-11,076	43.96
	-2	-522.5	-12,702	43.84
	-3	-517.5	-12,778	44.06
	-4	-505.4	-12,619	42.86
	-5	-487.9	-12,080	43.58
	Average	-498.3	-12,251	43.66
C	4282-1	-381.9	- 9,258	43.28
	-2	-461.6	-11,288	43.53
	-3	-423.6	-10,374	43.37
	-4	-423.3	-10,275	43.77
	-5	-410.8	-10,019	43.37
	Average	-420.2	-10,243	43.46

TABLE 7. STATIC COMPRESSION TEST RESULTS ON LAMINATE A SPECIMENS WITH 1.27 CM LONG DELAMINATION BETWEEN PLIES 1 AND 2, ACROSS THE ENTIRE WIDTH (1-D)

Specimen ID	Measurements at Failure*			
	Average Stress (MPa)	Average Strain (μ cm/cm)	Strain At The Center Of Buckled, Flawed Region (μ cm/cm)	Maximum Out-of-Plane Delfection In the Buckled, Flawed Region (cm)
4238-8	-307.68	--	--	--
-10	-257.48	-6392	--	.0025**
-11	-330.31	-7551	1747	.0053
-12	-298.84	-6787	--	.0025**
-13	-307.65	-6963	--	.0064
Average	-303.99	-6923	1747	.0059

* Imbedded delamination propagated to failure (to the tab region) in an unstable manner.

Most of the presented quantities, except for the average stress, were linearly extrapolated to correspond to the failure stress.

** Dial indicator was placed a small distance away from the center. These readings, therefore, are not used to obtain the average value.

TABLE 8. STATIC COMPRESSION TEST RESULTS ON LAMINATE A SPECIMENS WITH 1.27 CM DIAMETER DELAMINATION (2-D) BETWEEN PLIES 1 AND 2.

Specimen ID	Measurements At Failure*			
	Average Stress (MPa)	Average Strain (μ cm/cm)	Strain At the Center of Buckled, Flawed Region (μ cm/cm)	Maximum Out-of-Plane Deflection In the Buckled Flawed Region (cm)
4284-31	-358.17	-7762	9694	--
4284-32	-380.86	-8896	10,585	--
4284-46	-356.18	-7705	--	0.0038**
4284-51	-352.31	-8016	--	--
4284-54	-342.33	-7879	--	0.0432
Average	-357.97	-8052	10,140	.0432

*Imbedded delamination propagated to failure (to the tab region) in an unstable manner.

Most of the presented quantities, except for the average stress, were extrapolated to correspond to the failure stress.

** Dial indicator located off-center.

TABLE 9. STATIC COMPRESSION TEST RESULTS ON LAMINATE A SPECIMENS WITH 1.27 CM DIAMETER DELAMINATION (2-D) BETWEEN PLIES 4 AND 5

Specimen ID	Measurements At Failure*			
	Average Stress (MPa)	Average Strain (μ cm/cm)	Strain At the Center of Buckled, Flawed Region (μ cm/cm)	Maximum Out-of-Plane Deflection In the Buckled Flawed Region (cm)
4284-71	-324.70	-8278	--	0.0036**
4284-72	-338.94	-8146	--	0.0030**
4284-73	-308.38	-7345	--	0.0203
4284-74	-375.19	-7179	--	0.0127
4284-75	-357.56	-7628	+2132	0.0305
Average	-340.95	-7715	+2132	0.0212

*Imbedded delamination propagated to failure (to the tab region) in an unstable manner.

Most of the presented quantities, except for the average stress, were extrapolated to correspond to the failure stress.

**Dial indicator located off-center

TABLE 10. STATIC COMPRESSION TEST RESULTS ON LAMINATE B SPECIMENS WITH 1.27 CM DIAMETER DELAMINATION (2-D) BETWEEN PLIES 1 AND 2

Specimen ID	Measurements At Failure*		
	Average Stress (MPa)	Average Strain (μ cm/cm)	Maximum Out-of-Plane Deflection In the Buckled Flawed Region (cm)
4255-10	-531.89	-13,215	0.0318
4255-11	-506.12	-12,065	0.0508
4255-12	-529.98	-13,390	0.0635
4255-13	-504.65	-12,565	0.0508
4255-14	-519.30	-12,603	
Average	-518.39	-12,768	0.0492

*Imbedded delamination propagated to failure (to the tab region) in an unstable manner.

Most of the presented quantities, except for the average stress, were extrapolated to correspond to the failure stress.

TABLE 11. STATIC COMPRESSION TEST RESULTS ON LAMINATE B SPECIMENS WITH 1.27 CM DIAMETER DELAMINATION (2-D) BETWEEN PLIES 4 AND 5

Specimen ID	Measurements At Failure*		
	Average Stress (MPa)	Average Strain (μ cm/cm)	Maximum Out-of-Plane Deflection In the Buckled Flawed Region (cm)
4256-27	-374.38	-9951	--
4256-28	-403.20	-9785	--
4256-29	-406.77	-10,235	--
4256-30	-398.58	-10,154	--
4256-31	-420.37	- 9,831	.0038
Average	-400.66	-9991	.0038

*Imbedded delamination propagated to failure (to the tab region) in an unstable manner.

Most of the presented quantities, except for the average stress, were extrapolated to correspond to the failure stress.

TABLE 12. STATIC COMPRESSION TEST RESULTS ON LAMINATE C SPECIMENS WITH 1.27 CM DIAMETER DELAMINATION (2-D) BETWEEN PLIES 1 AND 2

Specimen ID	Measurements At Failure*		
	Average Stress (MPa)	Average Strain (μ cm/cm)	Maximum Out-of-Plane Deflection In the Buckled Flawed Region (cm)
4282-11	-521.58	-12,973	0.0381**
4282-12	-491.57	-12,098	--
4282-13	-510.73	-13,015	--
4282-14	-456.46	-11,097	--
4282-15	-510.73	-13,060	--
Average	-498.21	-12,449	--

*Imbedded delamination propagated to failure (to the tab region) in an unstable manner.

Most of the presented quantities, except for the average stress, were extrapolated to correspond to the failure stress.

**Dial indicator located off-center

TABLE 13. STATIC COMPRESSION TEST RESULTS ON LAMINATE C SPECIMENS WITH 1.27 CM DIAMETER DELAMINATION (2-D) BETWEEN PLIES 4 AND 5

Specimen ID	Measurements At Failure*		
	Average Stress (MPa)	Average Strain (μ cm/cm)	Maximum Out-of-Plane Deflection In the Buckled Flawed Region (cm)
4282-31	-306.44	-7060	0.0051
4282-32	-357.51	-8375	0.0127
4282-33	-306.44	-7110	0.0051
4282-34	-384.96	-8876	0.0102
4282-35	-351.12	-7484	0.0051
Average	-341.29	-7781	0.0076

*Imbedded delamination propagated to failure (to the tab region) in an unstable manner.

Most of the presented quantities, except for the average stress, were extrapolated to correspond to the failure stress.

TABLE 14. SUMMARY OF STATIC COMPRESSION TEST RESULTS

Laminate Type	Delamination Type	Delamination Located Between Plies	Measurements at Delamination Failure		
			Average Stress (GPa)	Average Strain (μcm/cm)	Maximum Out-of-Plane Deflection (cm)
A	None*	--	-519.4	-12,434	--
	1-D	1 and 2	-304.0	- 6,923	.0059
	2-D	1 and 2	-358.0	- 8,052	.0432
	2-D	4 and 5	-341.0	- 7,715	.0212
B	None*	--	-498.3	-12,251	--
	2-D	1 and 2	-518.4	-12,768	.0492
	2-D	4 and 5	-400.7	- 9,991	.0038
C	None*	--	-420.2	-10,243	--
	2-D	1 and 2	-498.2	-12,449	--
	2-D	4 and 5	-341.3	- 7,781	.0076

*These are results from tests on unflawed, virgin specimens, and correspond to a different failure mode.

TABLE 15. COMPRESSION FATIGUE LIFE TEST DATA ON LAMINATE A SPECIMENS WITH 1.27 CM LONG DELAMINATION (1-D) BETWEEN PLIES 1 AND 2

Test Series	Specimen ID	S*	Cycles to Failure (N_f)
3	4238-14	0.65	1300
	4284-21	0.80	400
	4284-24	0.65	1780
	4284-25	0.60	3500
	4284-25	0.60	4890
	4361-21	0.60	7200
4	4284-27	0.47	45,000
	4284-28	0.47	120,000
	4284-29	0.47	200,000
	4361-22	0.50	19,200
	4361-23	0.47	300,000
5	4284-22	0.39	$>10^{6+}$
	4284-23	0.45	61,700
	4361-24	0.43	$>10^{6+}$
	4361-25	0.45	102,000
	4361-26	0.45	102,500

*S is the ratio of the maximum compressive fatigue load to the static failure load for a given laminate-flaw type-flaw location combination; R=10; ω = 10 Hertz.

+Run-outs (no fatigue failure in a million cycles).

TABLE 16. COMPRESSION FATIGUE LIFE TEST DATA ON LAMINATE A SPECIMENS WITH 1.27 CM DIAMETER DELAMINATION (2-D) BETWEEN PLIES 1 AND 2

Test Series	Specimen ID	S*	Cycles to Failure (N_f)
7	4284-38	0.66	4460
	4284-55	0.66	4400
	4284-56	0.66	3000
	4361-12	0.66	1500
	4361-13	0.66	1700
9	4284-35	0.58	13,870
	4284-37	0.58	10,080
	4284-57	0.58	6,000**
	4284-58	0.58	8,000**
	4361-18	0.58	14,060
11	4284-39	0.55	22,540
	4284-45	0.55	>83,000+
	4284-47	0.55	62.430
	4284-48	0.55	33,660
	4284-66	0.55	312,000
	4284-67	0.55	>85,580+
	4361-16	0.55	17,000

*S is the ratio of the maximum compressive fatigue load to the static failure load for a given laminate-flaw type-flaw location combination; R=10; ω = 10 Hertz.

**Tests were prematurely stopped before delamination failure occurred. The numbers presented here are extrapolated values.

+Machine malfunctioned and the load exceeded the ultimate failure value.

TABLE 17. COMPRESSION FATIGUE LIFE TEST DATA ON LAMINATE A SPECIMENS WITH 1.27 CM DIAMETER DELAMINATION (2-D) BETWEEN PLIES 4 AND 5

Test Series	Specimen ID	S*	Cycles to Failure (N_f)
14	4284-70	0.83	420**
	4284-76	0.77	740
	4284-88	0.77	10,150
	4284-96	0.77	43,880
16	4284-81	0.72	310,010
	4284-84	0.72	54,000
	4284-93	0.72	688,030
	4284-99	0.72	6,750
	4284-100	0.72	9,980
	4361-3	0.72	10,840
18	4284-69	0.60	$>10^6$ +
	4284-85	0.66	550,000
	4284-103	0.66	251,400
	4284-104	0.66	284,000
	4361-5	0.66	$>10^6$ +

*S is the ratio of the maximum compressive fatigue load to the static failure load for a given laminate-flaw type-flaw location combination; R=10; ω= 10 Hertz.

**Specimen was cycled at S=0.7 for 8,000 cycles, and at S=0.75 for another 17,000 cycles, prior to cycling at S=0.83.

+Run-out

TABLE 18. COMPRESSION FATIGUE LIFE TEST DATA ON LAMINATE B SPECIMENS WITH 1.27 CM DIAMETER DELAMINATION (2-D) BETWEEN PLIES 1 AND 2

Test Series	Specimen ID	S*	Cycles to Failure (N_f)
7	4255-9	0.55	6790
	4255-15	0.61	14,170
	4255-16	0.61	1560
	4255-19	0.73	2300**
	4255-21	0.61	7350
	4255-24	0.61	2900
8	4255-20	0.54	21,040
	4255-22	0.54	18,000
	4255-23	0.54	34,300
	4255-25	0.54	52,180
	4255-26	0.54	30,300

*S is the ratio of the maximum compressive fatigue load to the static failure load for a given laminate-flaw type-flaw location combination; R=10; ω = 10 Hertz.

**Specimen was cycled at S=0.49 for 10,000 cycles before being cycled at S=0.73.

TABLE 19. COMPRESSION FATIGUE LIFE TEST DATA ON LAMINATE B SPECIMENS WITH 1.27 CM DIAMETER DELAMINATION (2-D) BETWEEN PLIES 4 AND 5

Test Series	Specimen ID	S*	Cycles to Failure (N_f)
14	4256-37	0.68	8840
	4256-38	0.66	10,630
	4256-39	0.66	29,290
	4256-40	0.66	22,250
	4256-41	0.66	7800
15	4256-32	0.61	133,100
	4256-33	0.61	184,100
	4256-35	0.61	260,600**
	4256-36	0.61	371,000
	4256-44	0.61	60,520

*S is the ratio of the maximum compressive fatigue load to the static failure load for a given laminate-flaw type-flaw location combination; R=10; ω= 10 Hertz.

**Delaminated near the surface away from the imbedded flaw (failure precipitated away from the imbedded flaw).

TABLE 20. COMPRESSION FATIGUE LIFE TEST DATA ON LAMINATE C SPECIMENS WITH 1.27 CM DIAMETER DELAMINATION (2-D) BETWEEN PLIES 1 AND 2.

Test Series	Specimen ID	S*	Cycles to Failure (N_f)
7	4282-16	0.69	640
	4282-17	0.62	920
	4282-18	0.62	6980
	4282-19	0.62	3470
	4282-21	0.62	780
8	4282-22	0.51	8650
	4282-23	0.49	61,000
	4282-24	0.49	52,000
	4282-25	0.49	94,650
	4282-26	0.49	138,160

*S is the ratio of the maximum compressive fatigue load to the static failure load for a given laminate-flaw type-flaw location combination; R=10; ω= 10 Hertz.

TABLE 21. COMPRESSION FATIGUE LIFE TEST DATA ON LAMINATE C SPECIMENS WITH 1.27 CM DIAMETER DELAMINATION (2-D) BETWEEN PLIES 4 AND 5

Test Series	Specimen ID	S*	Cycles to Failure (N_f)
14	4282-27	0.73	48,000
	4282-28	0.71	36,900**
	4282-29	0.75	99,730
	4282-30	0.75	84,770
	4282-41	0.75	10,710+
	4282-43	0.75	25,020
15	4282-36	0.67	120,740
	4282-37	0.67	59,760
	4282-38	0.67	257,080
	4282-40	0.67	96,000
	4282-44	0.67	303,150

*S is the ratio of the maximum compressive fatigue load to the static failure load for a given laminate-flaw type-flaw location combination; R=10; $=\omega$ 10 Hertz.

**Specimen was cycled at S=0.62 for 800,000 cycles prior to being cycled at S=0.71

+Delamination occurred near the surface away from the imbedded flaw location.

TABLE 22. RESIDUAL STRENGTH DATA FROM LAMINATE A SPECIMENS WITH 1.27 DIAMETER DELAMINATIONS BETWEEN PLIES 1 AND 2

Test Series	Specimen ID	Fatigue Loading (R=10; ω = 10 Hz) Prior to Residual Strength Testing		Residual Strength Test Data At			
				Delamination Failure		Ultimate Failure	
		S	N	Stress (MPa)	Strain (μ cm/cm)	Stress (MPa)	Strain+ (μ cm/cm)
8	4284-33	0.66	1000	-370.2	--	-481.2	--
	4284-36	0.66	1000**	-340.5	-9471	-456.2	-12,551
	4284-53	0.66	680	-241.7	--	-456.6	--
	4284-59	0.66	500	-321.1	--	-474.6	--
	4361-11	0.66	1000	-372.0	--	-578.6	--
10	4284-40	0.58	2800	-302.6	-7462	-498.3	-12,279
	4284 43	0.58	5000**	-326.9	-7535	-518.4	-12,901
	4284-60	0.58	700	-216.5	--	-460.0	--
	4284-61	0.58	5000	-290.3	--	-479.6	--
	4361-15	0.58	5000	-313.2	--	-599.3	--
12	4284-41	0.55	10,000	-339.2	-9465	-544.8	-11,587
	4284-42	0.55	8,000	-325.8	-7948	-509.8	-12,372
	4284-68	0.55	10,000	-289.0	--	-465.0	--
	4361-14	0.55	3,000	-328.5	--	-590.1	--
	4361-17	0.55	6,000	-304.5	--	-523.8	--

*The imbedded delamination propagated to the tab region in an unstable manner.

**Delamination failure occurred prior to residual strength testing.

+Linearly extrapolated from values prior to delamination failure.

TABLE 23. REISDUAL STRENGTH DATA FROM LAMINATE A SPECIMENS WITH 1.27 CM DIAMETER DELAMINATIONS BETWEEN PLIES 4 AND 5

Test Series	Specimen ID	Fatigue Loading (R=10; ω = 10 Hz) Prior to Residual Strength Testing		Residual Strength Test Data At			
				Delamination Failure		Ultimate Failure	
		S	N	Stress (MPa)	Strain (μ cm/cm)	Stress (MPa)	Strain+ (μ cm/cm)
15	4284-82	0.77	1000	329.7	-9620	-507.5	-14,444
	4284-83	0.77	1000	323.1	-8697	-525.7	-13,806
	4284-97	0.77	1000**	281.0	--	-427.6	--
	4284-98	0.77	550	263.9	--	-424.9	--
	4361-2	0.77	1000	293.0	--	-535.1	--
17	4284-86	0.72	7500	328.7	-8996	-538.3	-13,900
	4284-87	0.72	7500	309.4	--	-535.1	--
	4284-101	0.72	7500	310.4	--		--
	4284-102	0.72	7500	332.4	--		--
	4361-4	0.72	7500	311.0	--	-520.0	--
19	4284-89	0.66	100,000	319.0	--	-535.9	--
	4284-90	0.66	100,000	297.1	-7763	-501.5	-12,391
	4284-91	0.66	100,000	339.7	--	-534.0	--
	4284-105	0.66	100,000	307.1	--	-537.4	--
	4284-106	0.66	100,000	294.7	--	-448.4	--

*The imbedded delamination propagated to the tab region in an unstable manner.

**Delamination failure occurred prior to residual strength testing.

+Linearly extrapolated from values prior to delamination failure.

TABLE 24. ULTIMATE STRENGTH DATA ON FATIGUE LIFE TEST SPECIMENS

Laminate	Test Series	Specimen ID	Stress At Initial Delamination Failure* (MPa)	Ultimate Strength (MPa)
A	3	4284-21	307.1	560.5
	5	-22	308.8	482.5
	5	-23	264.5	527.7
	3	-24	296.7	503.2
	3	-25	219.0	517.9
	3	-26	290.5	572.0
	4	-28	255.4	570.5
	4	-29	254.6	528.9
	9	-35	348.8	487.1
	9	-37	446.1	543.1
	7	-38	341.2	476.4
	11	-39	313.7	513.0
	11	-47	367.3	531.7
	11	-48	327.9	544.4
	7	-55	422.9	541.8
	7	-56	506.7	560.2
	9	-57	405.5	544.4
	9	-58	358.1	511.2
	11	-66	290.3	454.2
	14	-76	350.0	561.6
	16	-81	442.4	446.2
	16	-84	283.7	509.3
	18	-85	313.7	504.5
	14	-88	348.7	507.2
	16	-93	420.1	568.0
	14	-96	300.3	518.5
	16	-99	324.8	522.7
	16	-100	360.0	513.0
	18	-103	336.4	535.4
	18	-104	483.7	511.9
	16	4361-3	300.8	507.7
	18	-5	385.4	532.1
	7	-12	422.2	547.8
	7	-13	413.6	562.0
	11	-16	330.3	605.5
	9	-18	338.0	547.0
	3	-21	336.5	499.7
	4	-22	246.4	585.3
	4	-23	404.8	536.1
	5	-24	331.5	613.9
	5	-25	272.0	558.8
	5	-26	300.9	615.6

*These specimens had already "failed" through the propagation of an imbedded delamination to the tab region. The stresses presented in this column correspond to the first unloading phenomenon observed during the ultimate strength test. This unloading was accompanied by a loud "popping" sound, characteristic of an interlaminar delamination.

TABLE 24. (CONCLUDED)

Laminate	Test Series	Specimen ID	Stress At Initial Delamination Failure* (MPa)	Ultimate Strength (MPa)
B	7	4255-15	344.0	550.6
	7	-16	--	508.4
	7	-19	--	536.3
	8	-20	492.7	545.6
	7	-21	--	610.3
	8	-22	409.2	519.4
	8	-23	--	551.6
	7	-24	525.0	538.1
	8	-25	492.9	570.7
	8	-26	455.7	547.6
	15	4256-32	376.7	530.7
	15	-33	443.7	494.5
	15	-35	324.1	499.3
	14	-37	481.7	549.7
	14	-38	364.0	528.7
	14	-39	319.3	533.8
	14	-40	460.1	512.8
	14	-41	420.5	530.5
	15	-44	486.9	545.2
C	7	4282-16	472.4	514.6
	7	-17	383.0	494.1
	7	-18	352.4	498.0
	7	-19	472.4	554.1
	7	-21	--	513.3
	8	-22	460.9	559.2
	8	-23	446.9	527.3
	8	-24	446.9	467.3
	8	-25	375.5	504.3
	14	-27	274.5	528.6
	14	-28	300.1	460.0
	14	-29	395.8	505.6
	14	-30	293.7	498.0
	15	-36	325.6	533.7
	15	-37	265.6	458.4
	15	-38	302.6	471.1
	15	-40	319.2	469.9
	14	-41	338.4	446.9
	14	-43	338.4	509.4
	15	-44	280.9	489.0

*These specimens had already "failed" through the propagation of an imbedded delamination to the tab region. The stresses presented in this column correspond to the first unloading phenomenon observed during the ultimate strength test. This unloading was accompanied by a loud "popping" sound, characteristic of an interlaminar delamination.

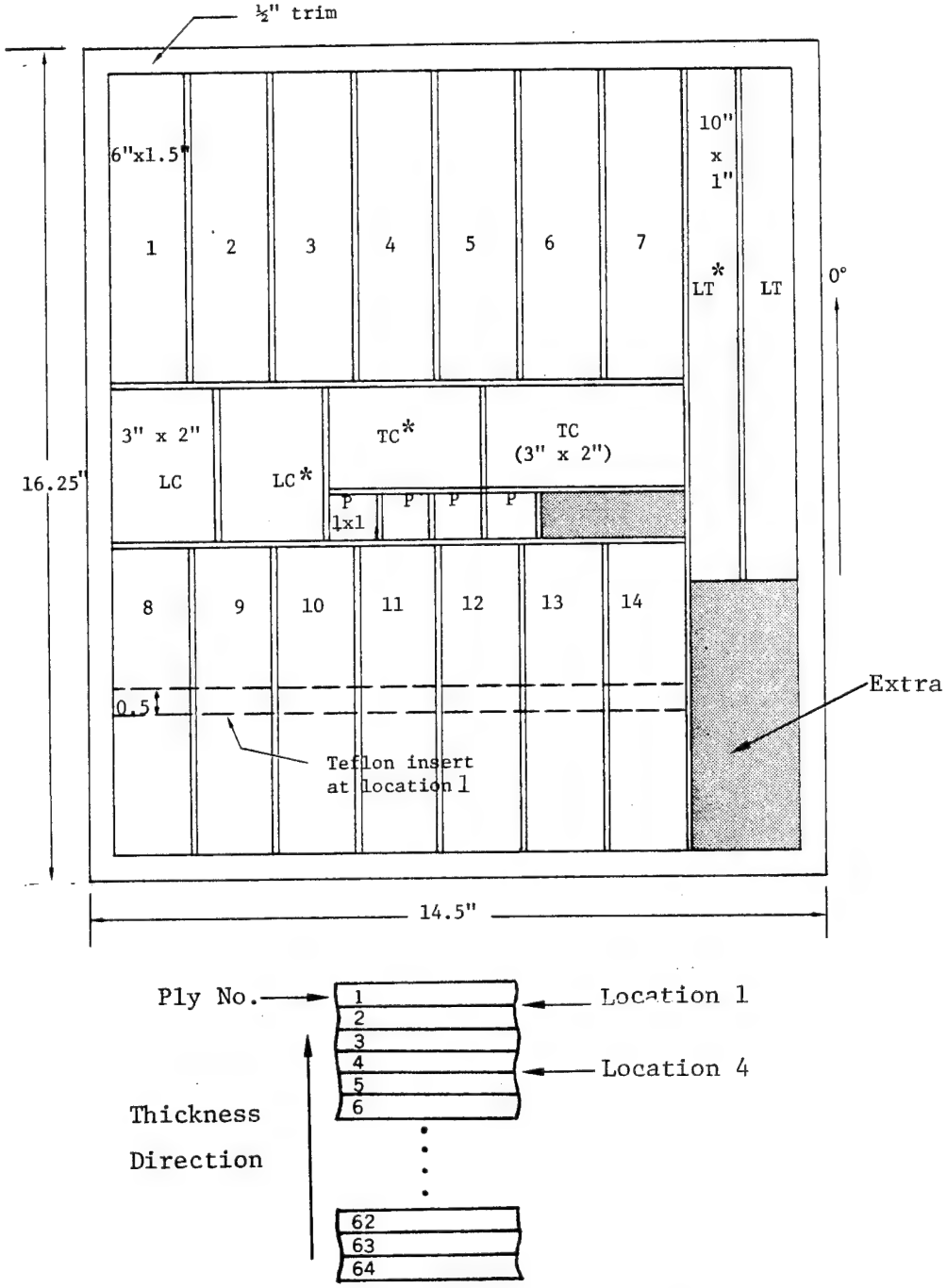

*Quality Control tests in longitudinal compression (LC), transverse compression (TC), and longitudinal tension (LT) to be conducted on these specimens.

Figure 1. Geometry of a Laminate A Panel (ID 4238)

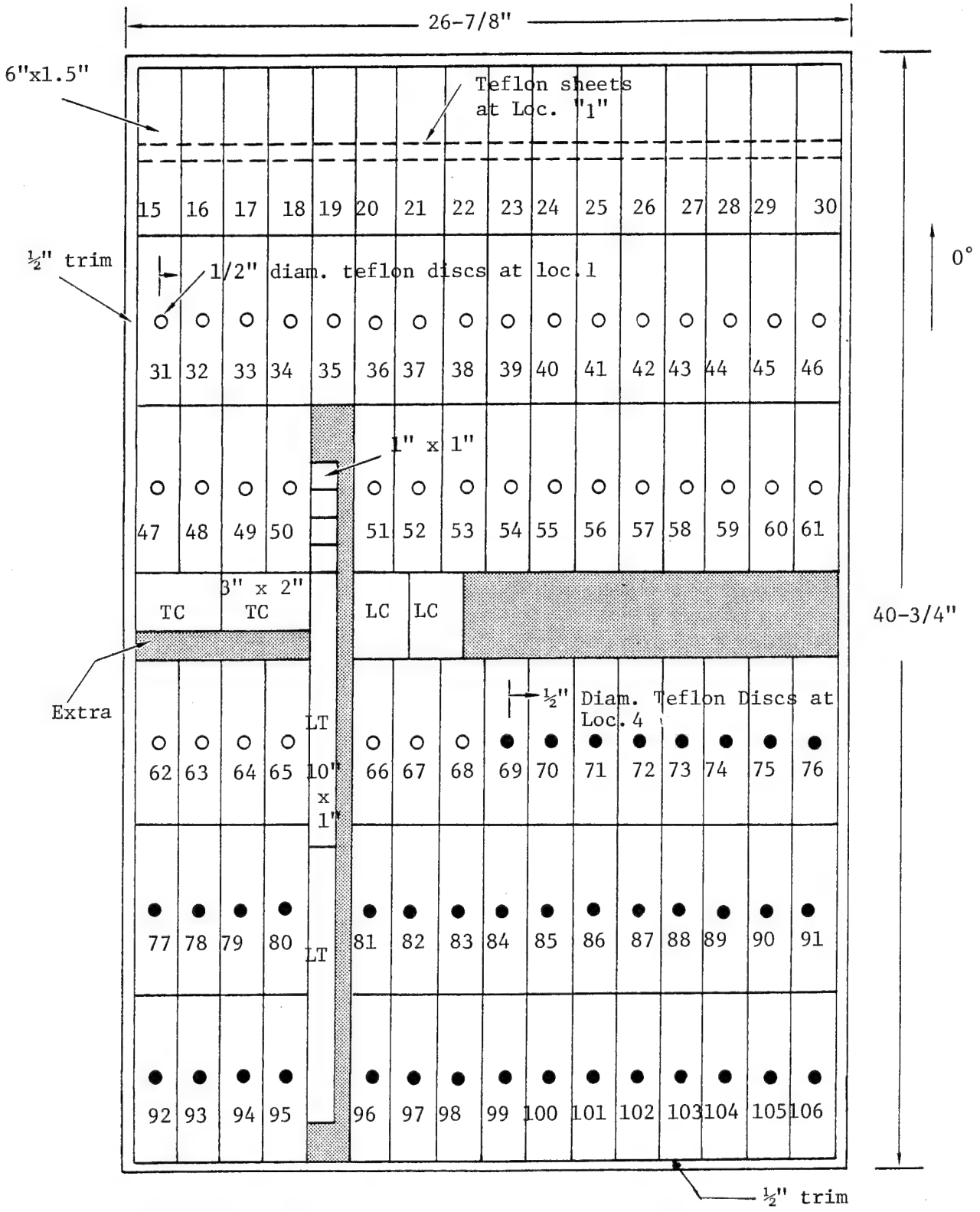

Figure 2. Geometry of the second Laminate A Panel (ID 4284)

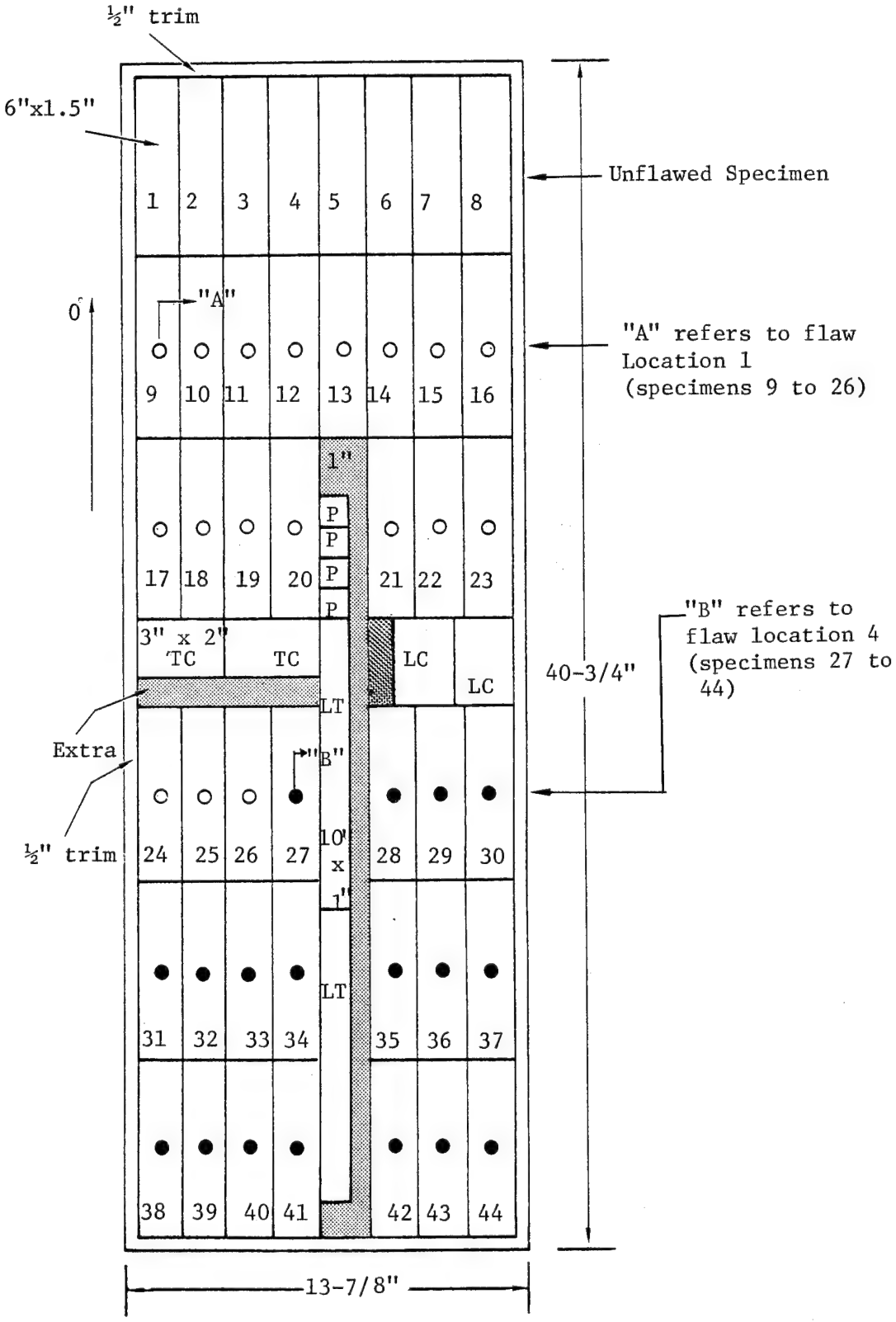

Figure 3. Geometry of a Laminate B Panel (ID 4255 and 4256) and a Lamimate C Panel (ID 4282)

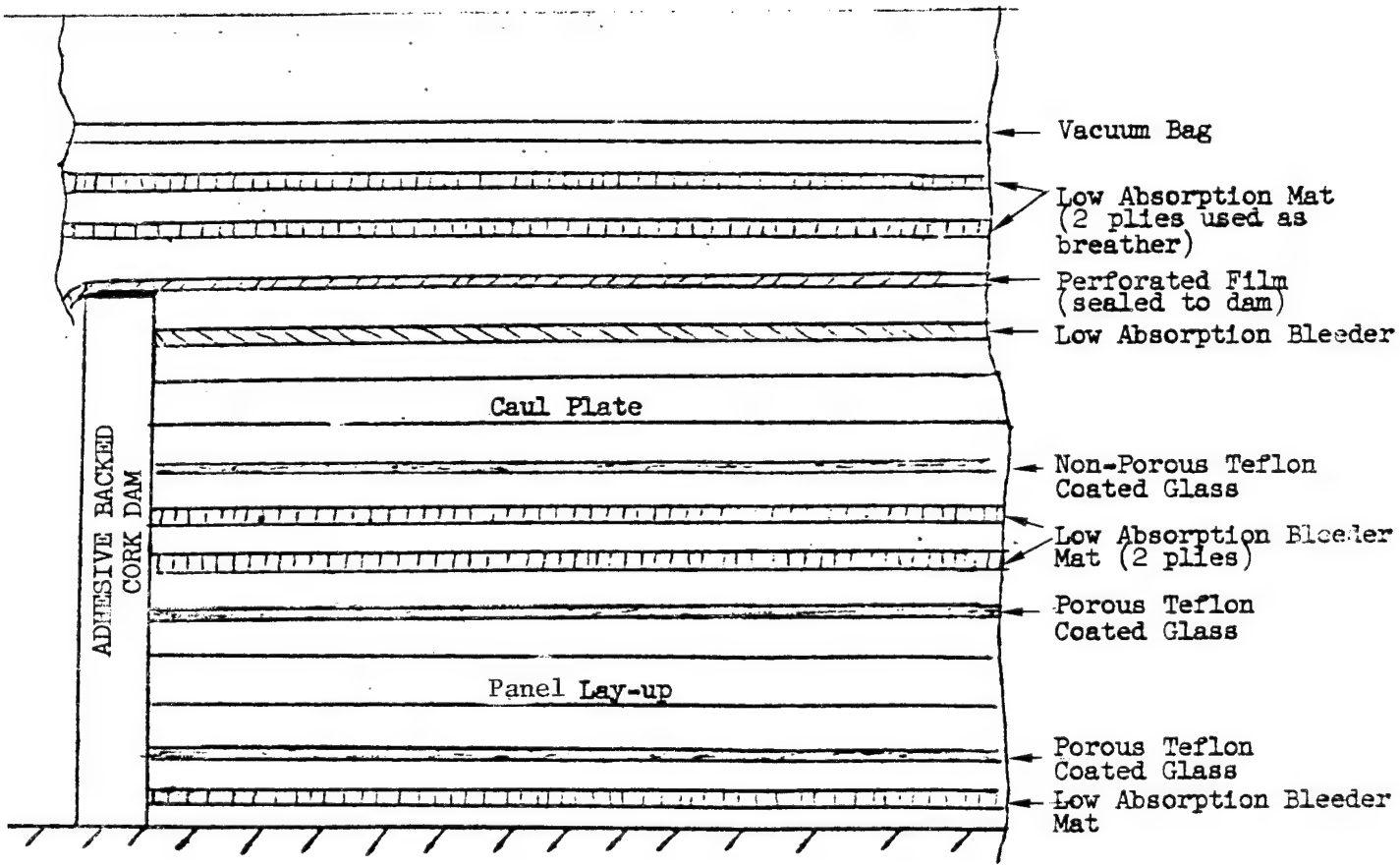

Note: The various elements (bleeder, glass ply, panel, caul plate, etc.) are separated in the figure for clarity.

Figure 4. Modified Bleeder Arrangement Used During The Layup Operation

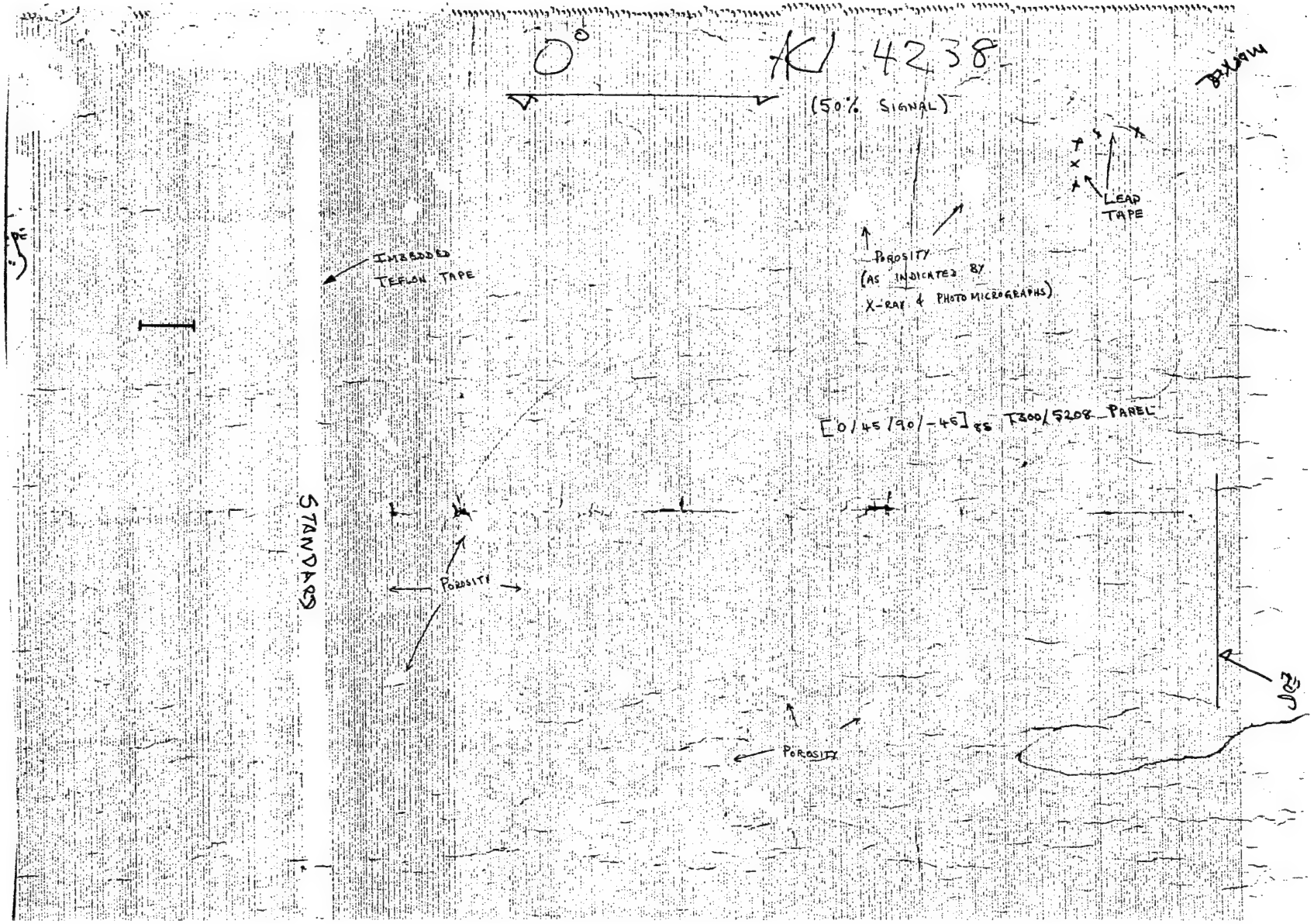

Figure 5. Ultrasonic C-Scan Record of a Laminate A Panel

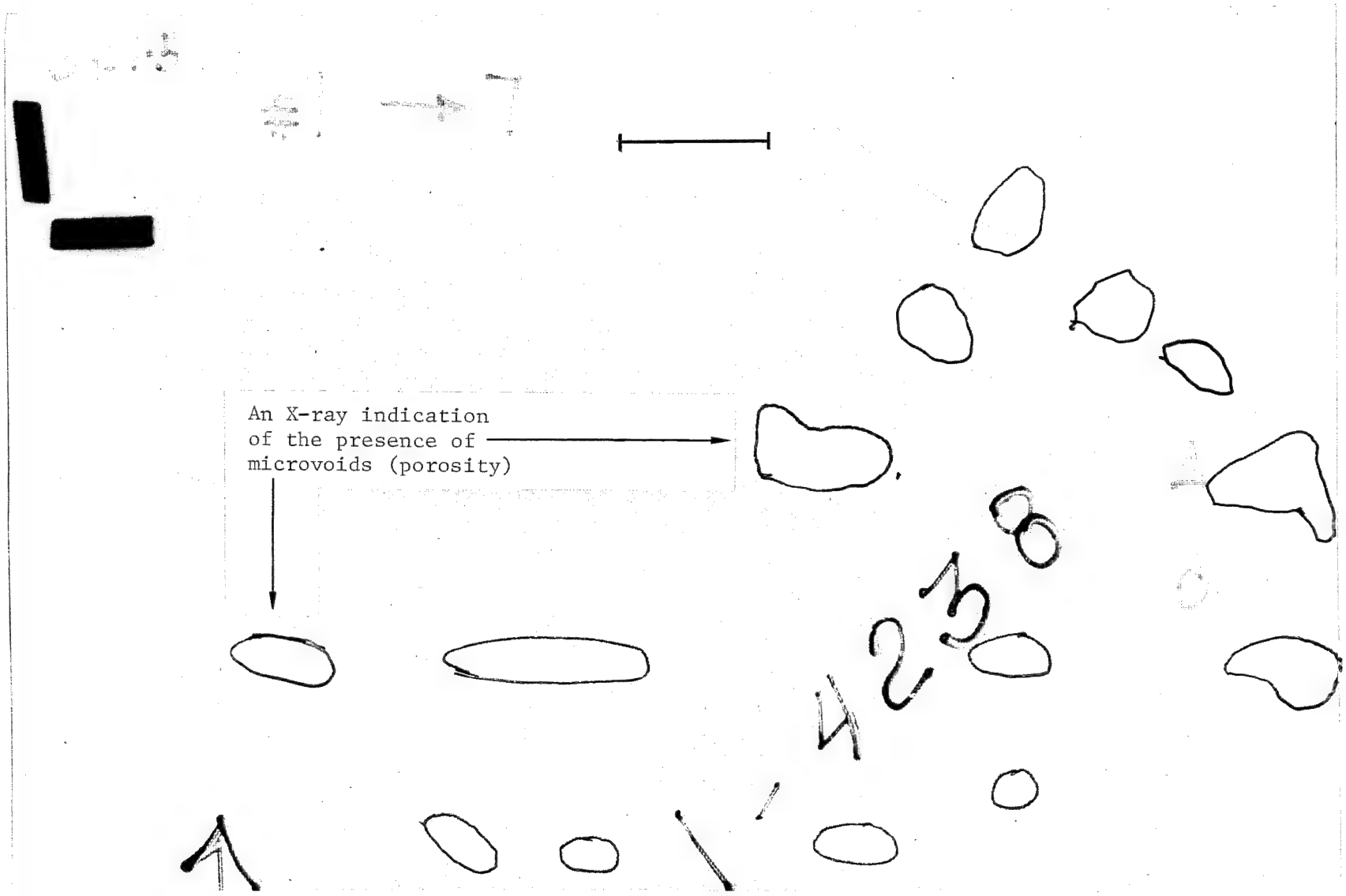

Figure 6. A Photoprint of an X-ray Record of the same portion of the Fabricated $[0/45/90/-45]_{8S}$ T300/5208 Panel shown in Figure 5.

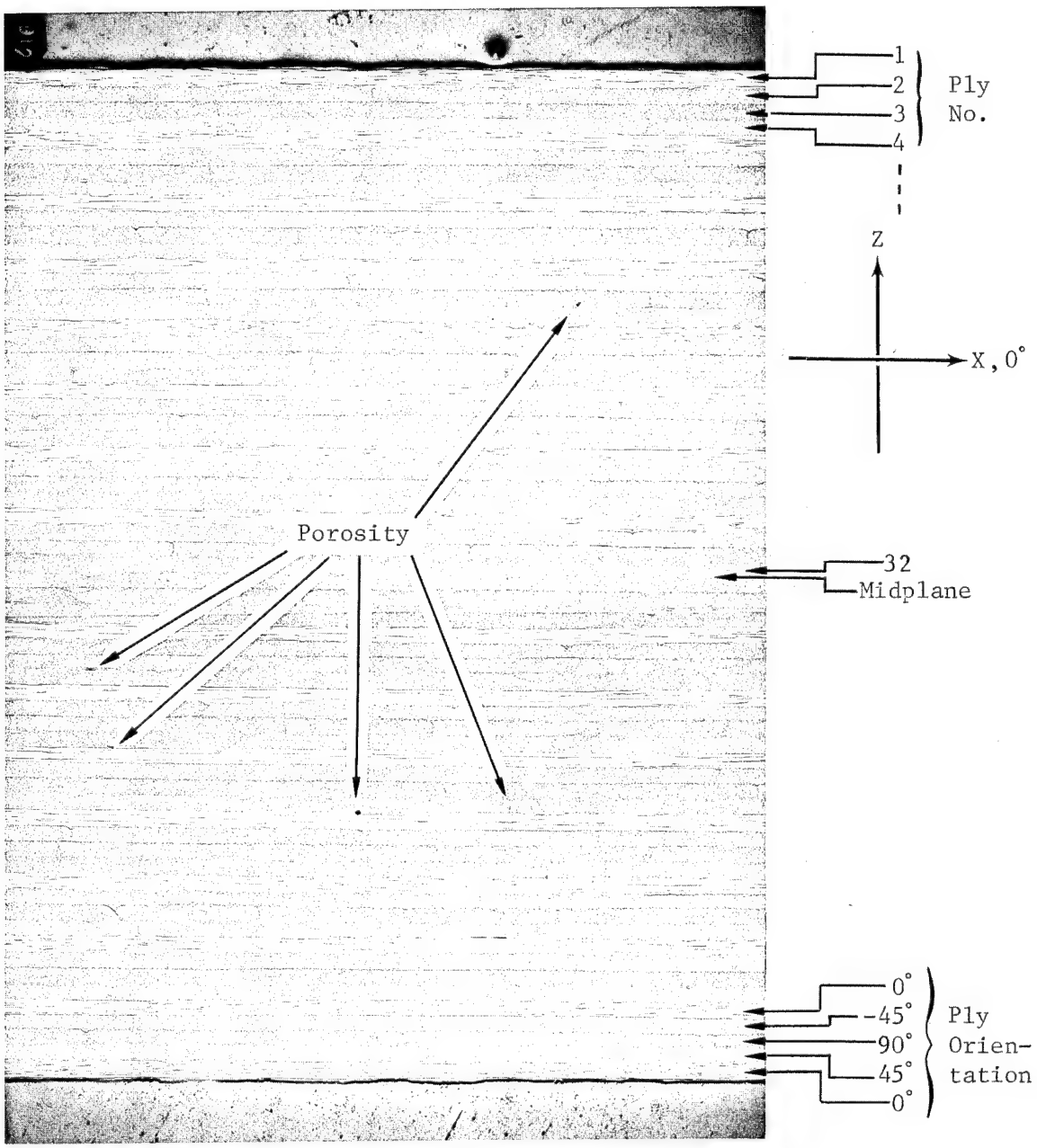

Figure 7. Photomicrograph of a Cross-Section of the Fabricated $[0/45/90/-45]_{8S}$ T300/5208 Panel Corresponding to a "Bad" C-Scan Location. The Picture at 16x Magnification Shows a Random Distribution of a Negligible Amount of Microvoids (Porosity) in the X-Z Plane.

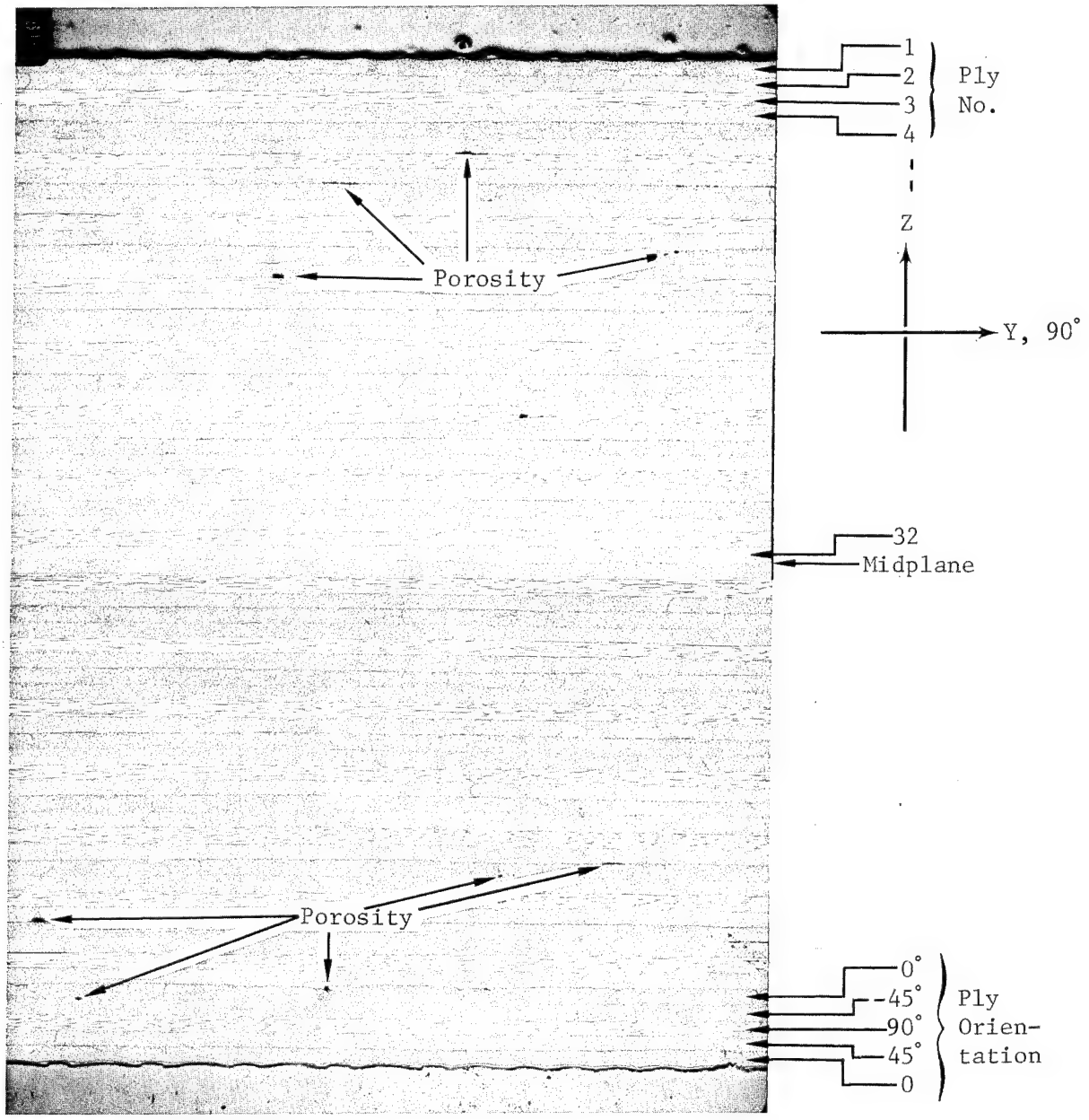

Figure 8. Photomicrograph of a Cross-Section of the Fabricated $[0/45/90/-45]_{8S}$ T300/5208 Panel Corresponding to a "Bad" C-Scan Location. The Picture at 16x Magnification Shows a Random Distribution of a Negligible Amount of Microvoids (Porosity) in the Y-Z Plane.

50 x Magnification

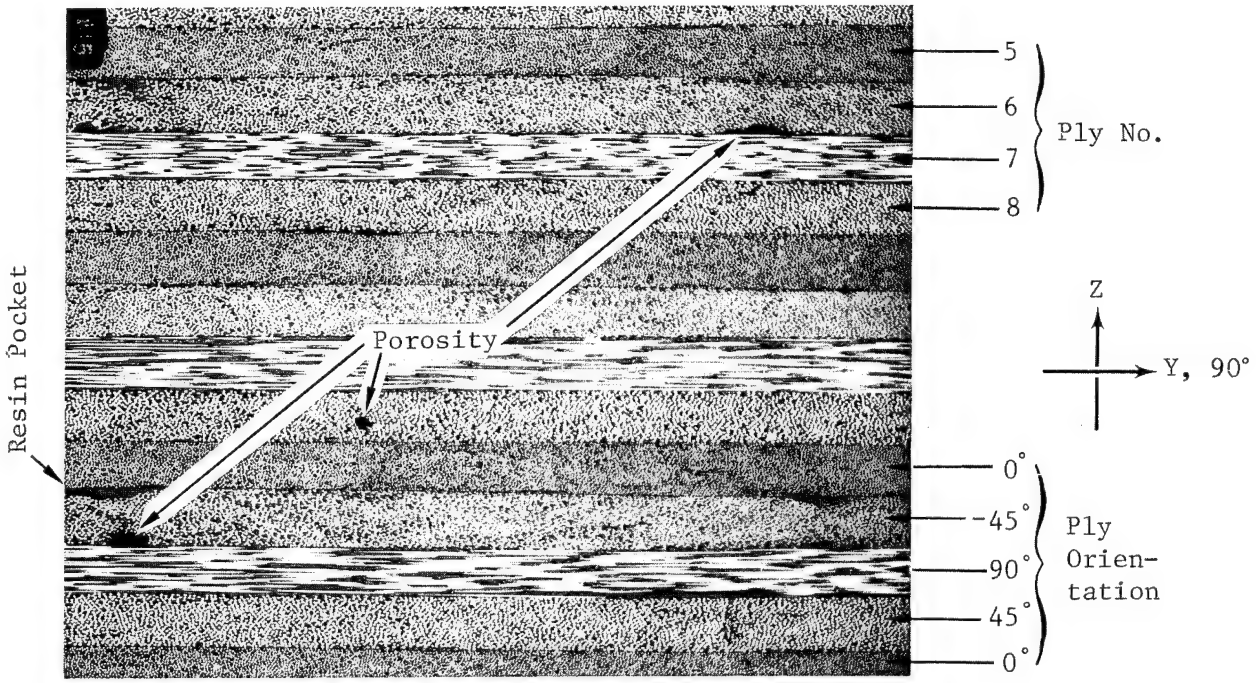

Figure 9. Photomicrograph of a Portion of the Y-Z Cross-Section in Figure 8 at 50x Magnification. In Addition to the Microvoids (Porosity), a Few Resin-Rich Regions are also Present in the Fabricated $[0/45/90/-45]_{8S}$ T300/5208 Panel.

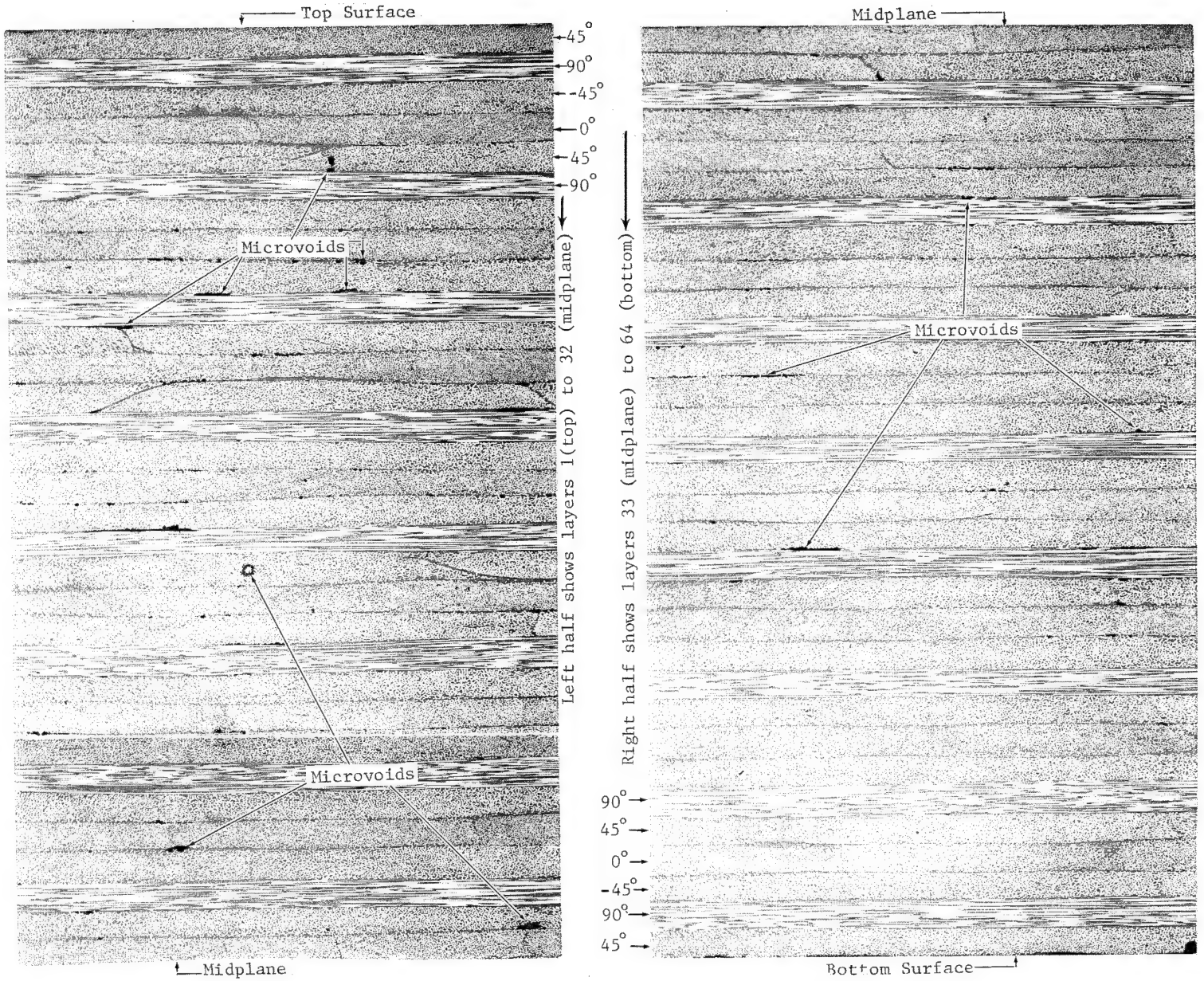

Figure 10. Photomicrograph of a YZ Cross-Section of the $45/90/-45/0_{8S}$ T300/520ε Test Laminate at 50x (The section corresponds to a bad C-scan location).

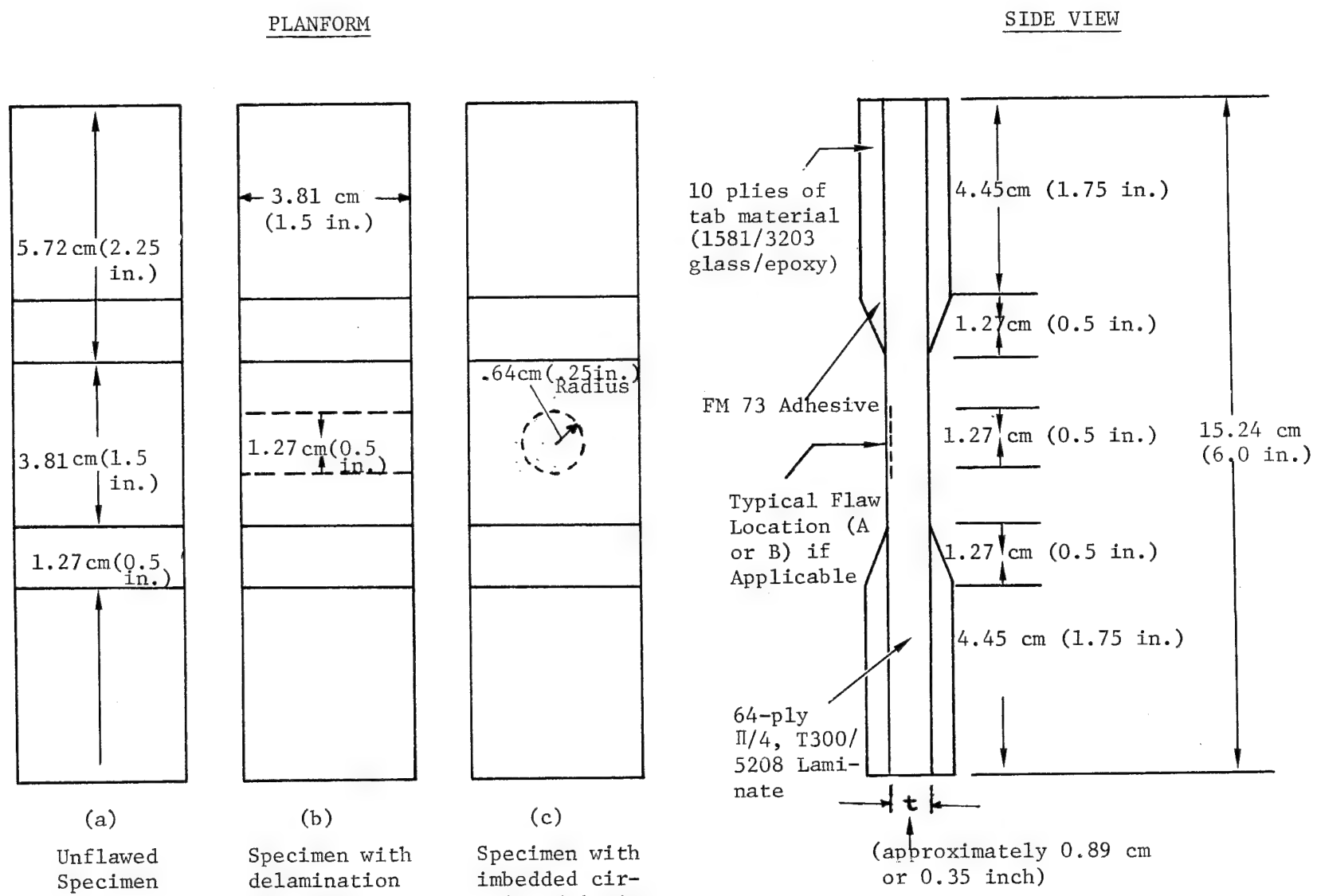

Figure 11. Test Specimen Geometry, Flaw Size and Location, and Tab Details

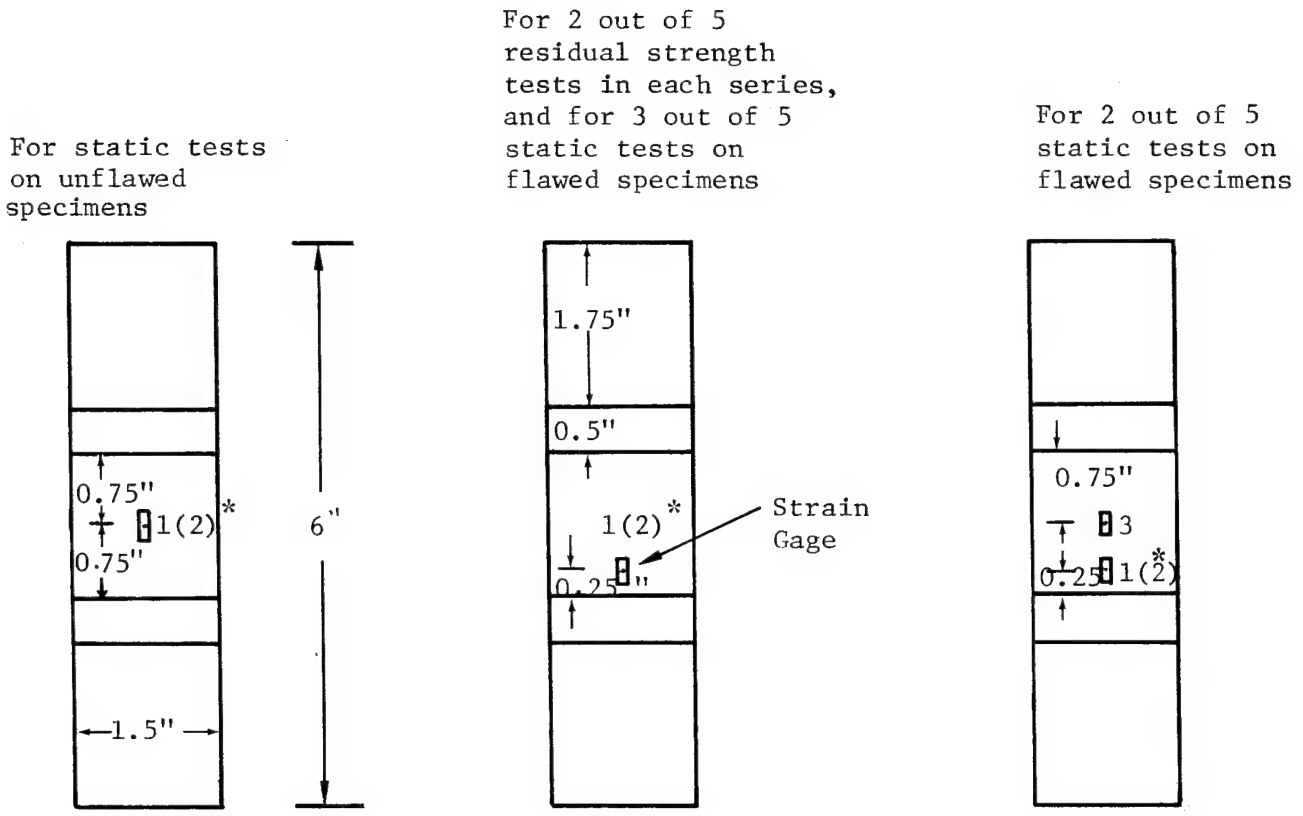

*Numbers in parentheses denote ID of back surface gage; or, 1 and 2 are back-to-back gages at the same location.

Figure 12. Strain Gage Arrangements For Static and Residual Strength Tests

Figure 13. Compression Fatigue Test Arrangement

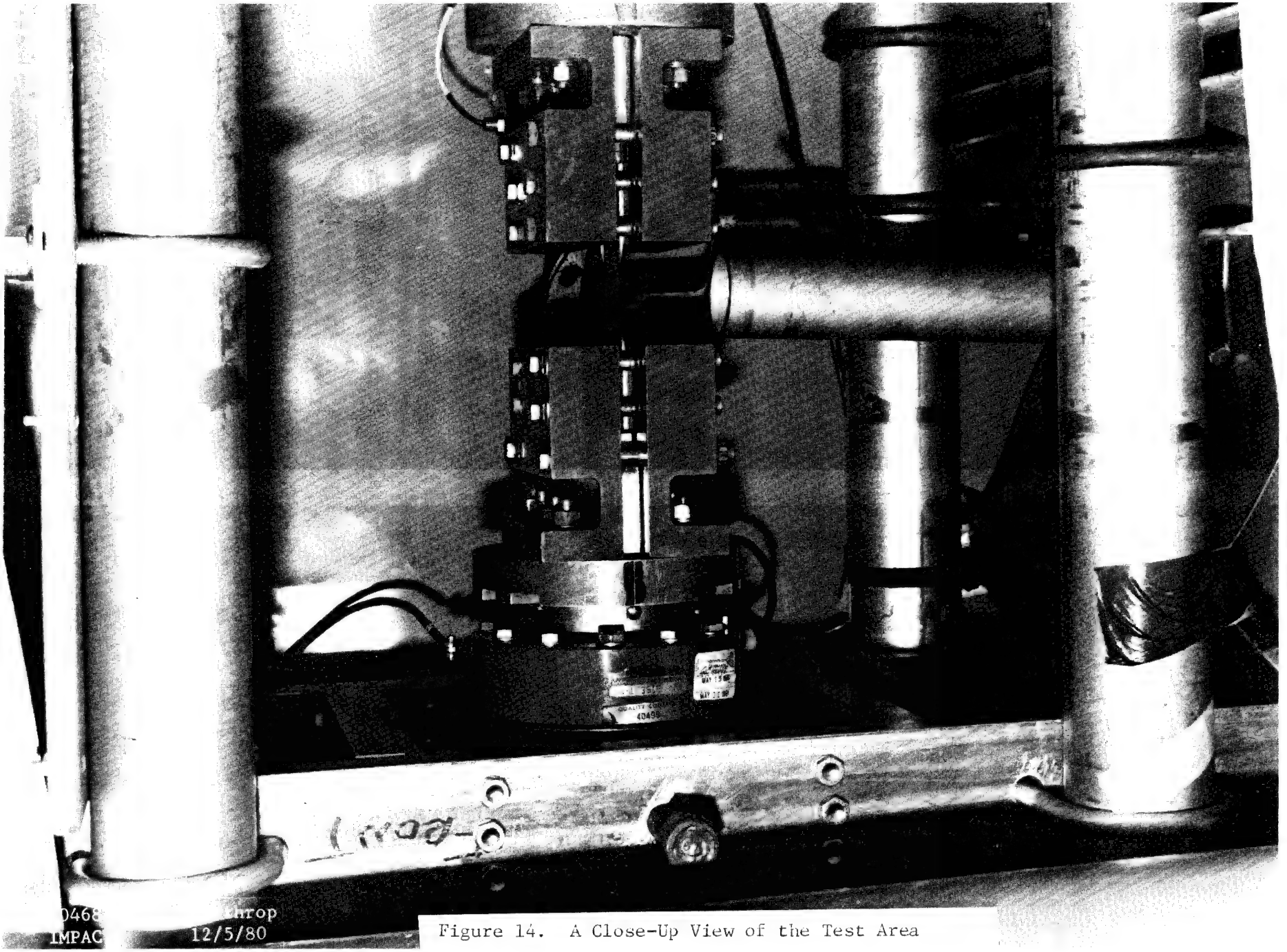

Figure 14. A Close-Up View of the Test Area

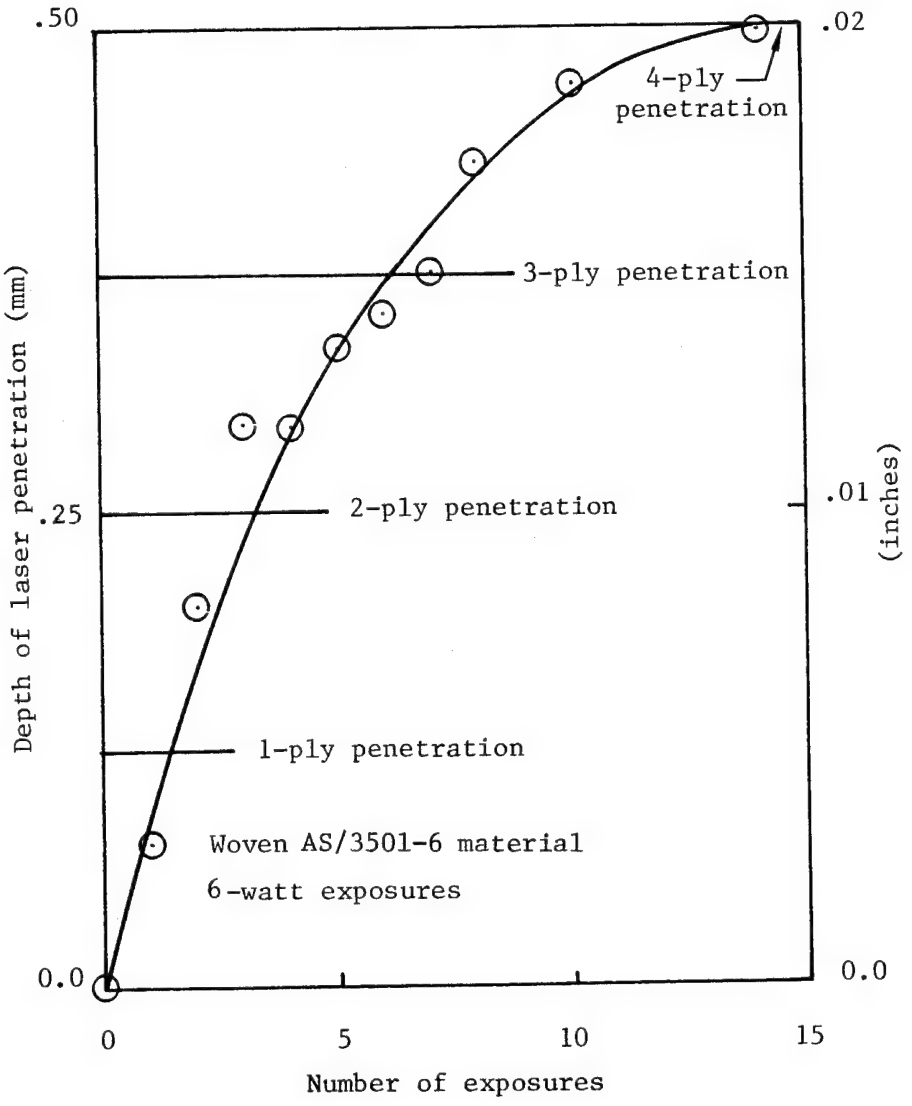

Figure 15. Effect of Laser Exposure on Depth of Penetration

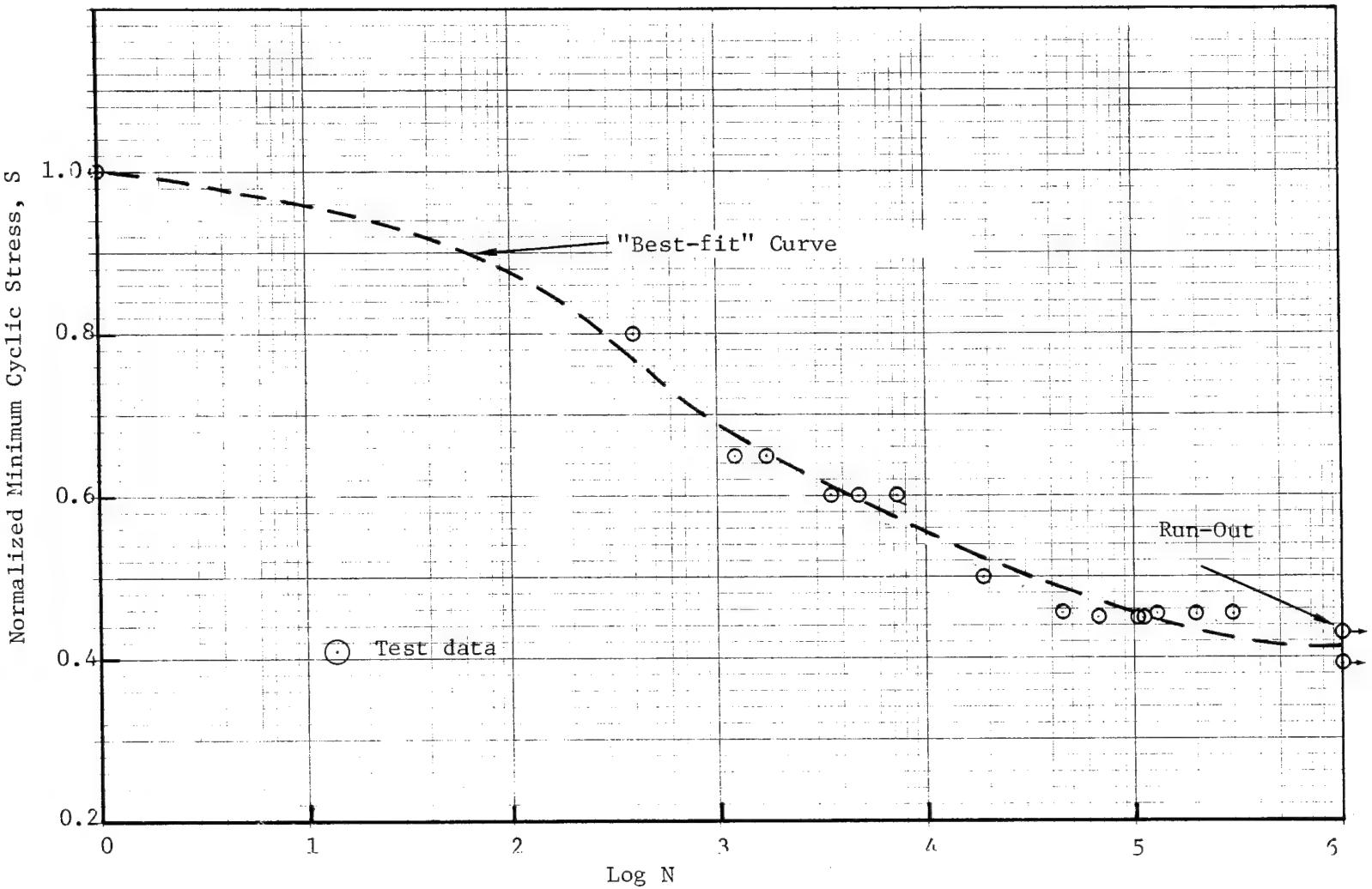

Figure 16. S-N data for Laminate A Specimens With 1.27 CM Long Delamination (1-D) Between Plies 1 and 2

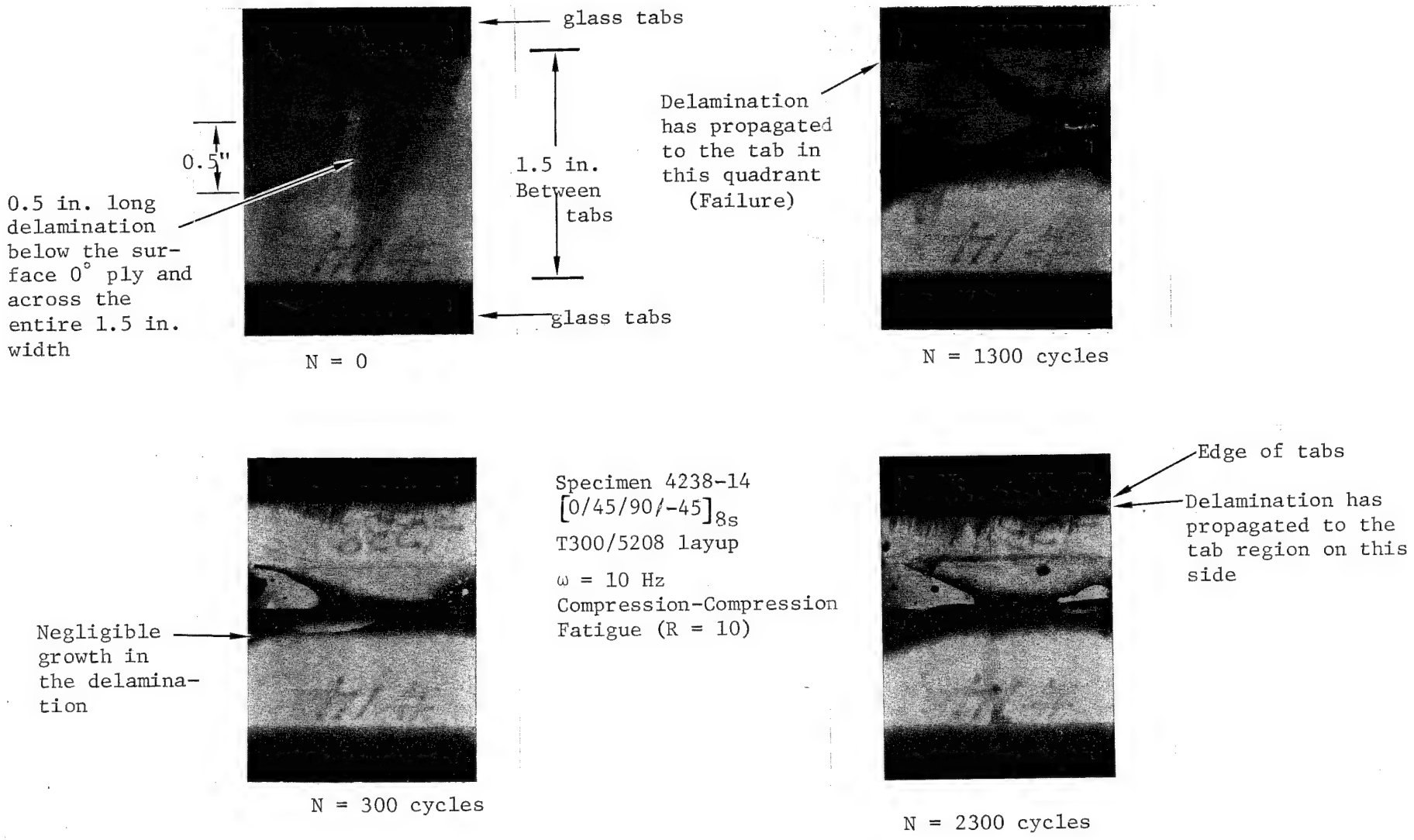

Figure 17. Delamination Growth in Specimen 4238-14; Laminate A; Test Series 3; S=0.65

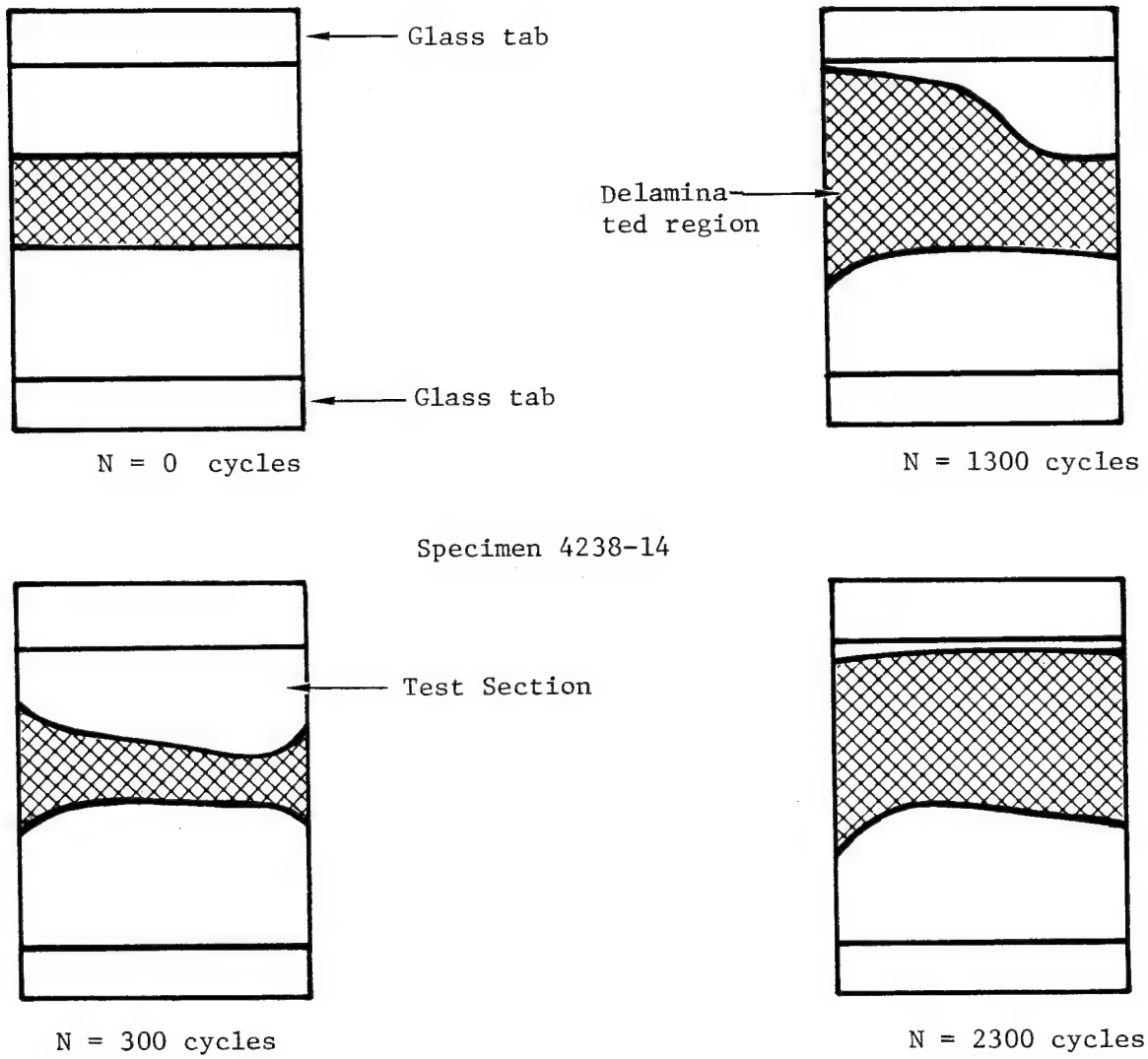

Figure 18. Outline of Delamination Boundaries Corresponding To Figure 17.

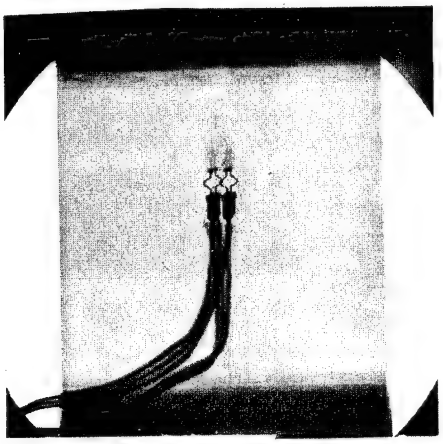

N = 0 cycles

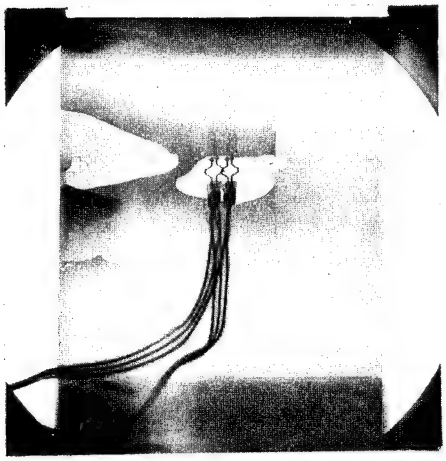

N = 1280 cycles

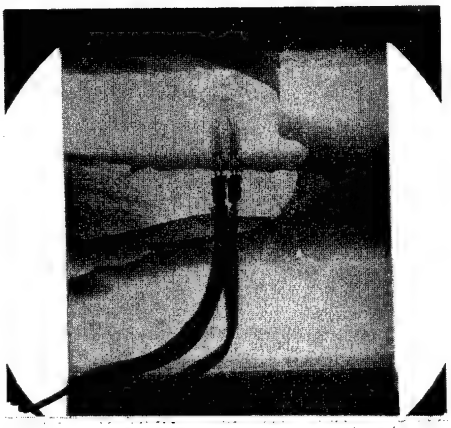

N=1780 cycles

Failed

Figure 19. Delamination Growth in Specimen 4284-24; Laminate A; Test Series 3; S=0.65

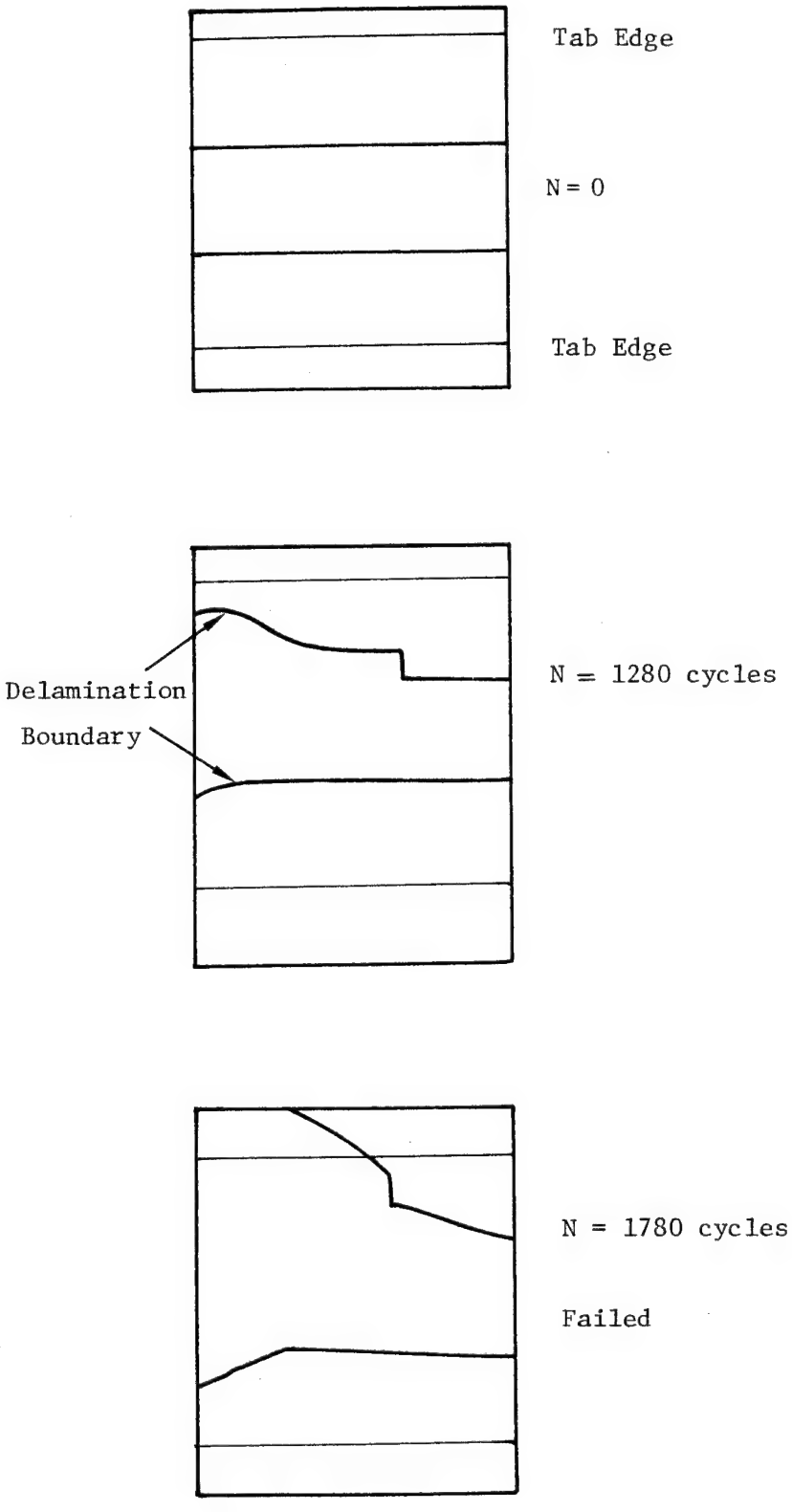

Figure 20 . Outline of the Delamination Boundaries Corresponding to Figure 19..

N = 0 cycle

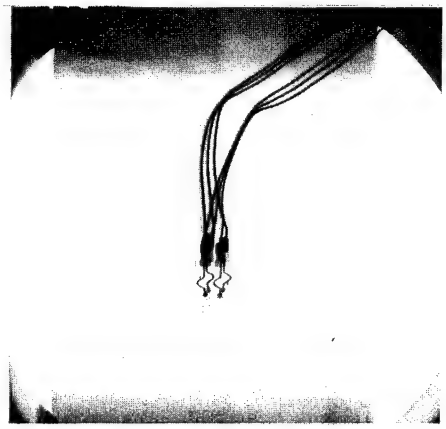

N = 1500 cycles

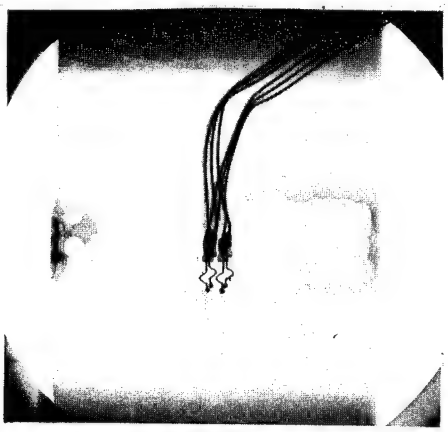

N = 500 cycles

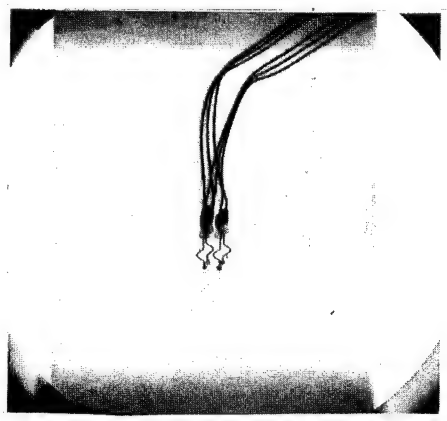

N = 2000 cycles

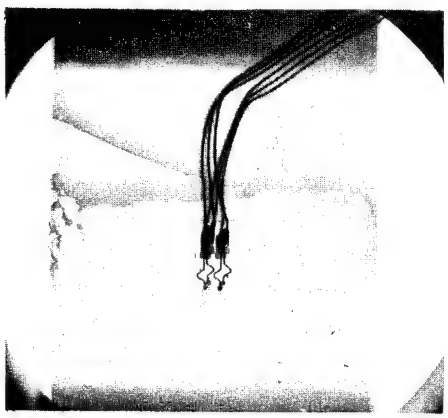

N = 1000 cycles

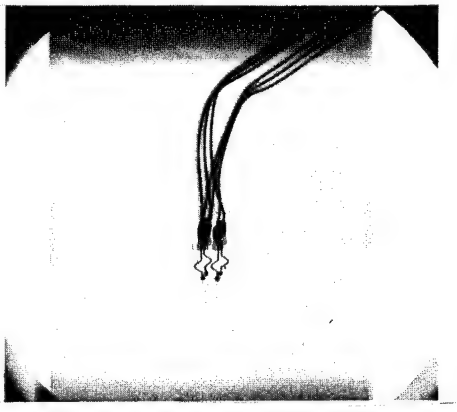

N = 2500 cycles

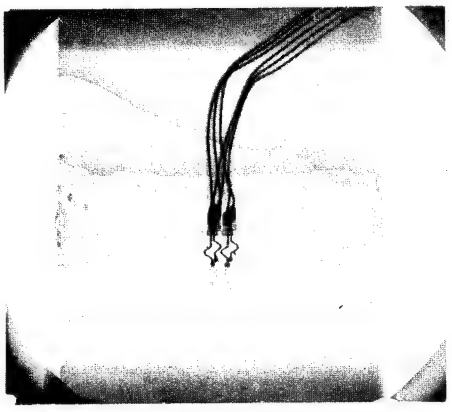

Figure 21. Delamination Growth in Specimen 4284-25; Laminate A; Test Series 3; S=0.60

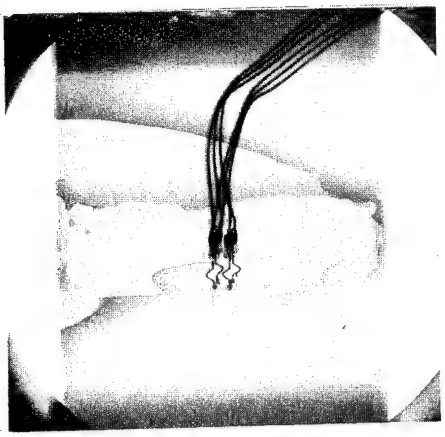

N = 3000 cycles

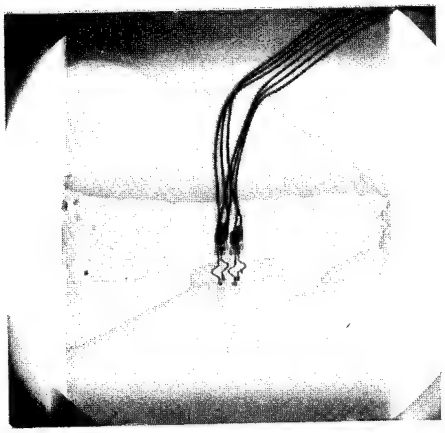

N = 3500 cycles

Failed

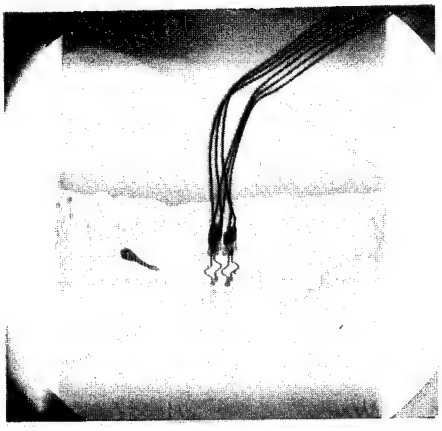

N = 4000 cycles

Failed

Figure 21. (Concluded)

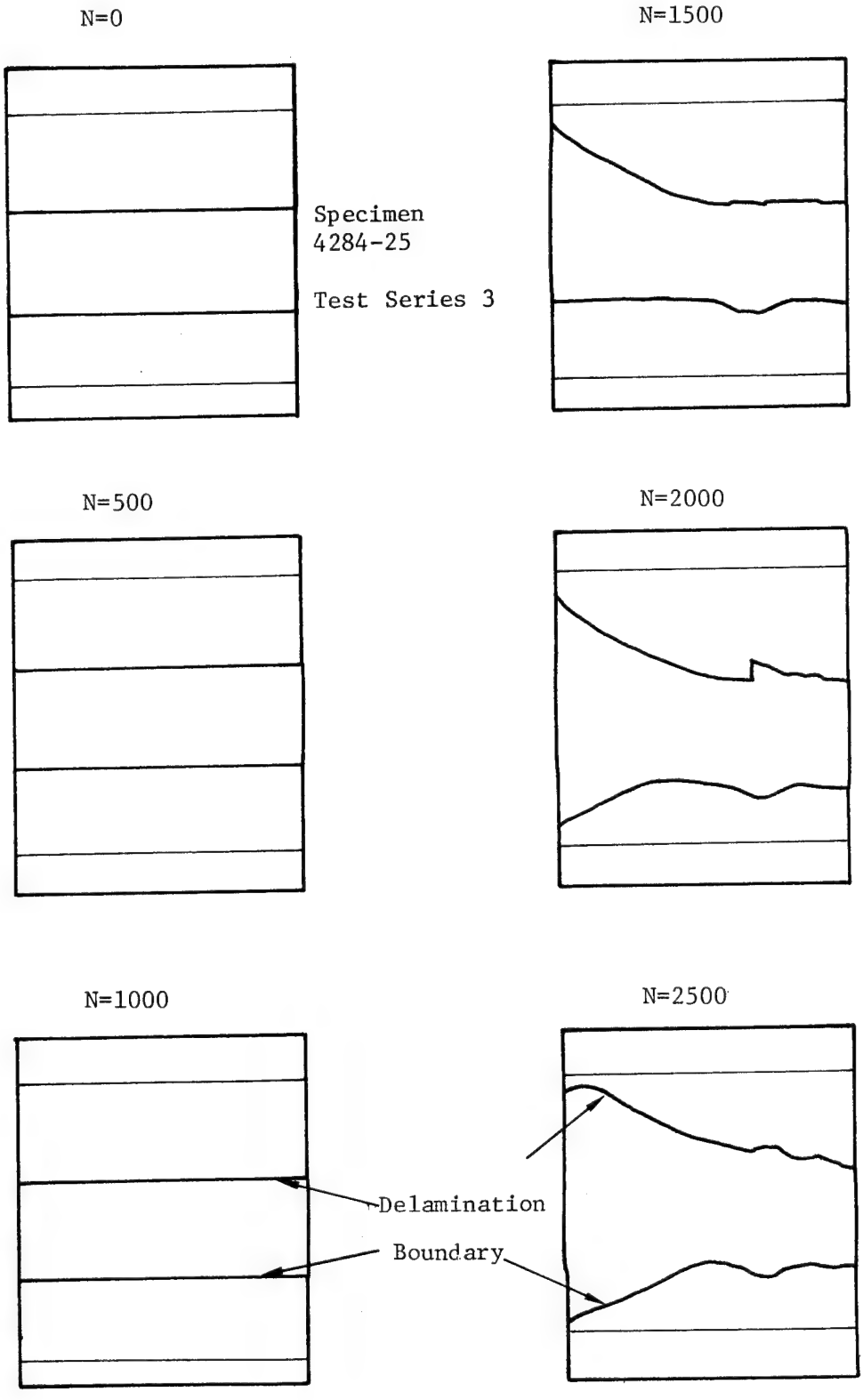

Figure 22. Outline of the Delamination Boundaries Corresponding to Figure 21.

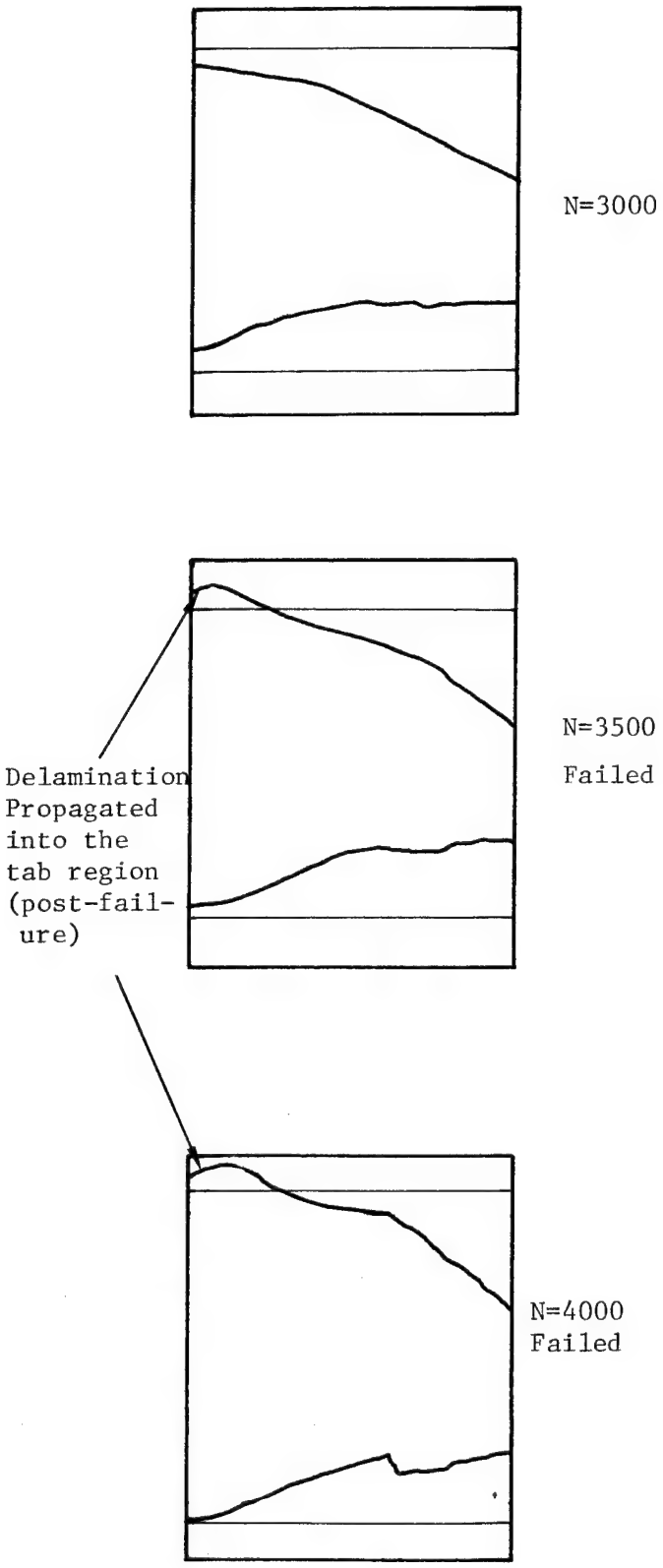

Figure 22. (Concluded)

N=0 cycle

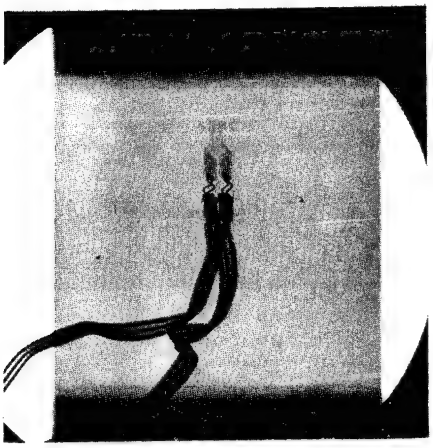

N=2500 cycles

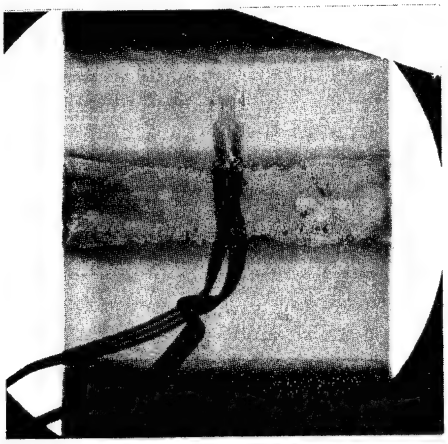

N=500 cycles

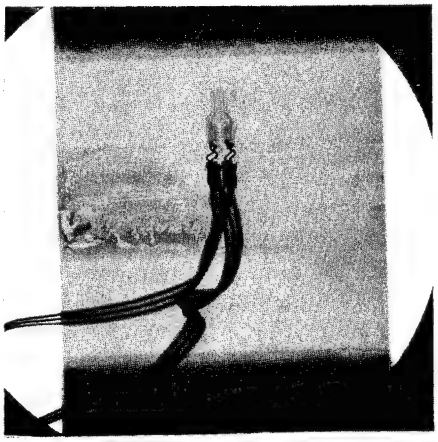

N=3000 cycles

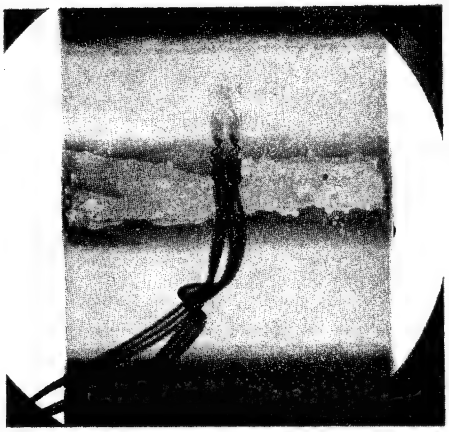

N=1500 cycles

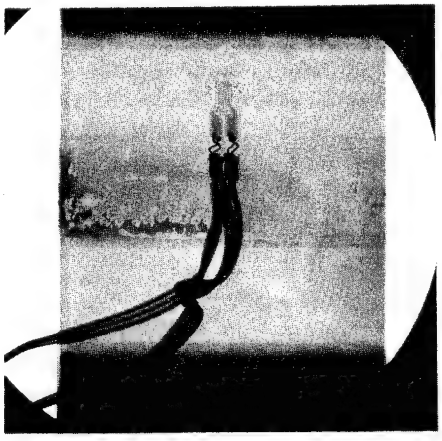

N=3500 cycles

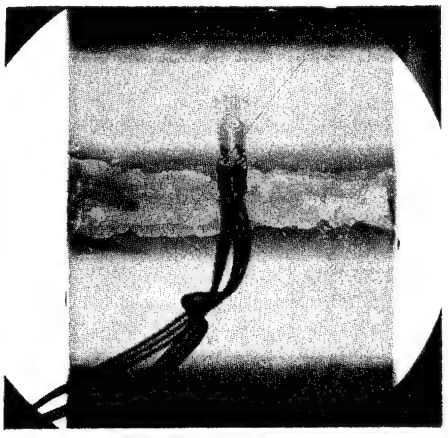

Figure 23. Delamination Growth in Specimen 4284-27; Laminate A; Test Series 4; S = 0.47.

N=4500 cycles

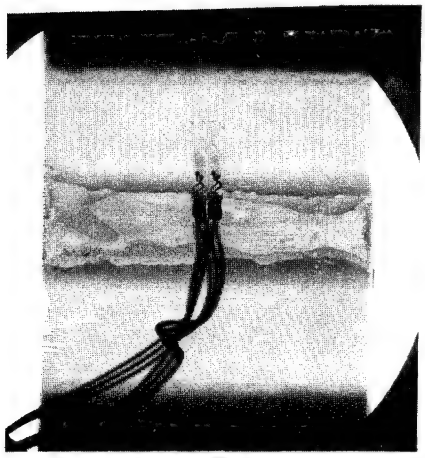

N=10,000 cycles

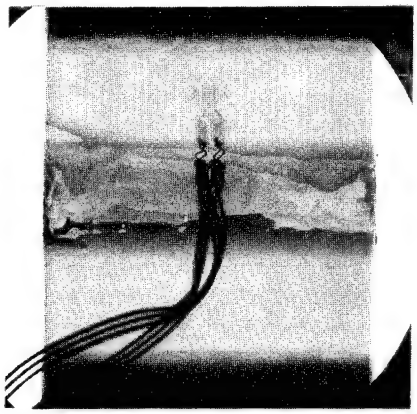

N=6000 cycles

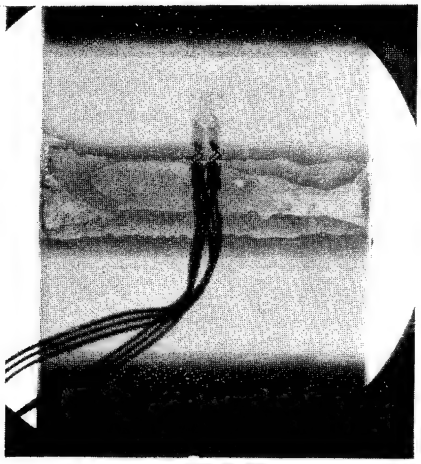

N=12,500 cycles

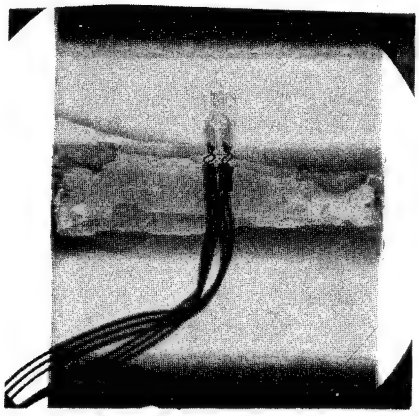

N=7500 cycles

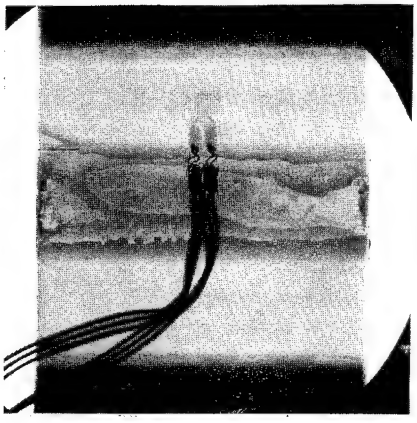

N=15,000 cycles

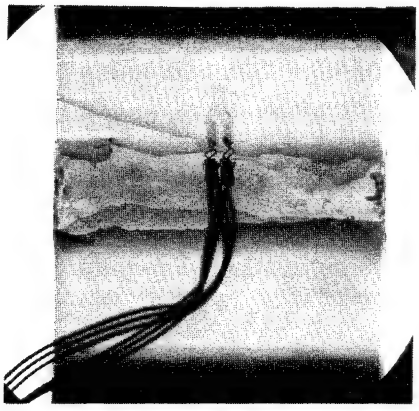

Figure 23. (Continued)

N=17,500 cycles

N=25,000 cycles

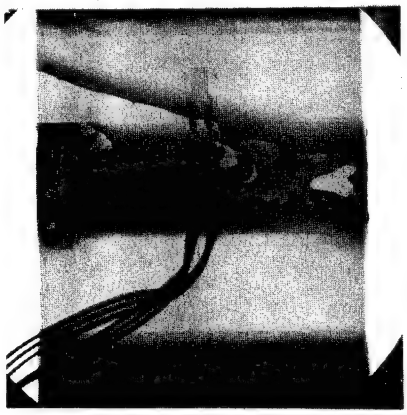

N=22,500 cycles

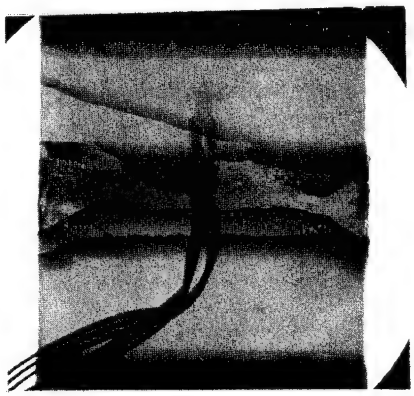

N=45,000 cycles

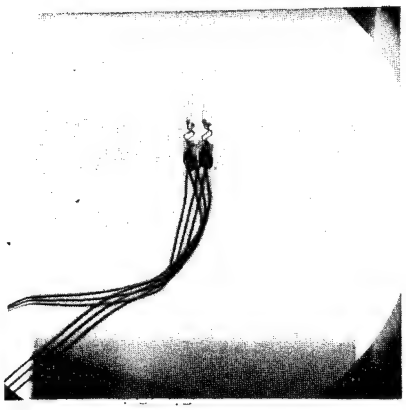

Failed

Figure 23. (Concluded)

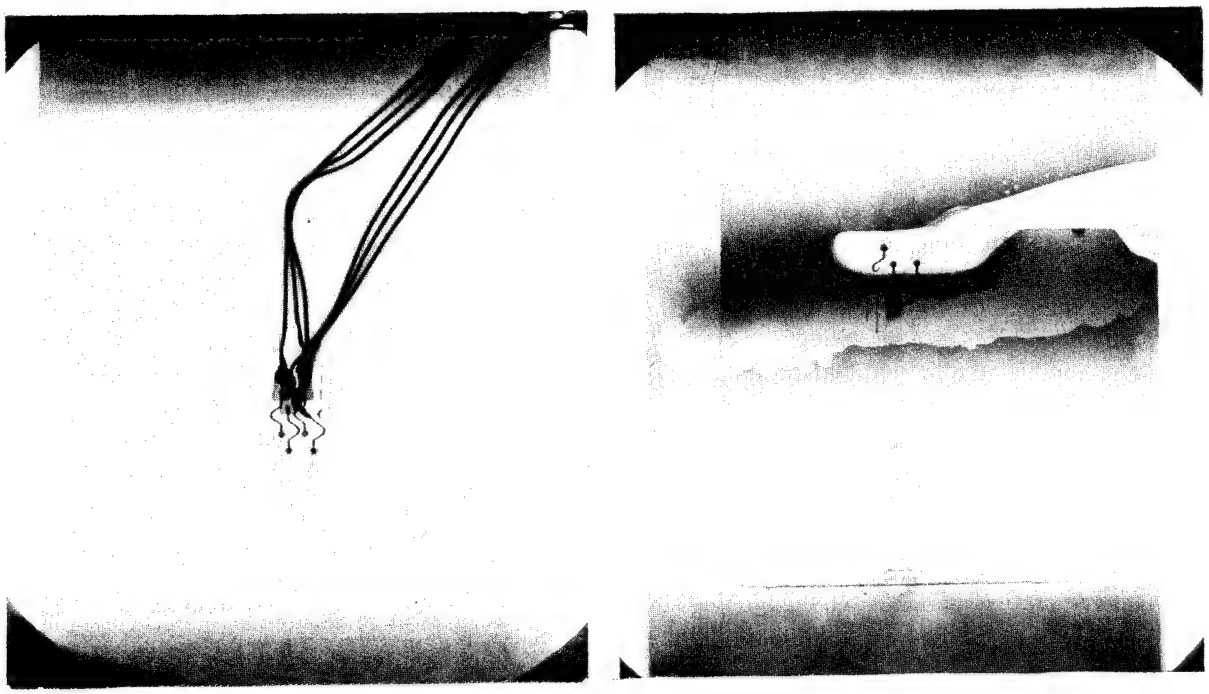

N=0

N=50,000

N=61,700 (Failure)

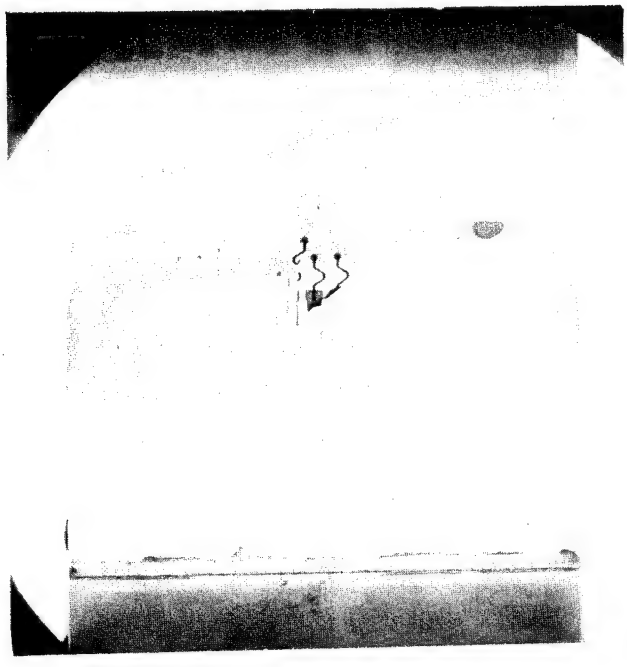

Figure 24. Delamination Growth in Specimen 4284-23; Laminate A; Test Series 5; S=0.45

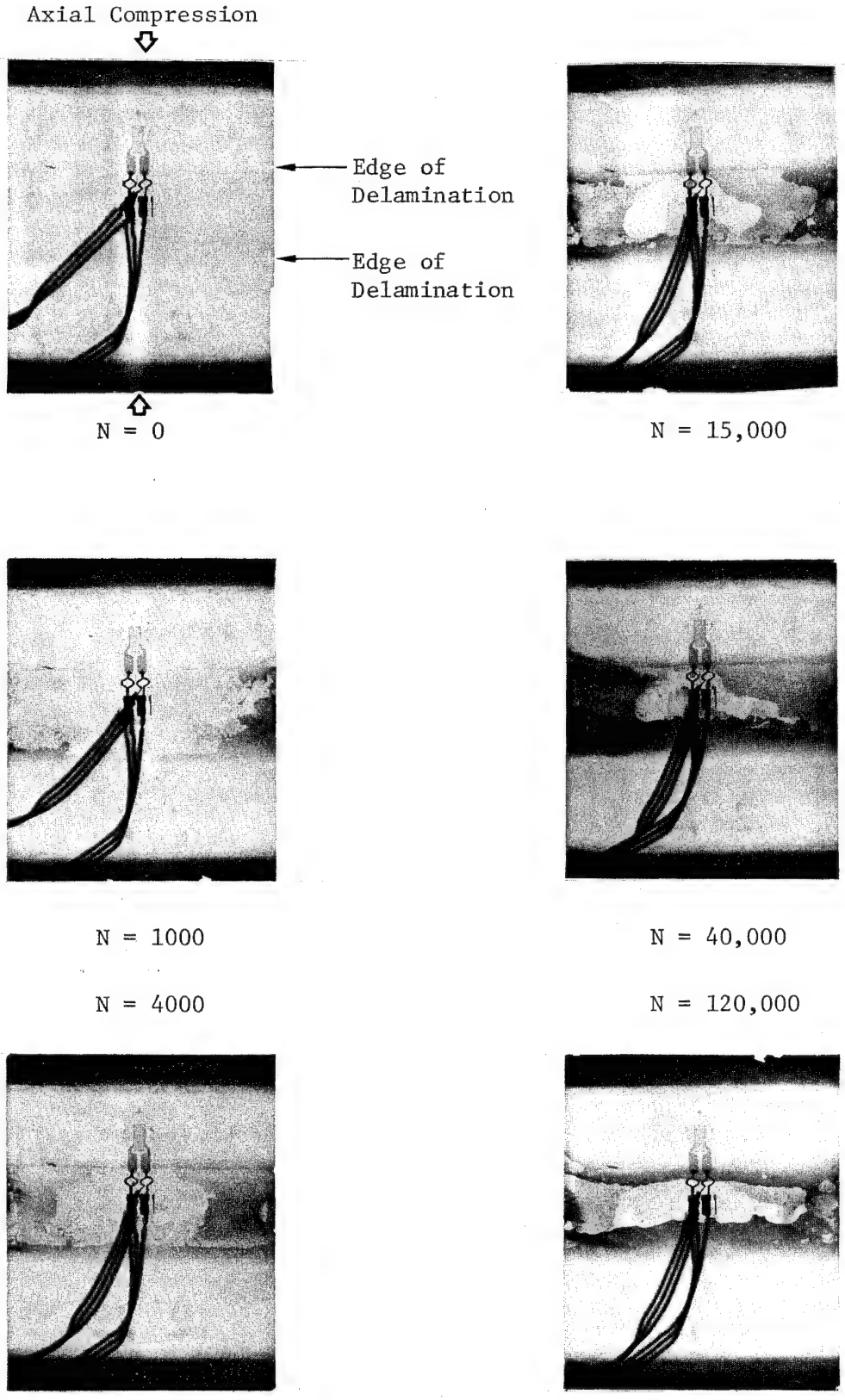

Figure 25. Delamination Growth in Specimen 4284-22; Laminate A; Test Series 5; S=0.39

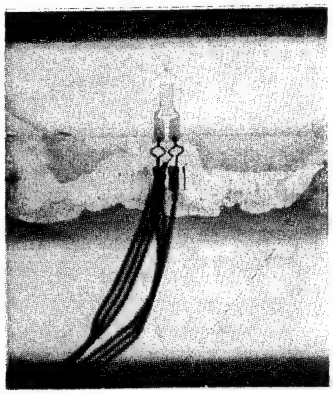

N = 200,000

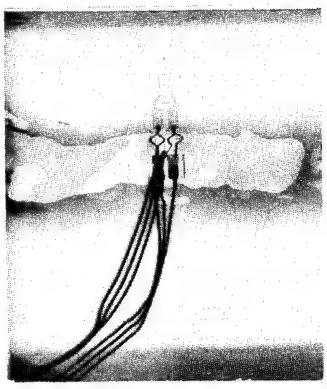

N = 500,000

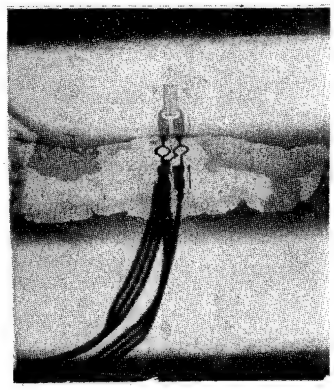

N = 300,000

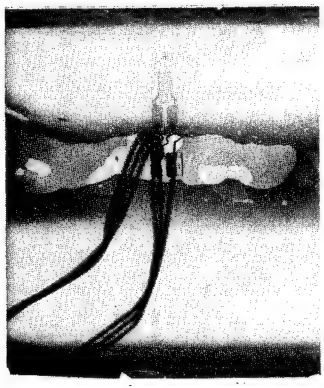

N = 600,000

N = 400,000

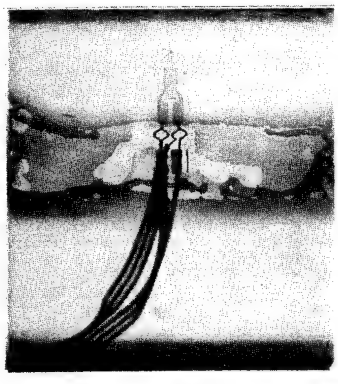

N = 10^6 (No Failure)

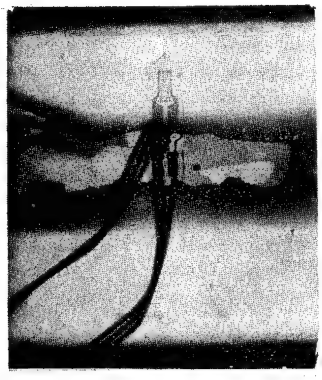

Figure 25. (Concluded)

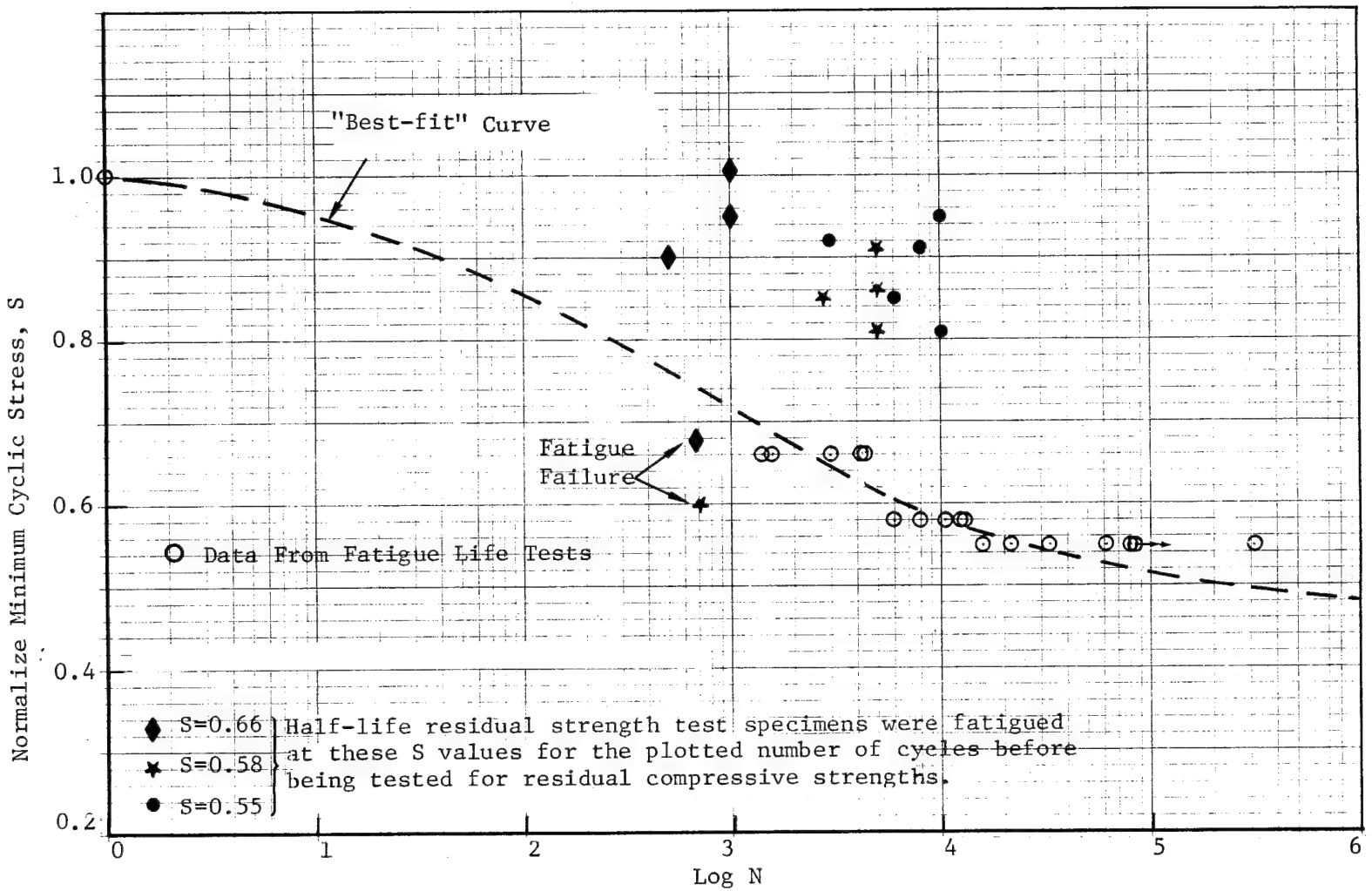

Figure 26. S-N Data and Half-Life Residual Strength Data for Laminate A Specimens With 1.27 cm Diameter Delamination (2-D) Between Plies 1 and 2.

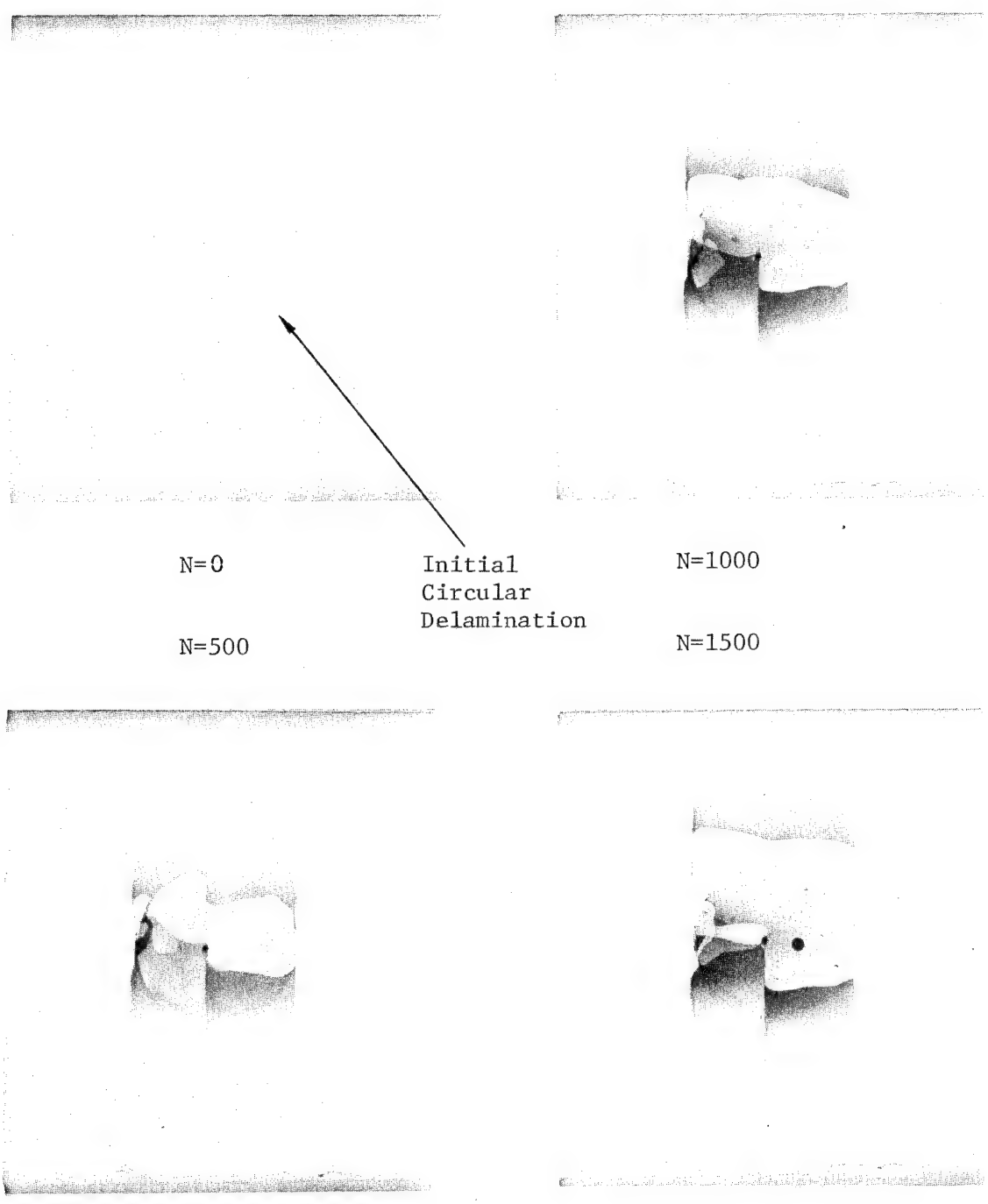

Figure 27. Delamination Growth in Specimen 4284-56; Laminate A; Test Series 7; S=0.66

N=2000

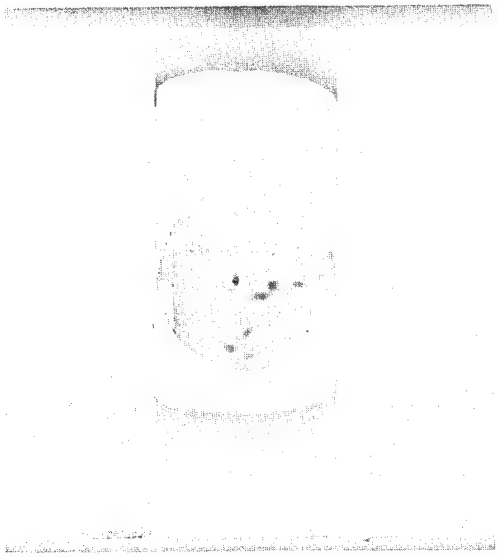

N=3000 (Failure)

N=2500

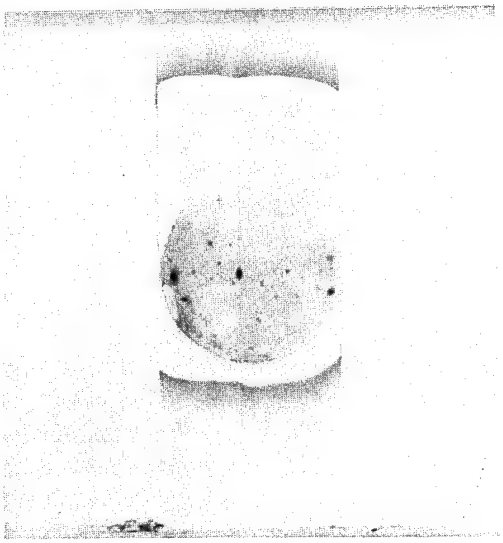

Figure 27. (Concluded)

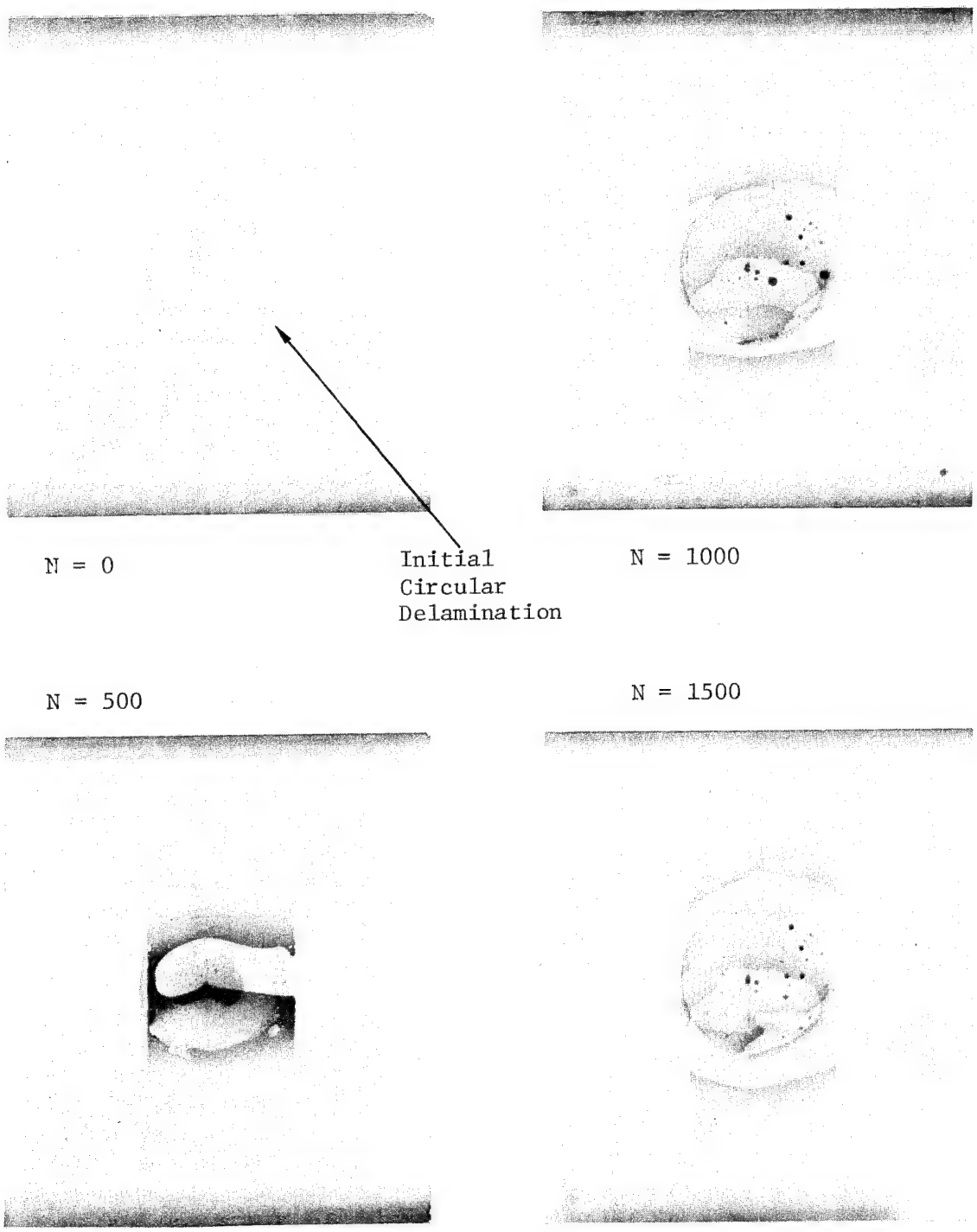

Figure 28. Delamination Growth in Specimen 4284-55; Laminate A; Test Series 7; S=0.66

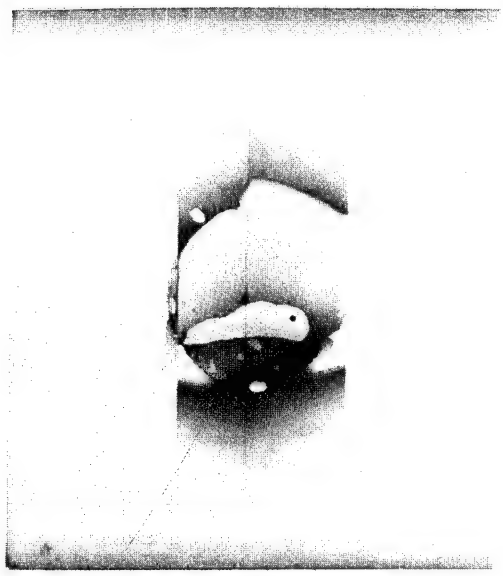

N = 2000

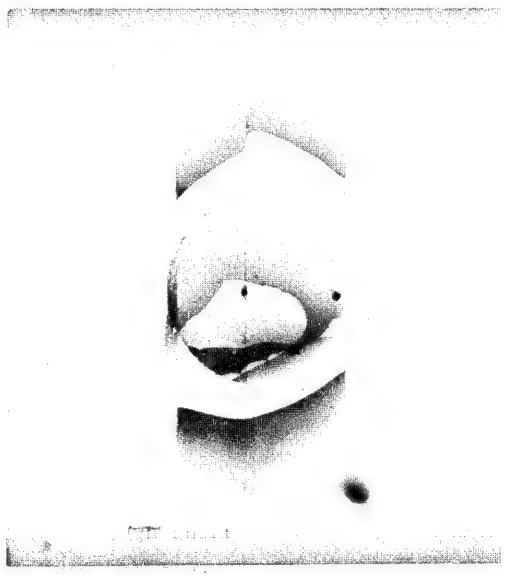

N = 3000

N = 2500

N = 3500

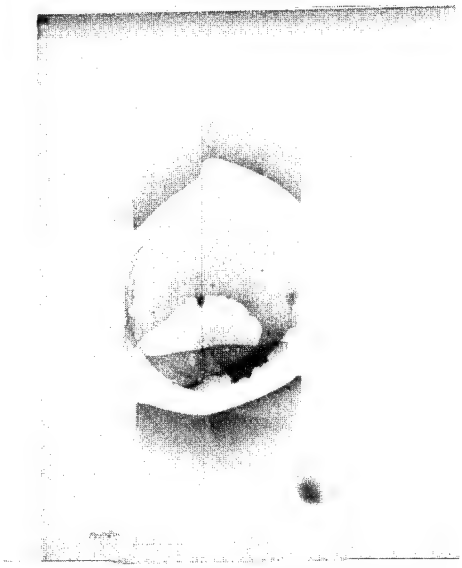

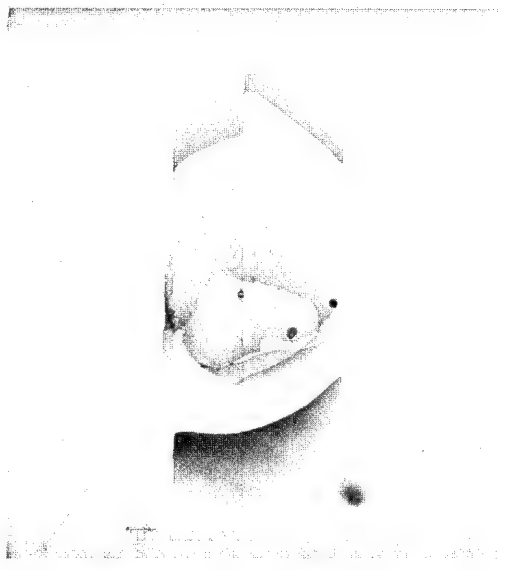

Figure 28. (Continued)

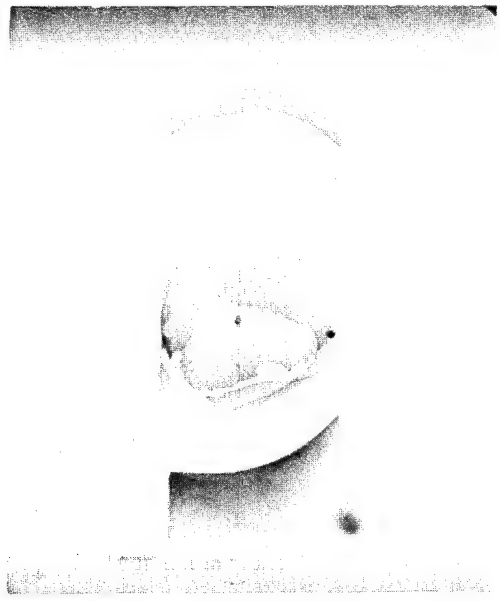

N = 4000

N = 4400

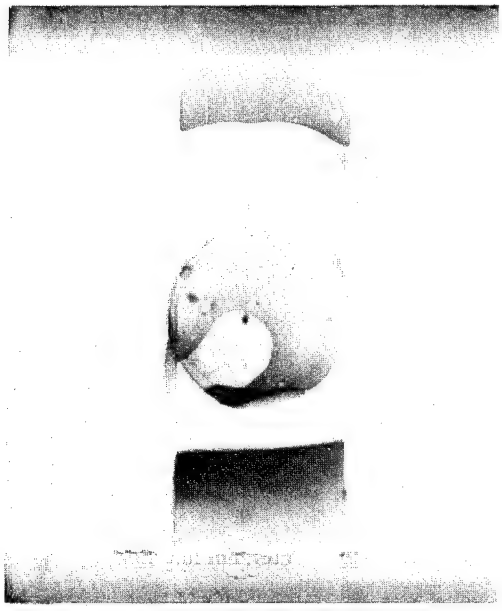

Figure 28. (Concluded)

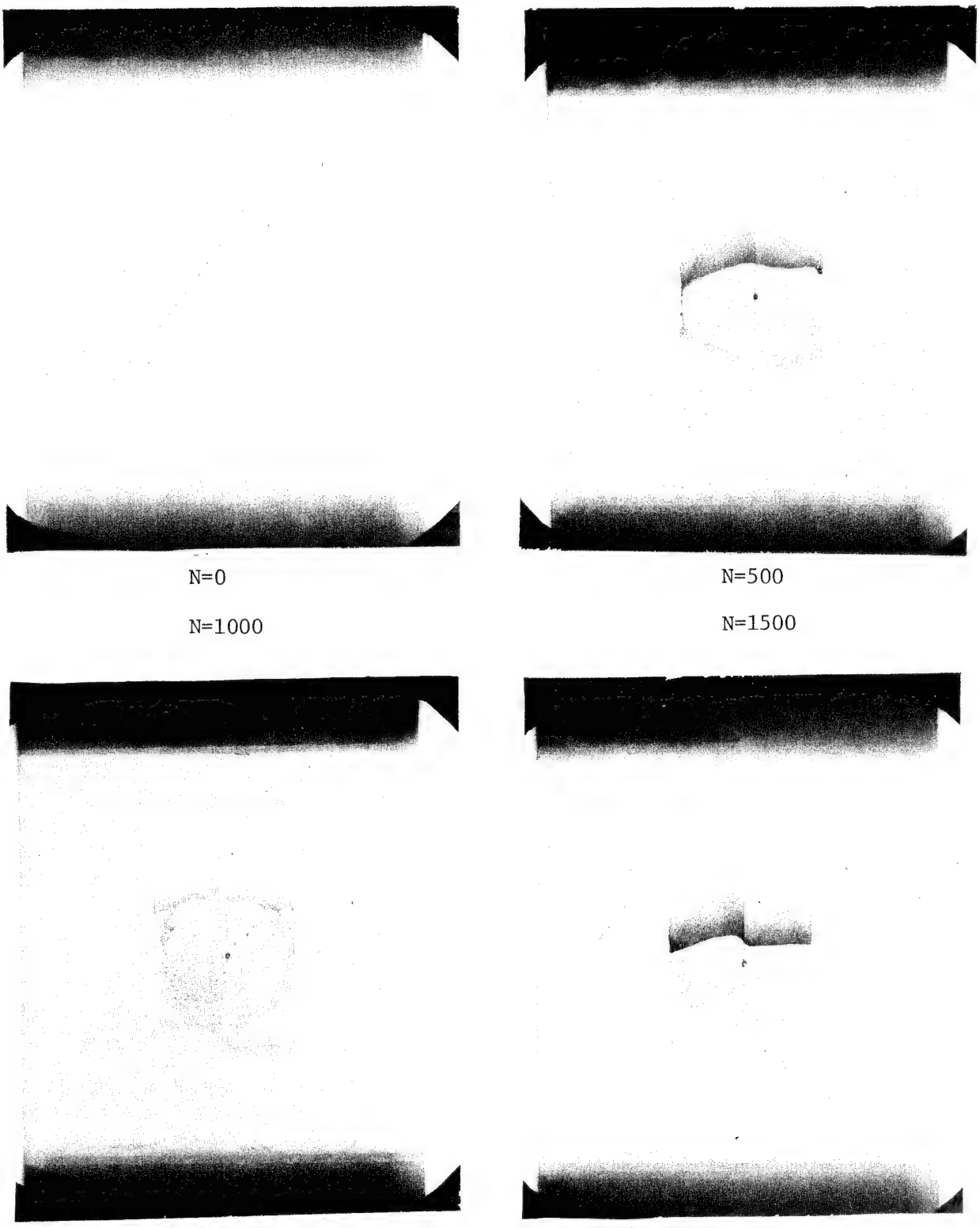

Figure 29. Delamination Growth in Specimen 4284-57; Laminate A; Test Series 9; S=0.58; Radiographs Taken With a 7.12 kN Load

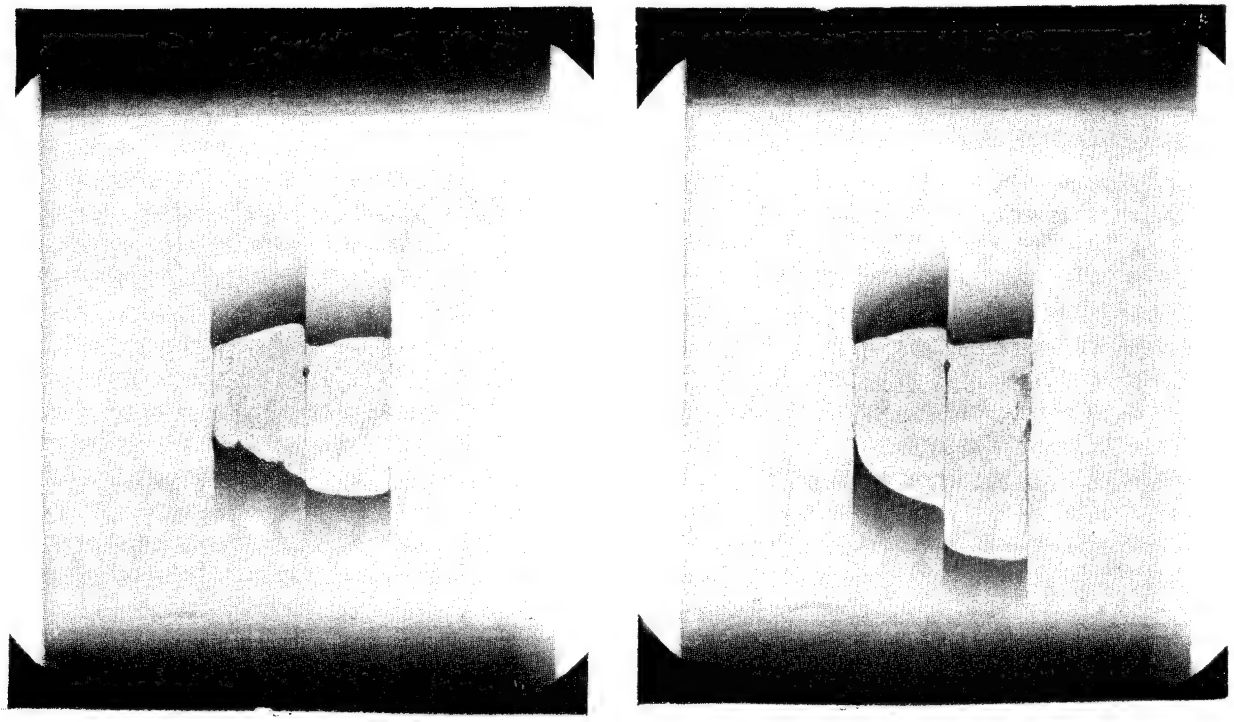

N=2000

N=3000

N=3470 (Imminent Failure)

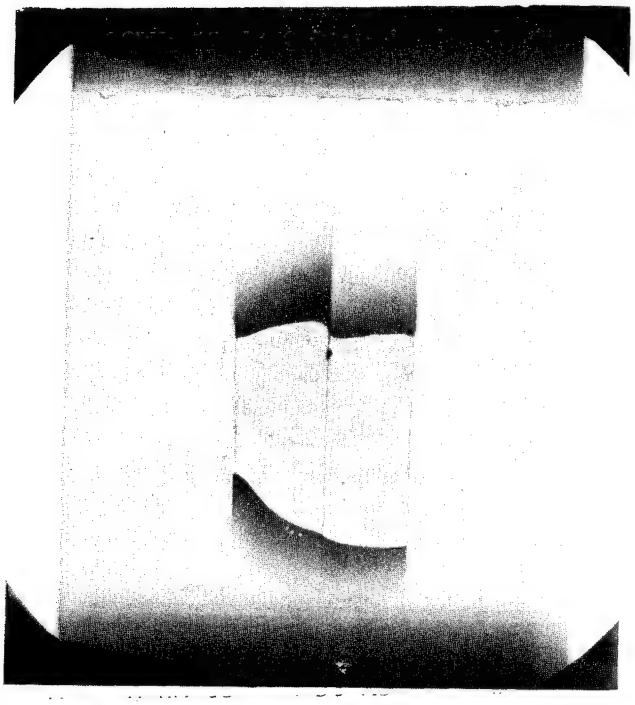

Figure 29. (Concluded)

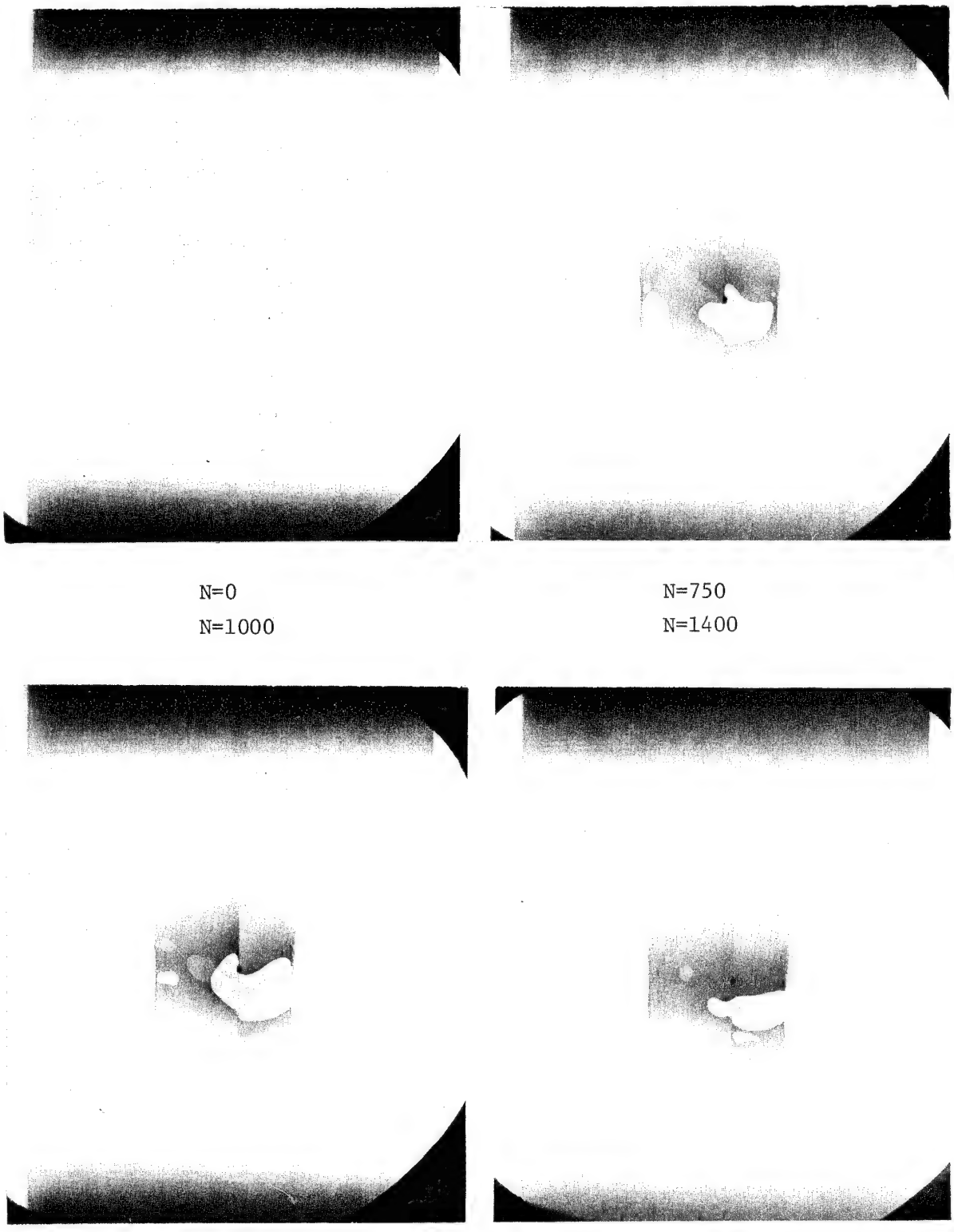

Figure 30. Delamination Growth in Specimen 4284-58; Laminate A; Test Series 9; S=0.58

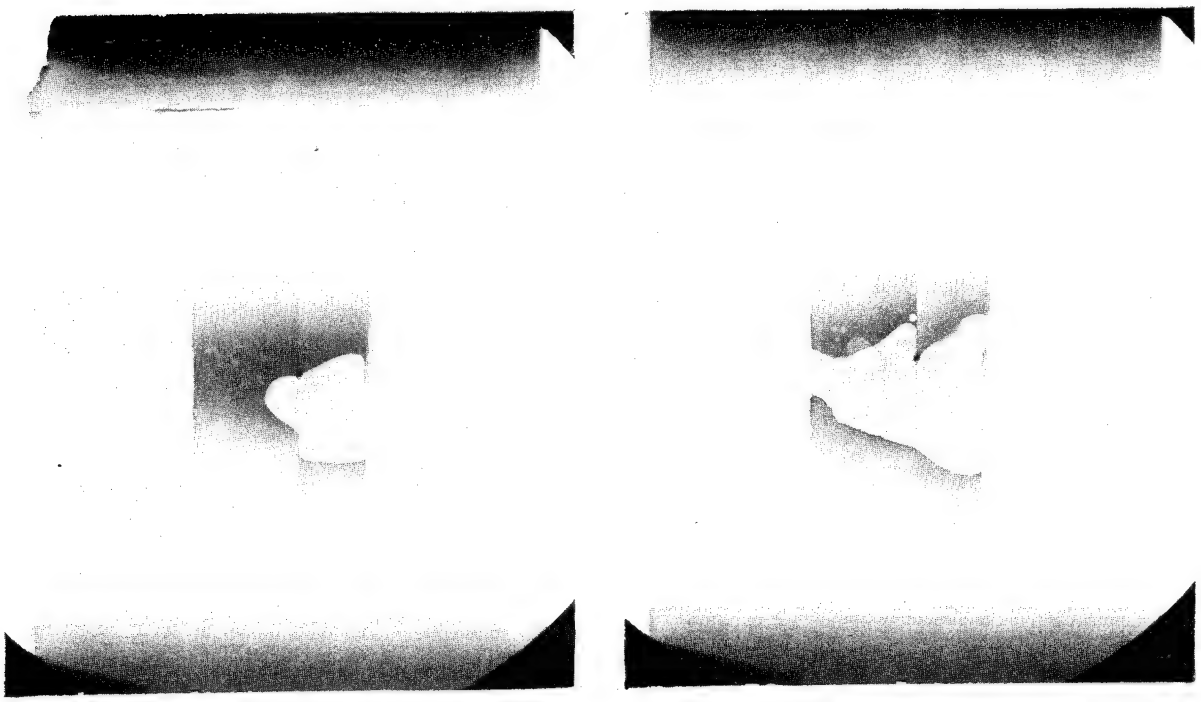

N=1900

N=3000

N=4000

N=4700

Figure 30. (Concluded)

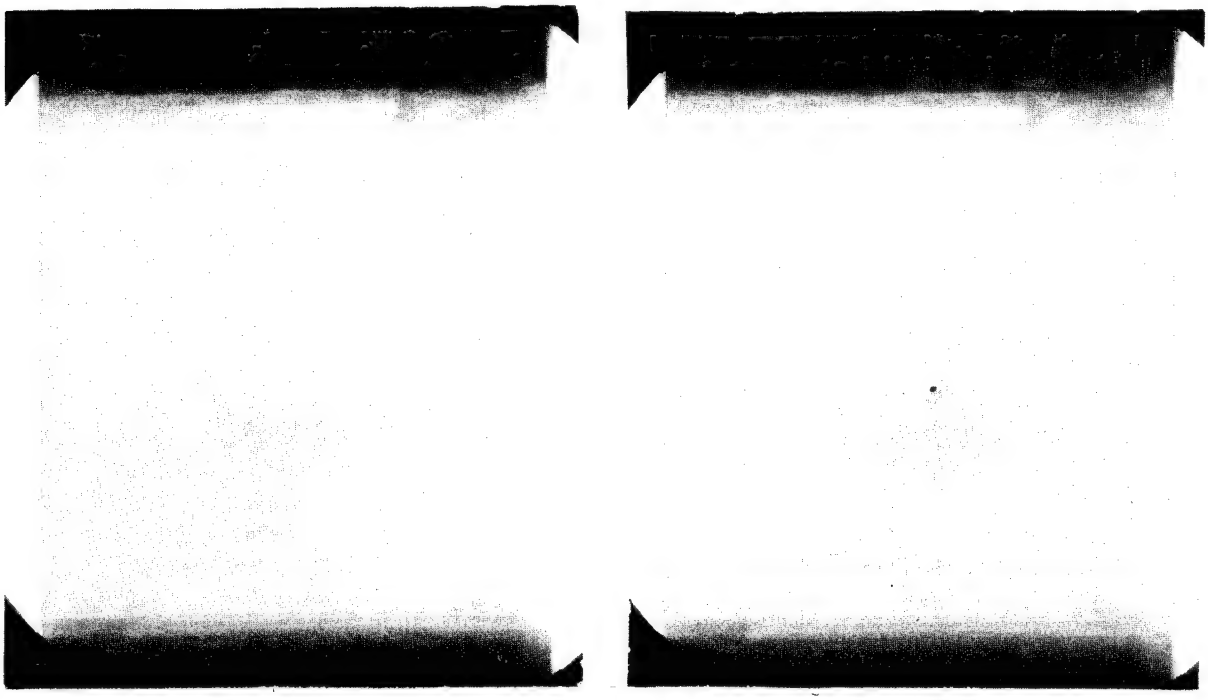

Figure 31. Delamination Growth in Specimen 4284-66; Laminate A; Test Series 11; S=0.55; Radiographs Taken With a 6.67 kN Load.

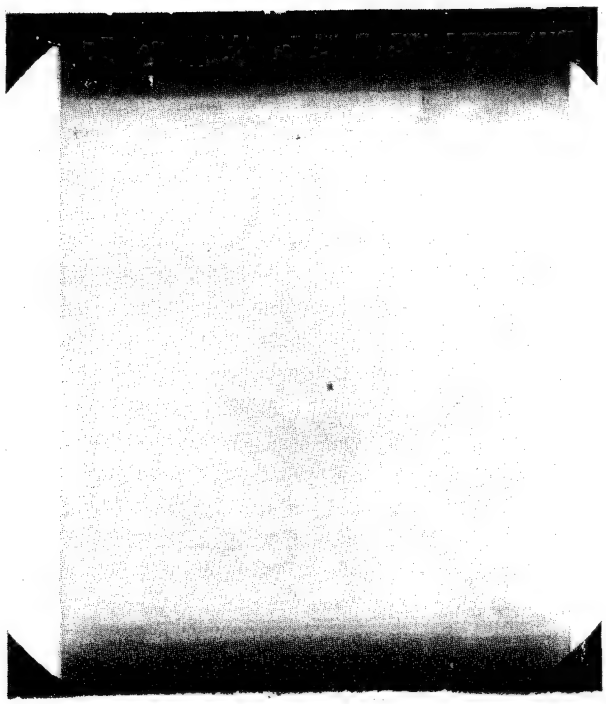

N=260,000

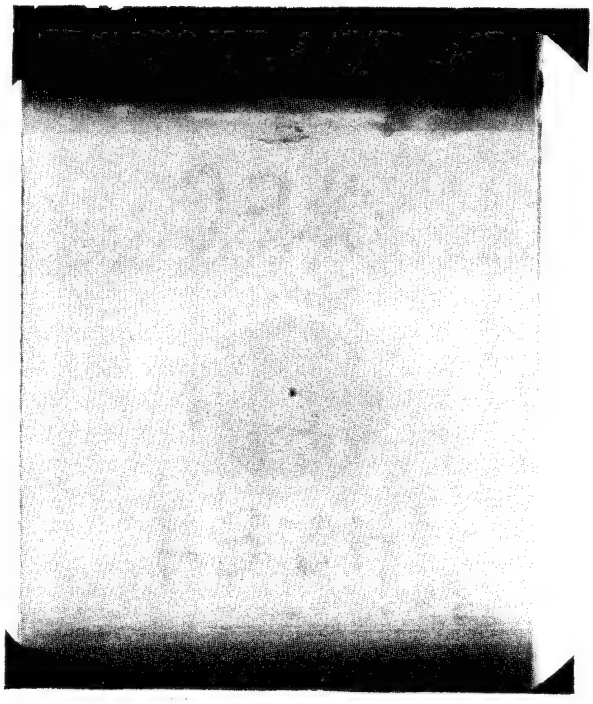

N=312,000 (Failure)
DIB injected only through
the laser-drilled hole.

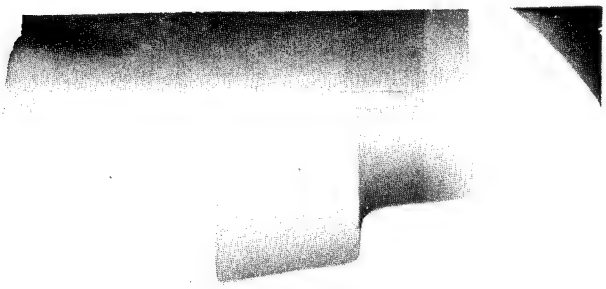

N=312,000 (Failure)
DIB injected into the
delaminated region
near the back surface.
The last two pictures
indicate that failure
was precipitated by
back-surface delamina-
tion and not at the
imbedded flaw location.

Figure 31. (Concluded)

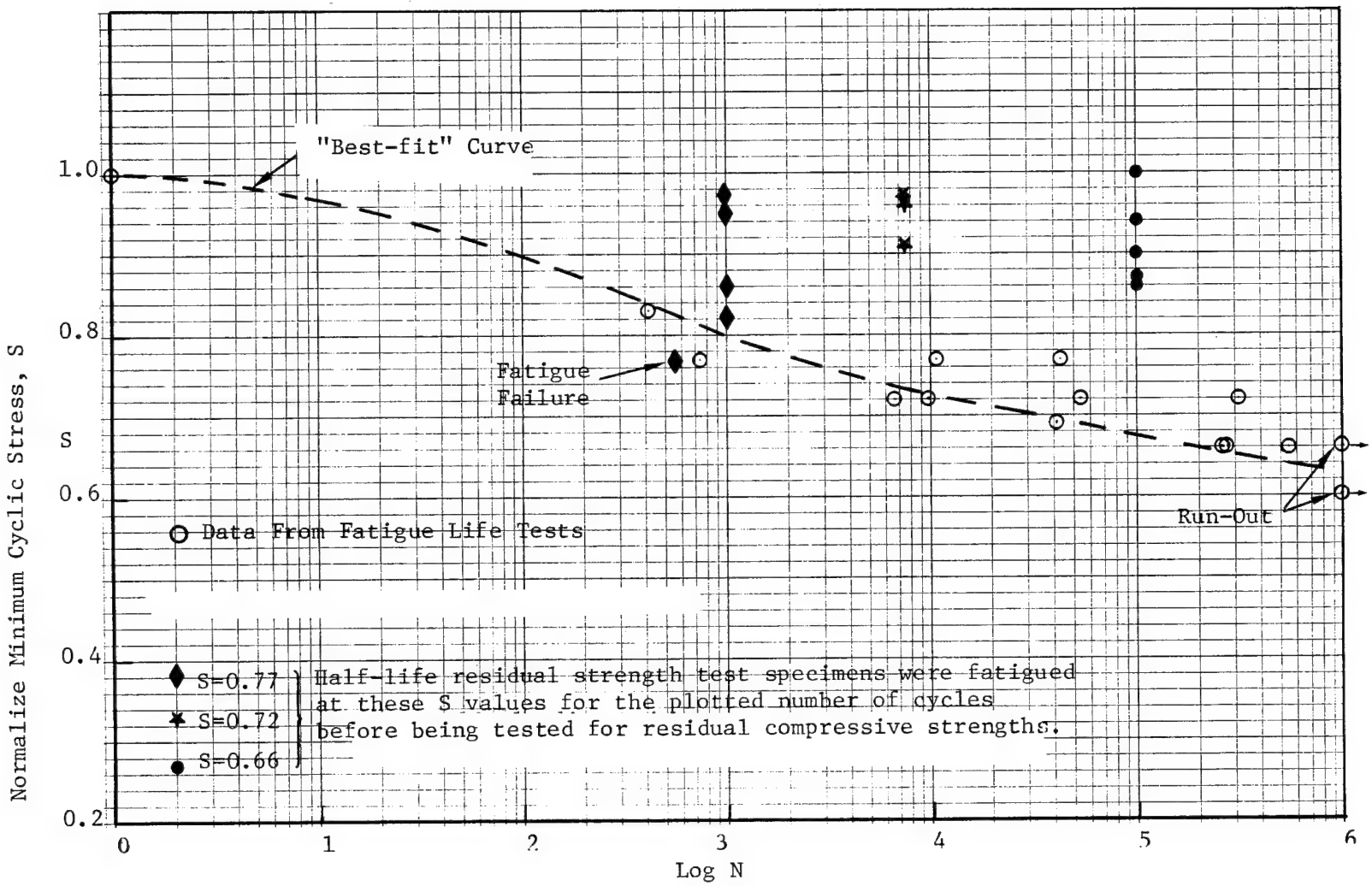

Figure 32. S-N Data for Laminate A Specimens with 1.27 cm Diameter Delamination (2-d) Between Plies 4 and 5

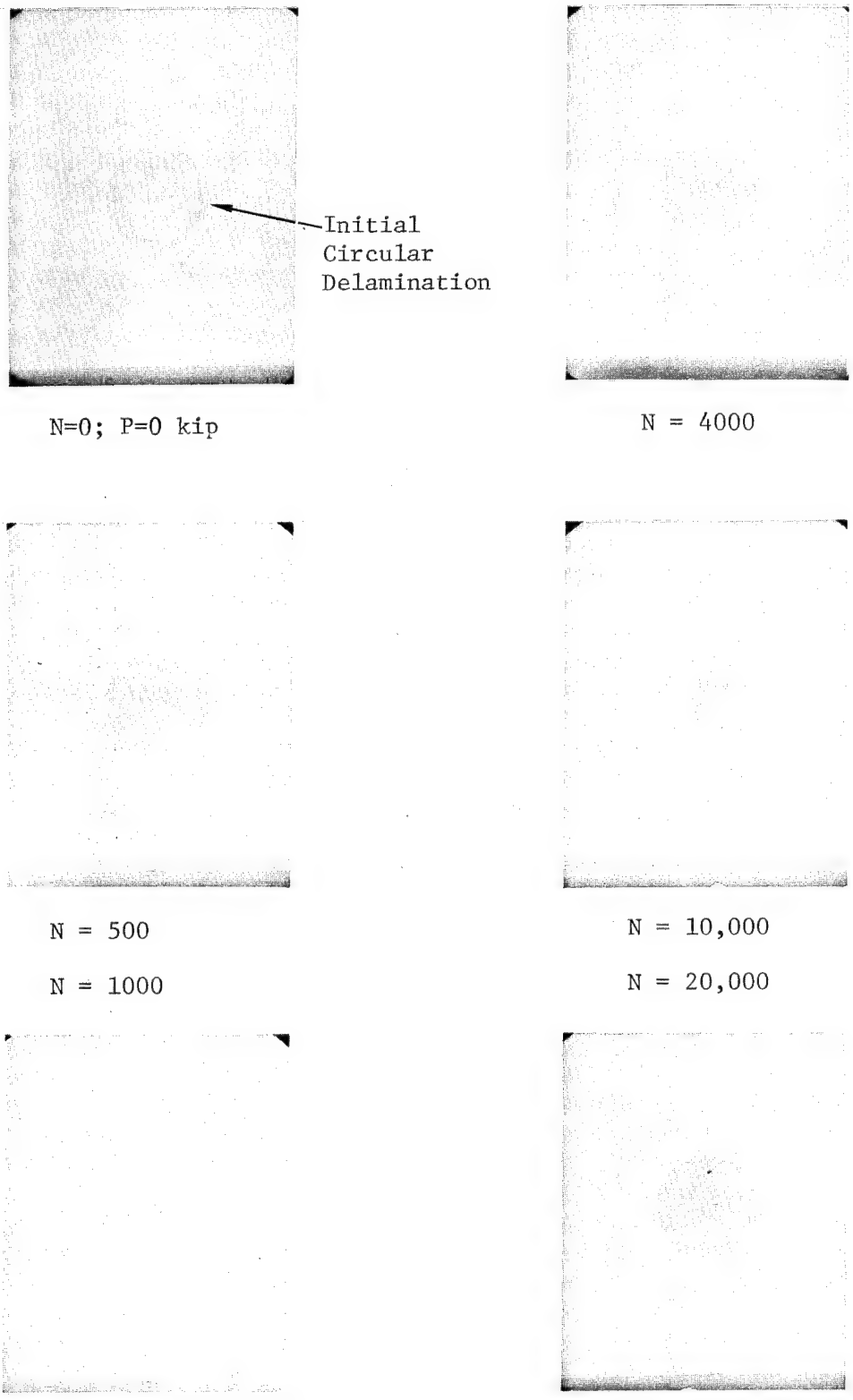

Figure 33. Delamination Growth in Specimen 4284-96; Laminate A; Test Series 14; S=0.77

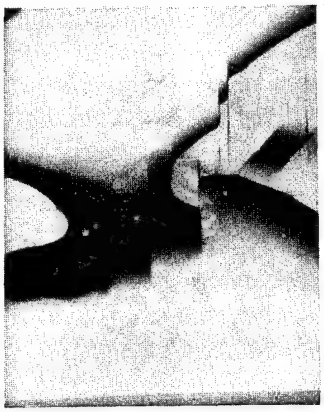

N = 43,880 (Failure)

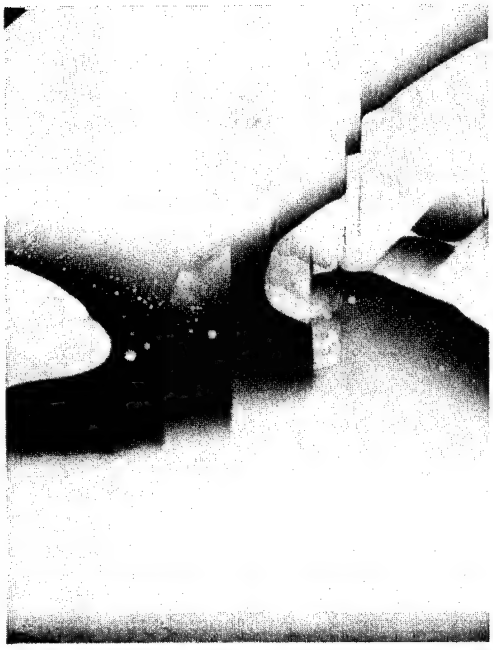

Magnified View of the Failed Test Section (N = 43,880) obtained by placing the Polaroid film farther from the specimen

Figure 33. (Concluded)

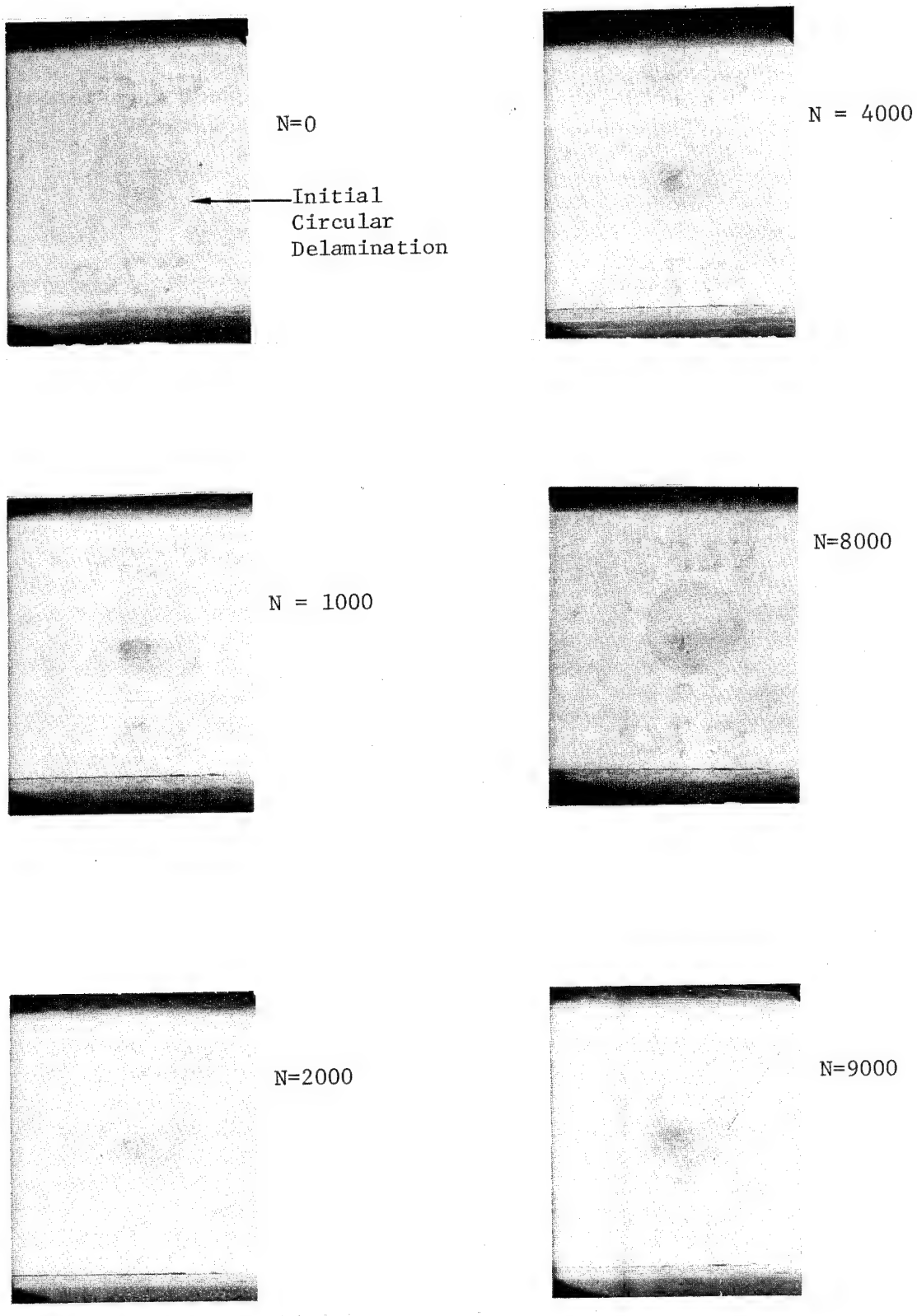

Figure 34. Delamination Growth in Specimen 4284-70; Laminate A; Test Series 14; S=0.83

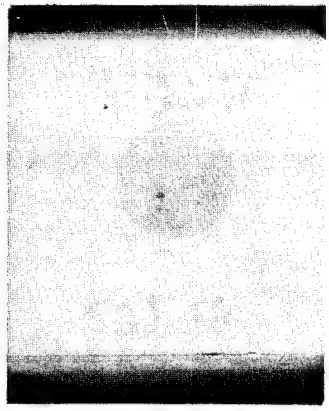

N=12,000

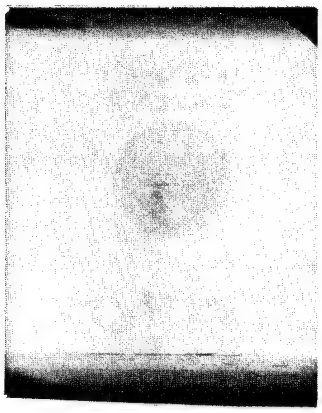

N = 25,000

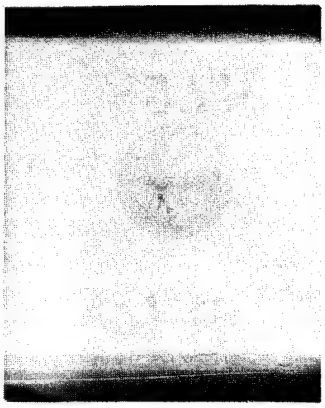

N = 20,000

N = 25,420 (Failure)

Figure 34. (Concluded)

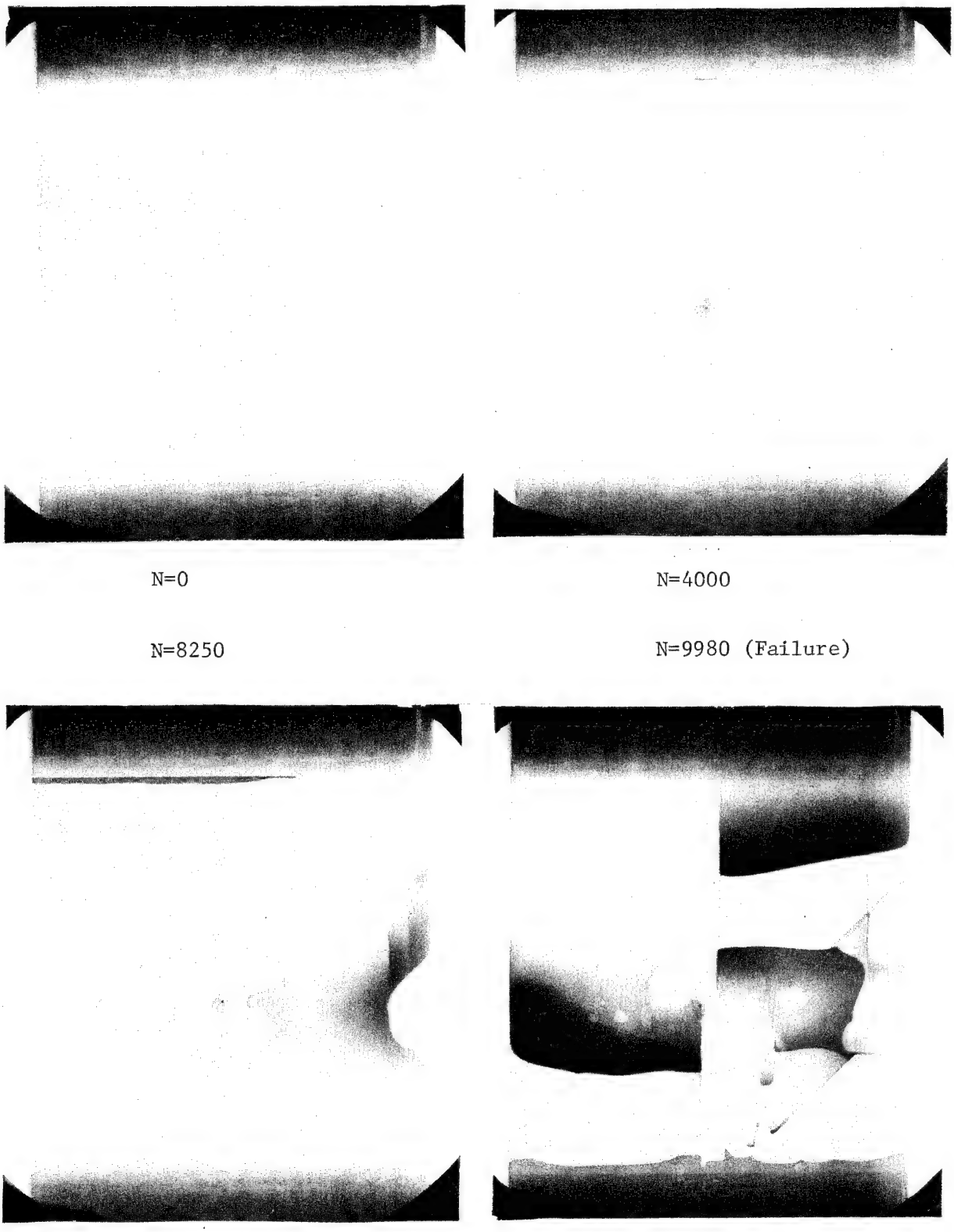

Figure 35. Delamination Growth in Specimen 4284-100; Laminate A; Test Series 16; S=0.72

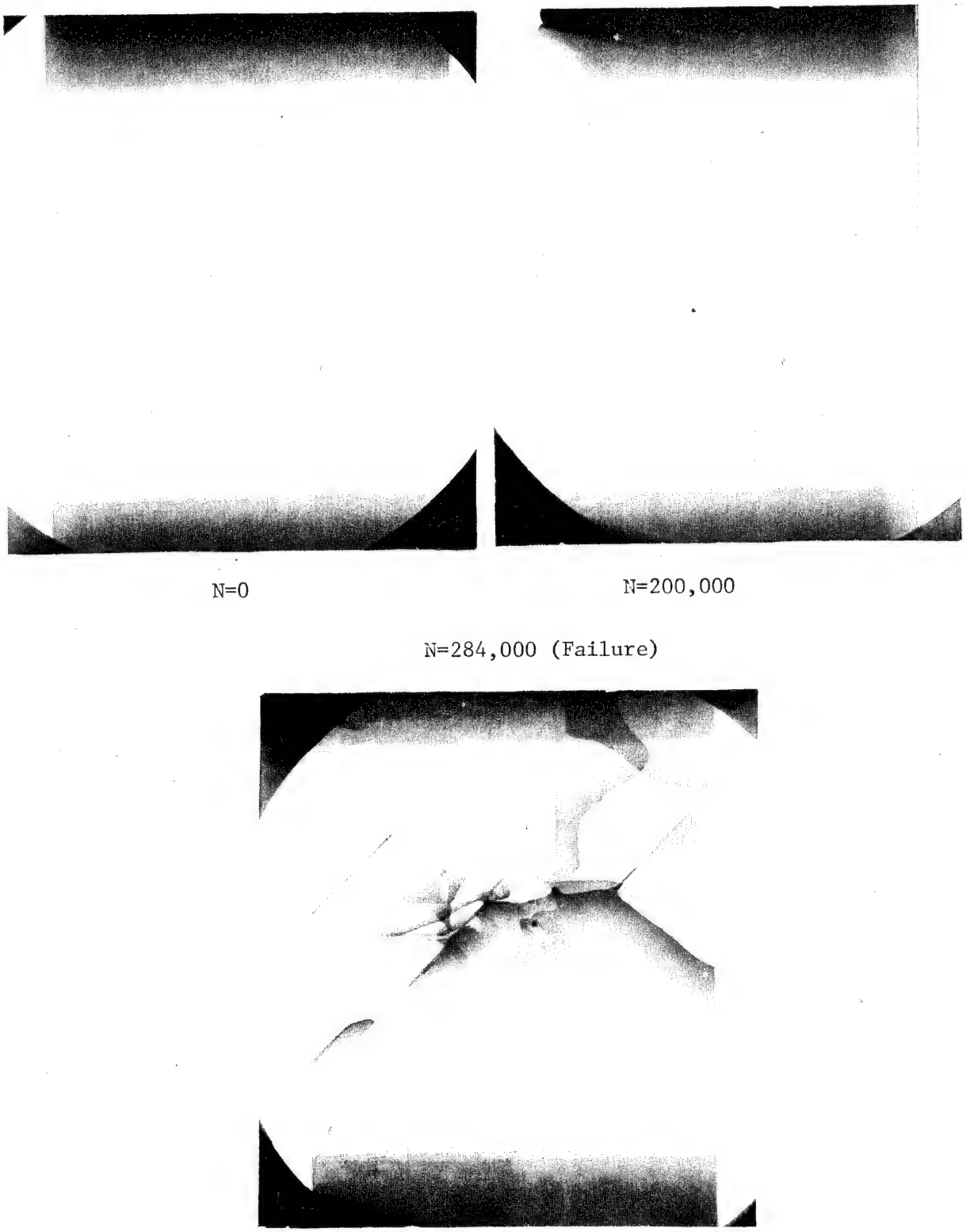

Figure 36. Delamination Growth in Specimen 4284-104; Laminate A; Test Series 18; S=0.66

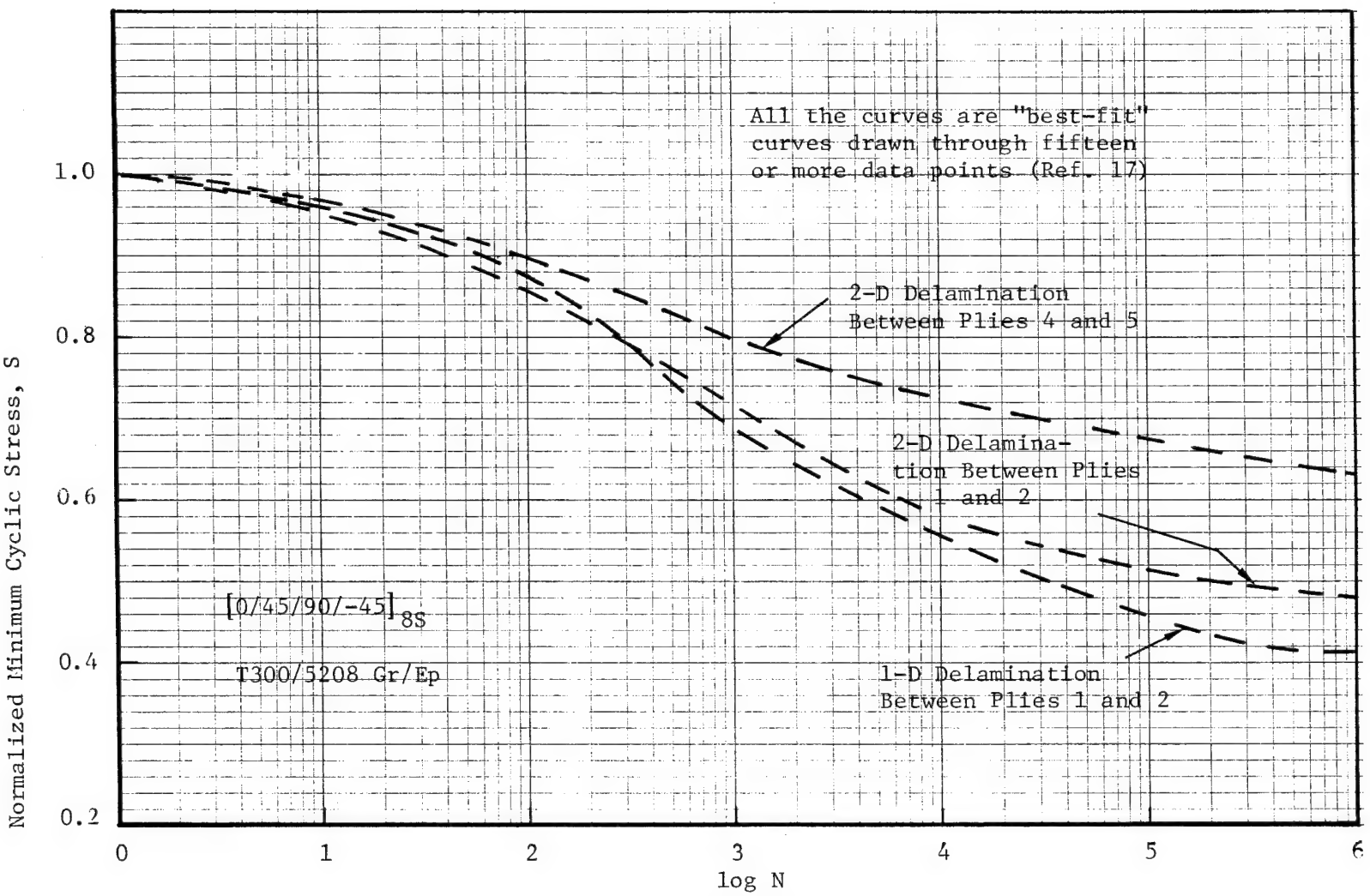

Figure 37. S-N Curves For Laminate A For Two Types and Two Locations of Interlaminar Delaminations

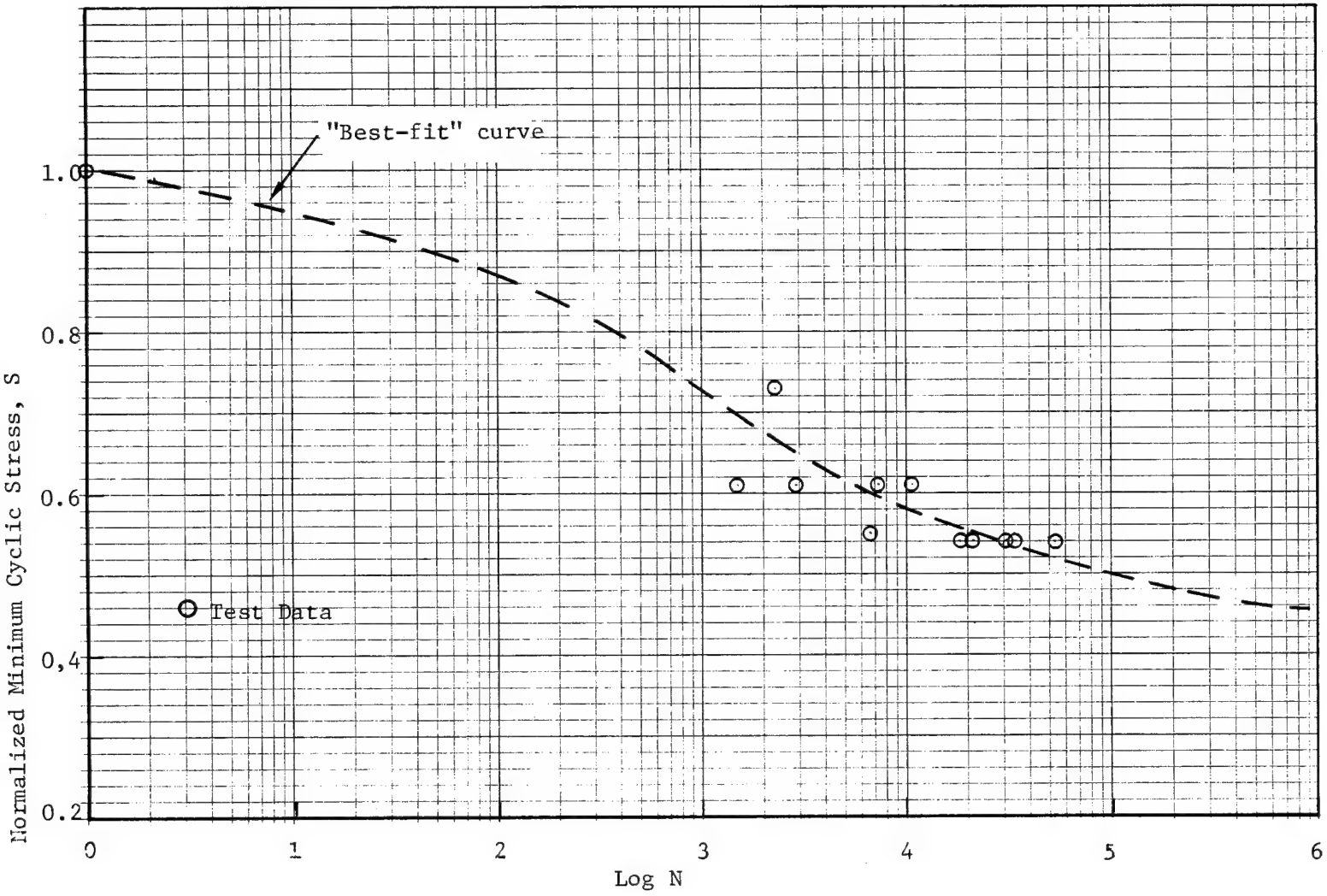

Figure 38. S-N Data for Laminate B Specimens With 1.27 cm Diameter Delamination (2-D) Between plies 1 and 2

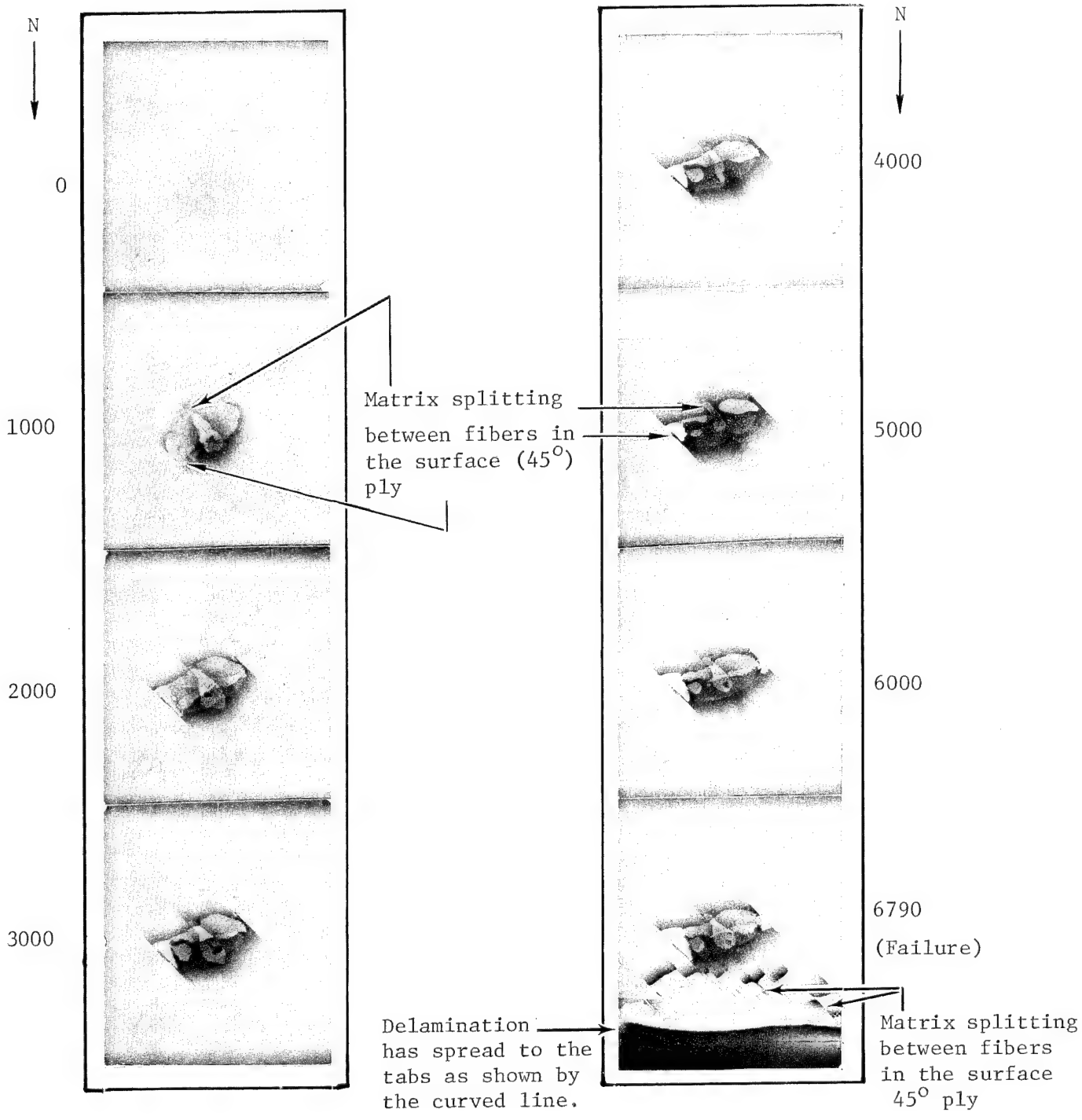

Figure 39. Delamination Growth in Specimen 4255-9; Laminate B; Test Series 7; S=0.55

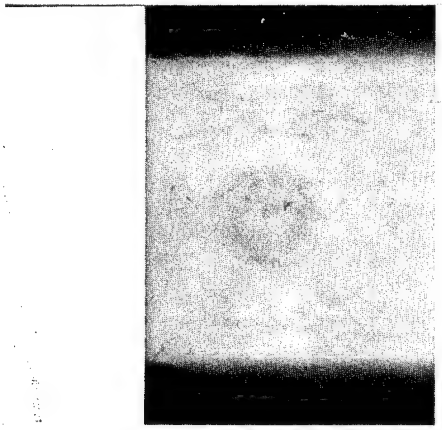

N=0

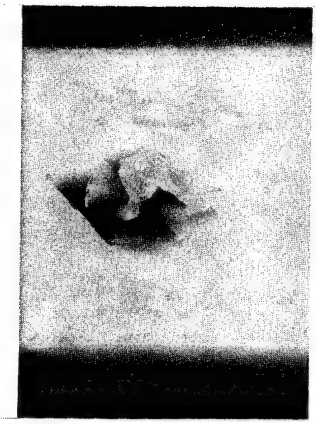

N=5000

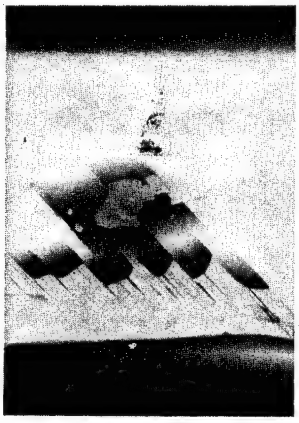

N=7350
(Failed)

Figure 40. Delamination Growth in Specimen 4255-21; Laminate B; Test Series 7;S=0.61.

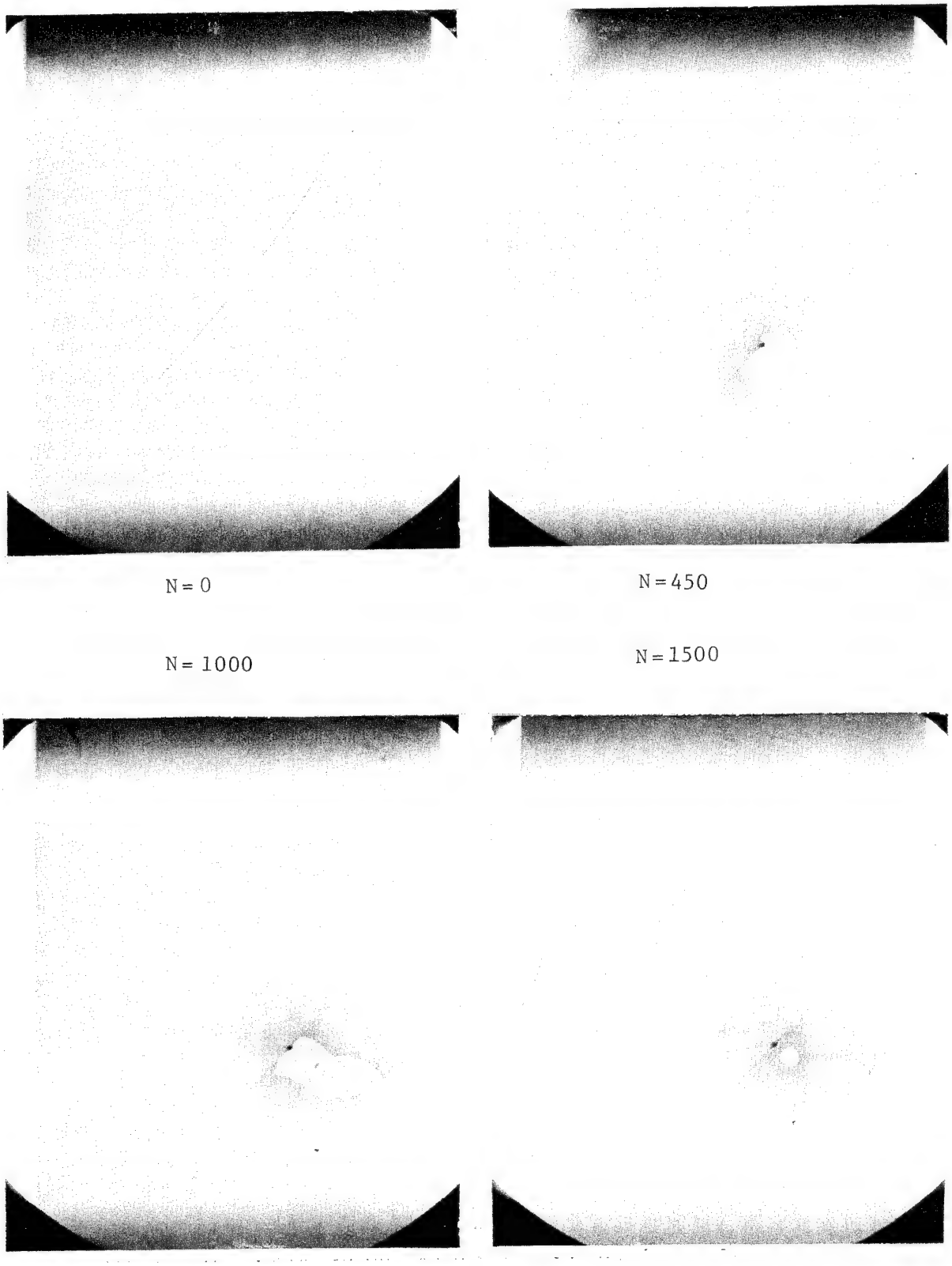

Figure 41. Delamination Growth in Specimen 4255-24; Laminate B; Test Series 7; S=0.61

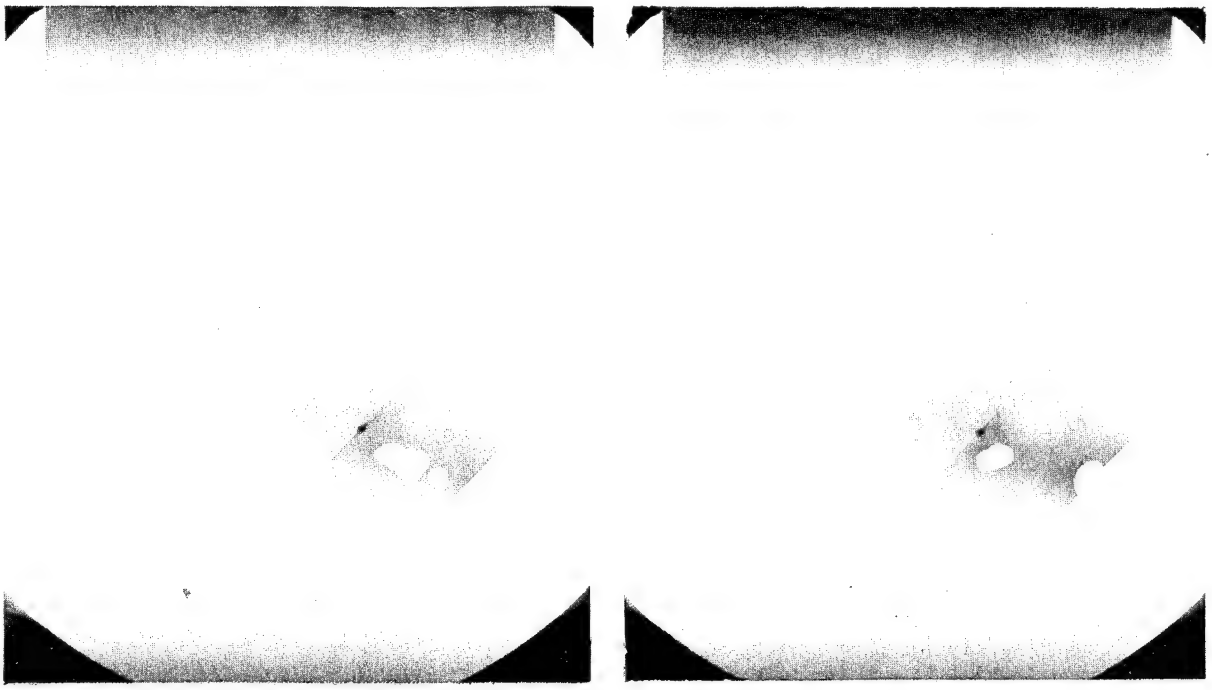

N=2500

N=2900 (Failure)

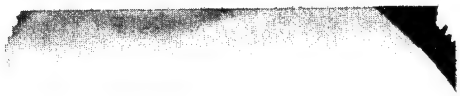

N=2900 (DIB injected into the delaminated region near the back surface. Imbedded flaw has not yet propagated to the tab region).

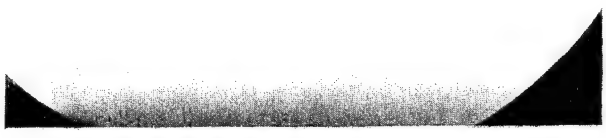

Figure 41. (Concluded)

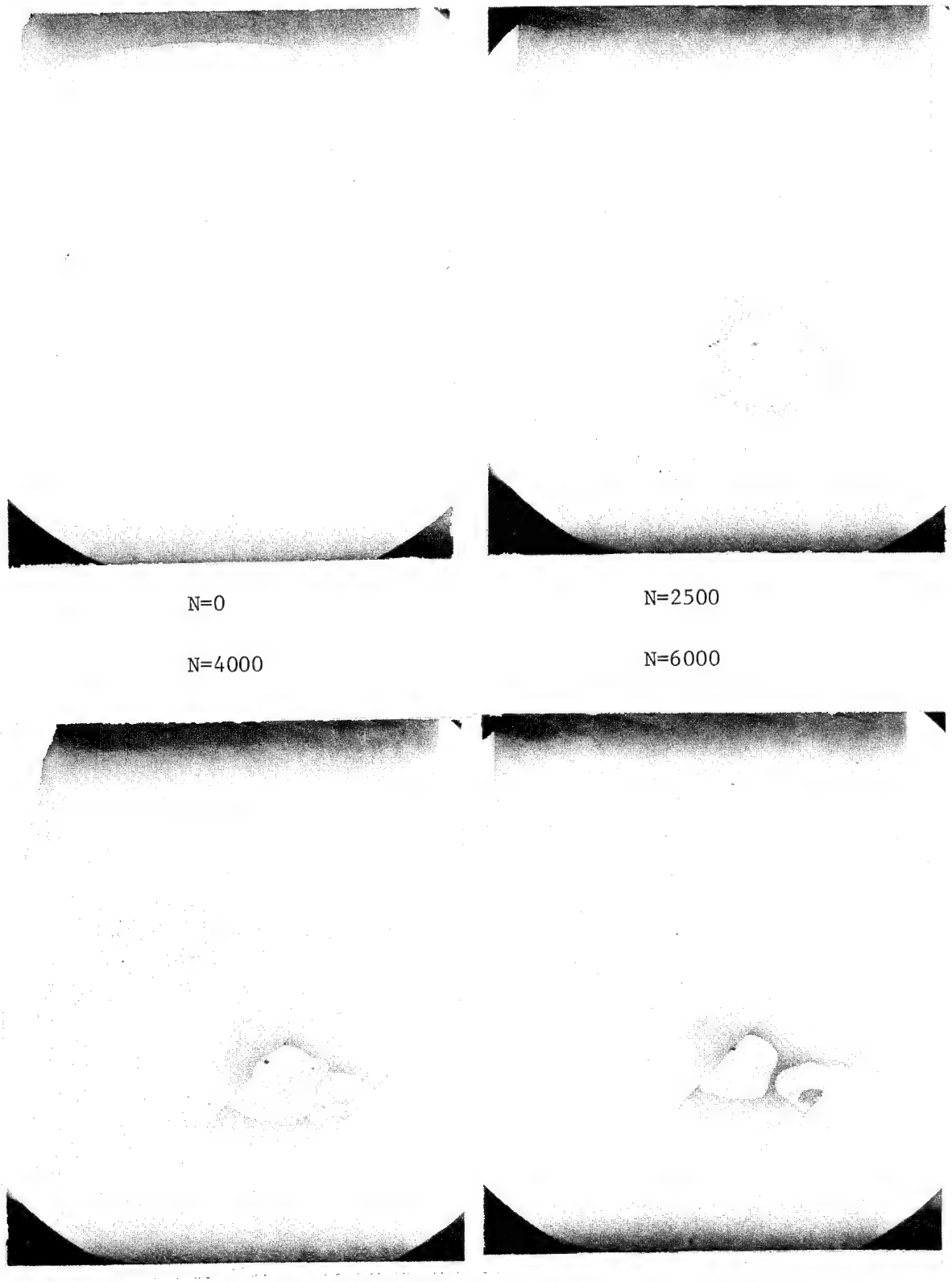

Figure 42. Delamination Growth in Specimen 4255-25; Laminate B; Test Series 8; S=0.54

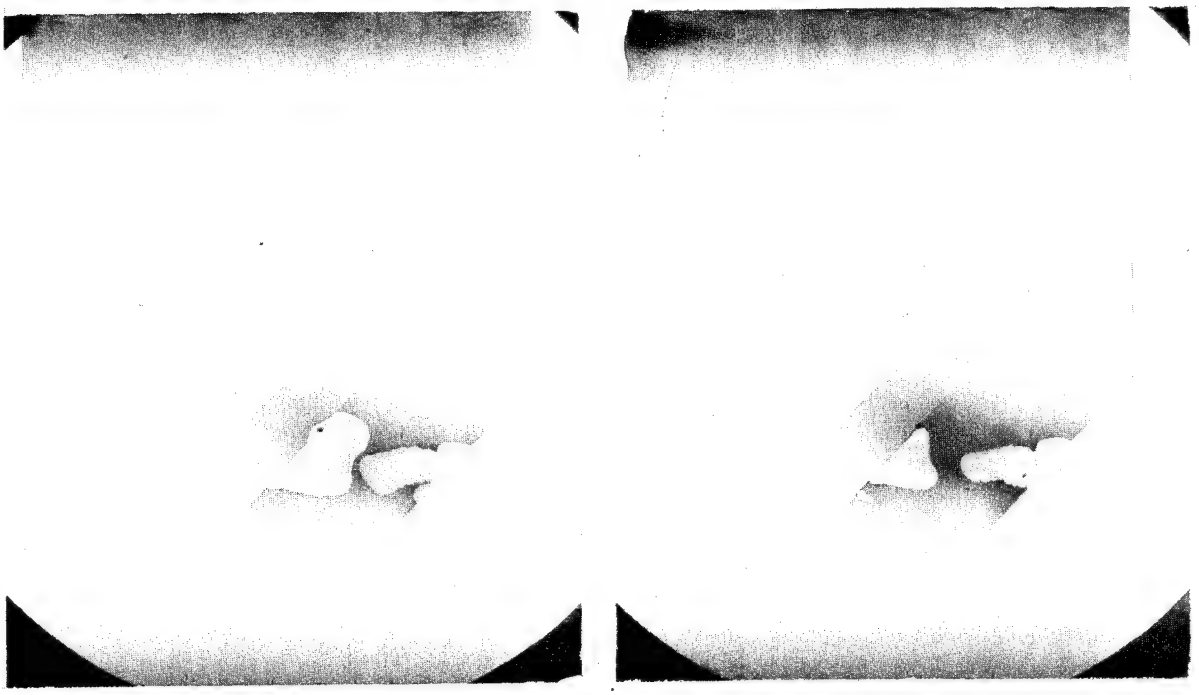

N=14,000

N=20,000

N=24,000

N=30,000

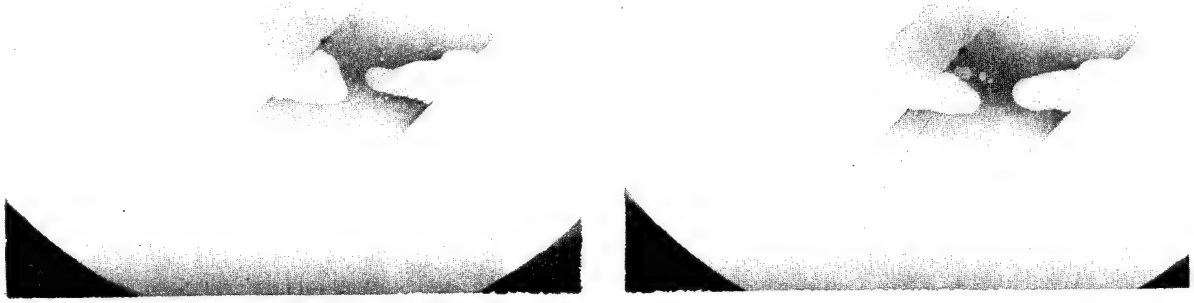

Figure 42. (Continued)

N=35,000

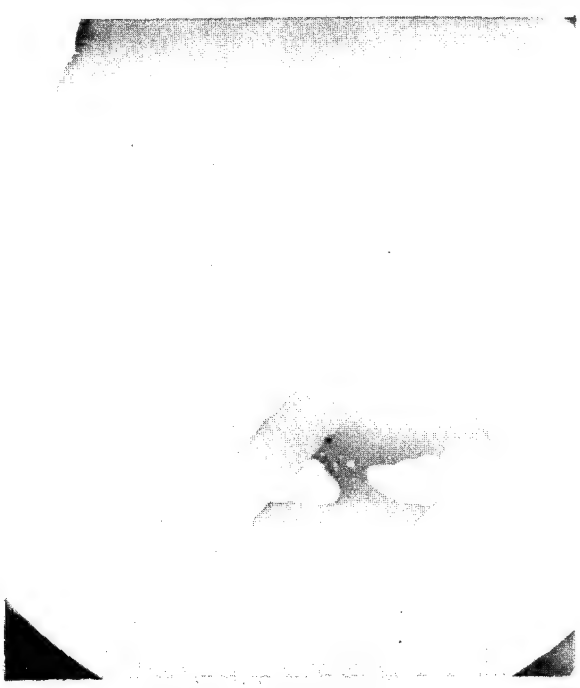

N=40,000

N=50,000

N=52,180 (Failure)

Figure 42. (Concluded)

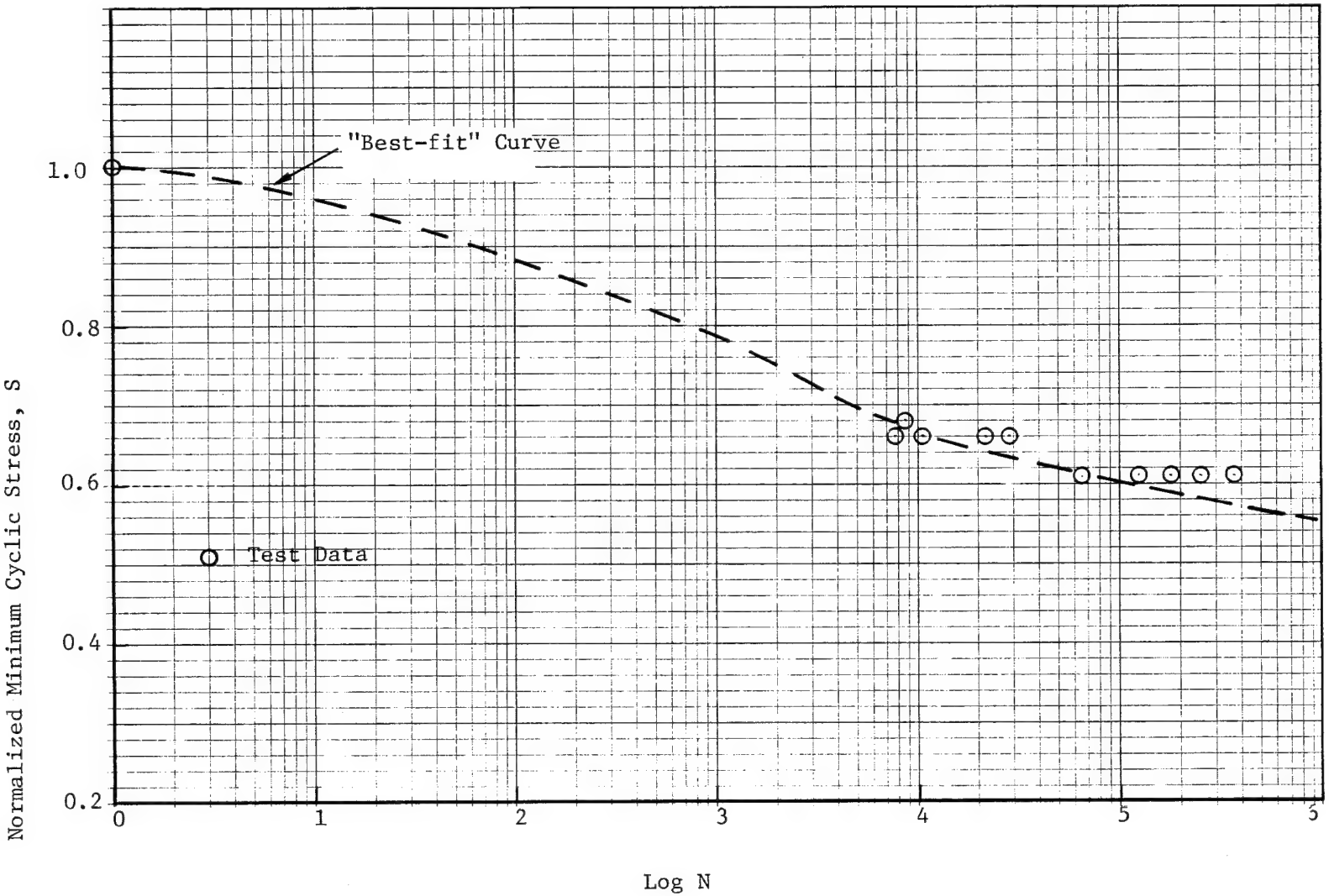

Figure 43. S-N Data for Laminate B Specimens With 1.27 cm Diameter Delamination (2-D) Between Plies 4 and 5.

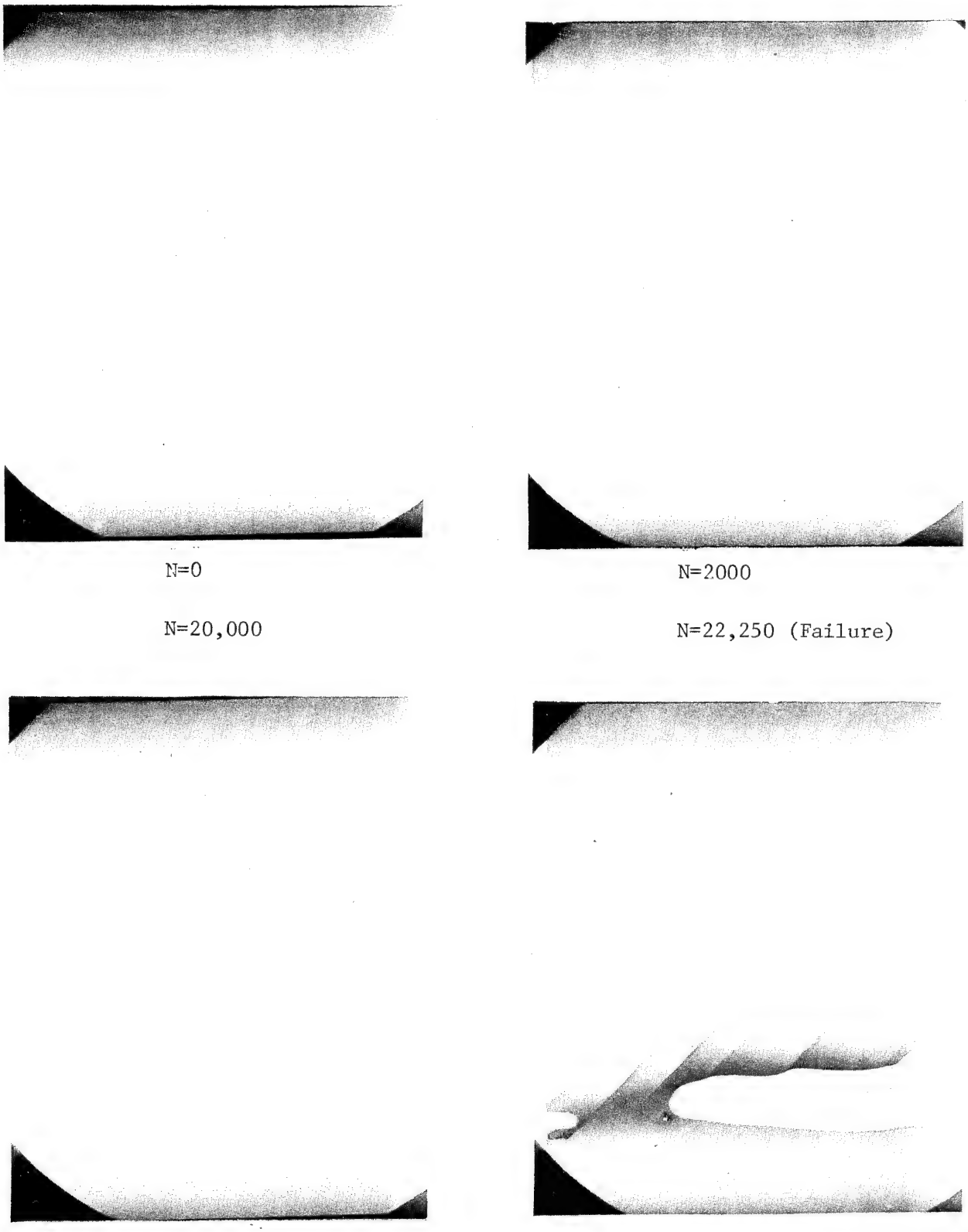

Figure 44. Delamination Growth in Specimen 4256-40; Laminate B; Test Series 14; S=0.66; Radiographs Taken with a 9.12 kN Load

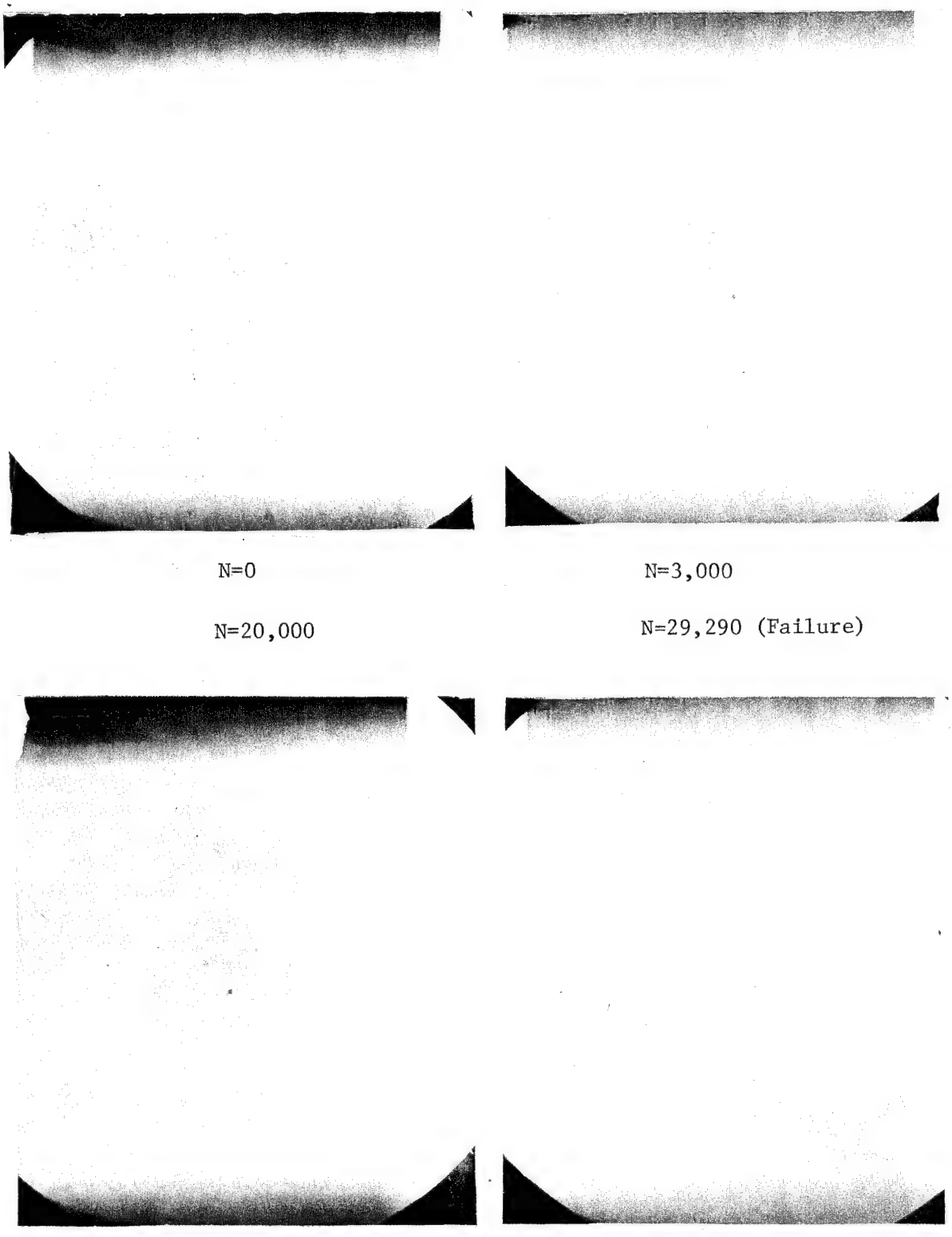

Figure 45. Delamination Growth in Specimen 4256-39; Laminate B; Test Series 14; S=0.66; Radiographs Taken with a 9.12 kN Load.

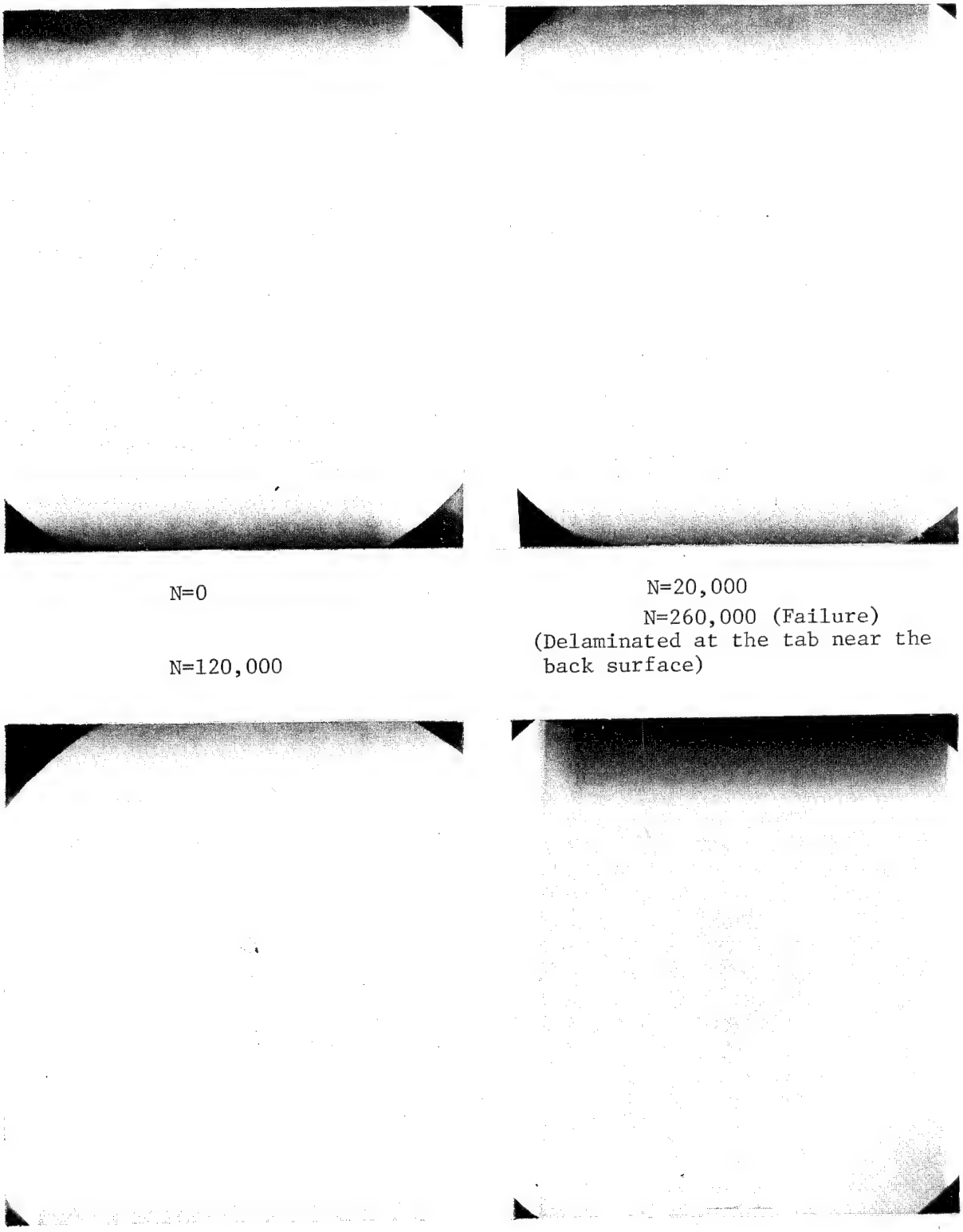

Figure 46. Delamination Growth in Specimen 4256-35; Laminate B; Test Series 15; S=0.61; Radiographs Taken with a 8.45 kN Load

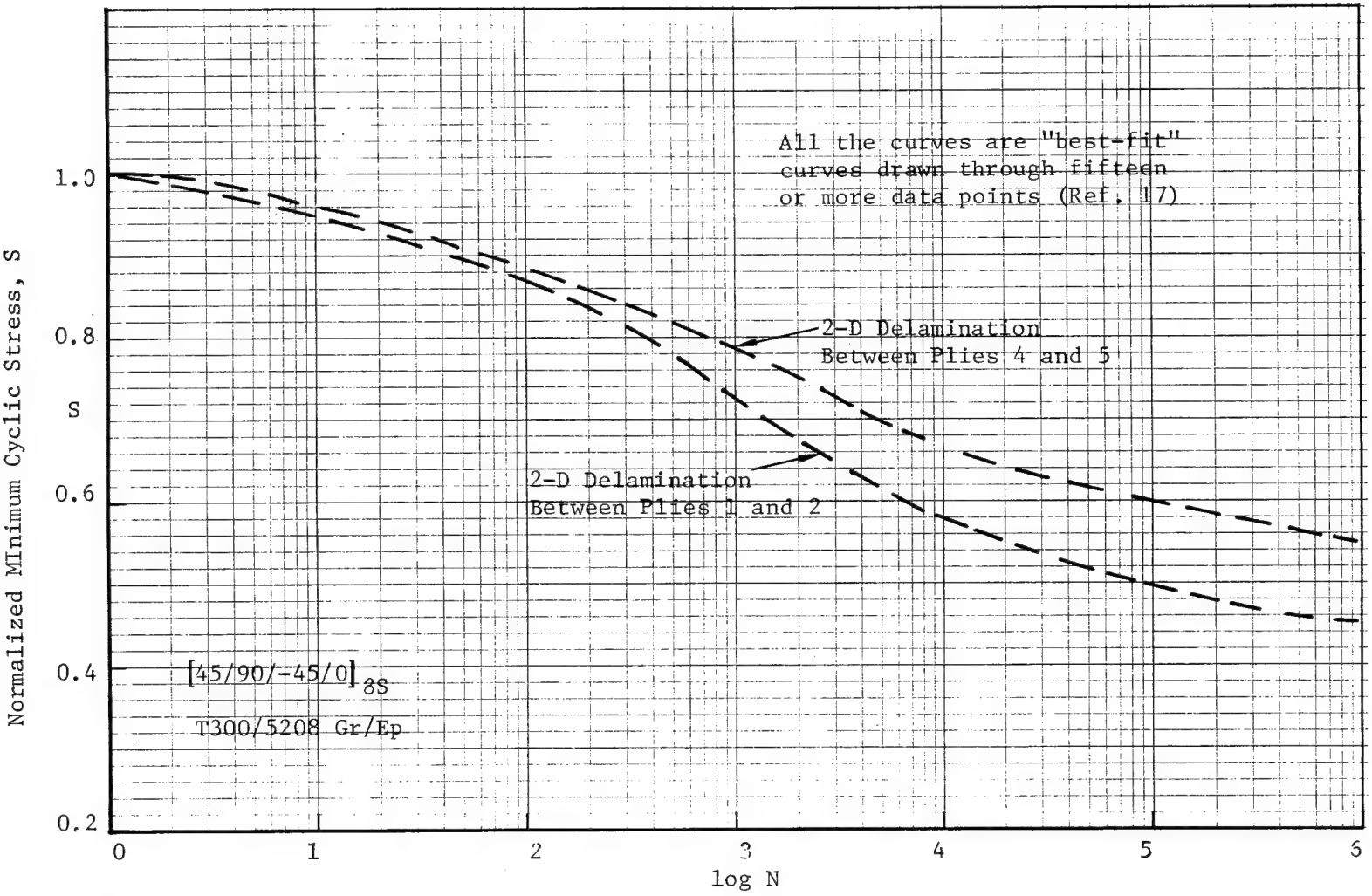

Figure 47. S-N Curves For Laminate B With 2-D Delaminations At Two Locations

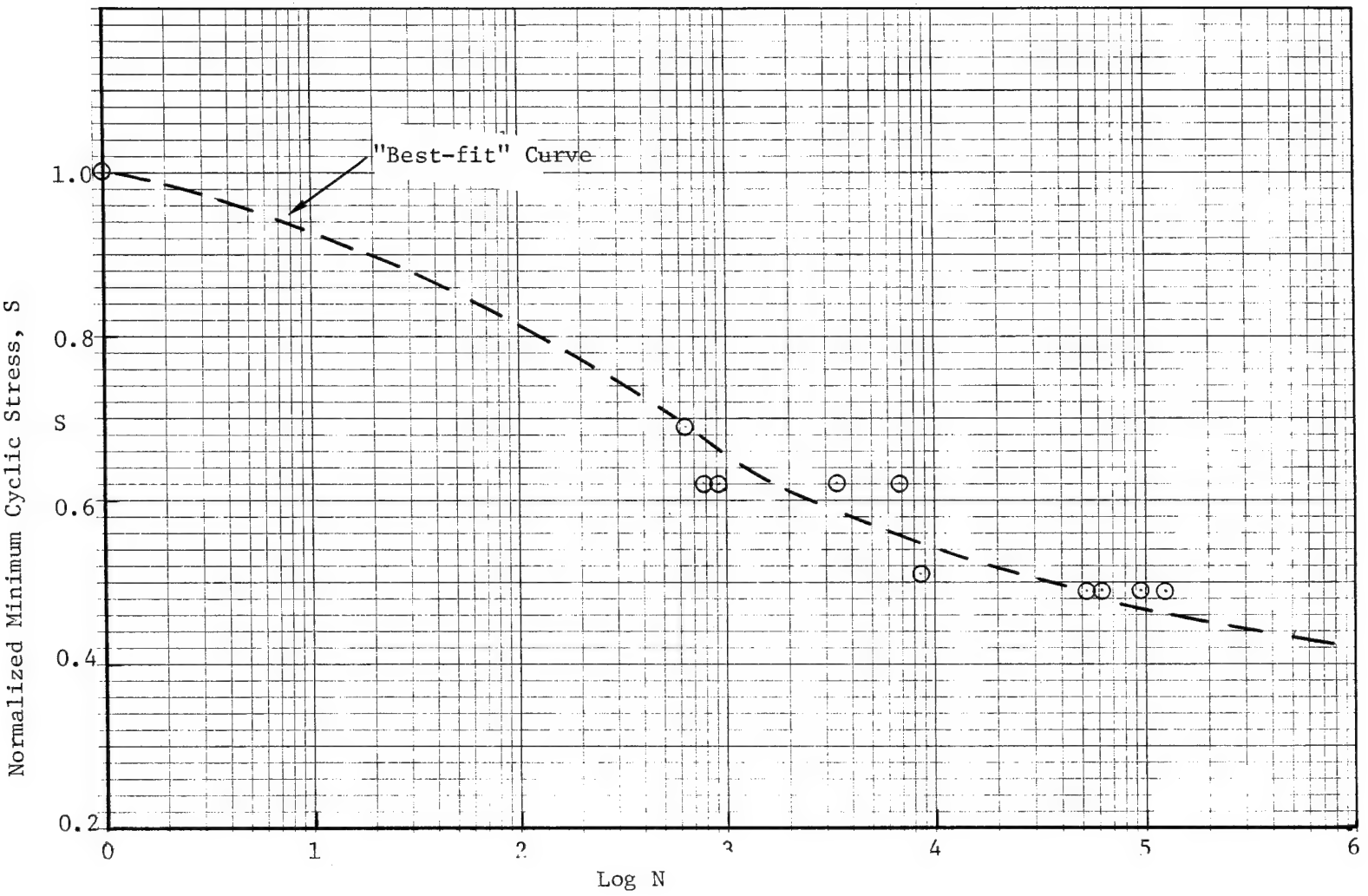

Figure 48. S-N Data for Laminate C Specimens With 1.27 cm Diameter Delamination (2-D) Between Plies 1 and 2.

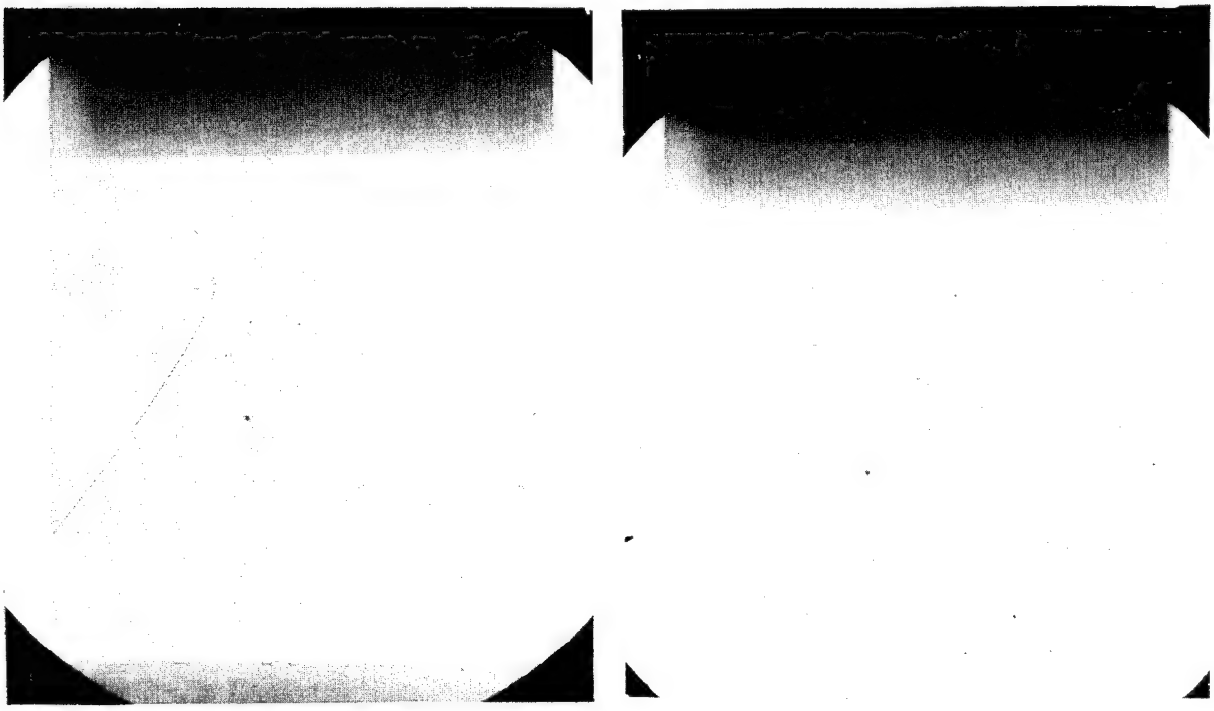

N=0

N=2500

N=6980 (Failed Near Upper Tab)

Figure 49. Delamination Growth in Specimen 4282-18; Laminate C: Test Series 7; S=0.62

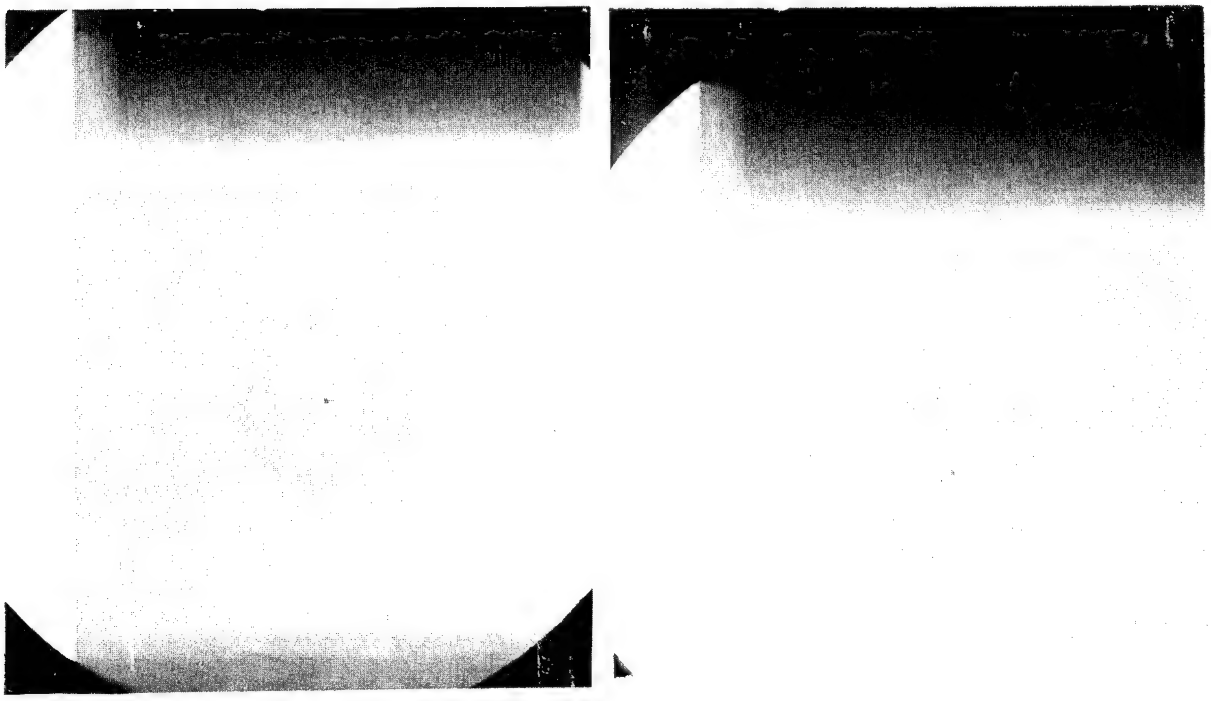

N=0

N=15,000

N=52,000 (Failure)

Figure 50. Delamination Growth in Specimen 4282-24; Laminate C; Test Series 8; S=0.49

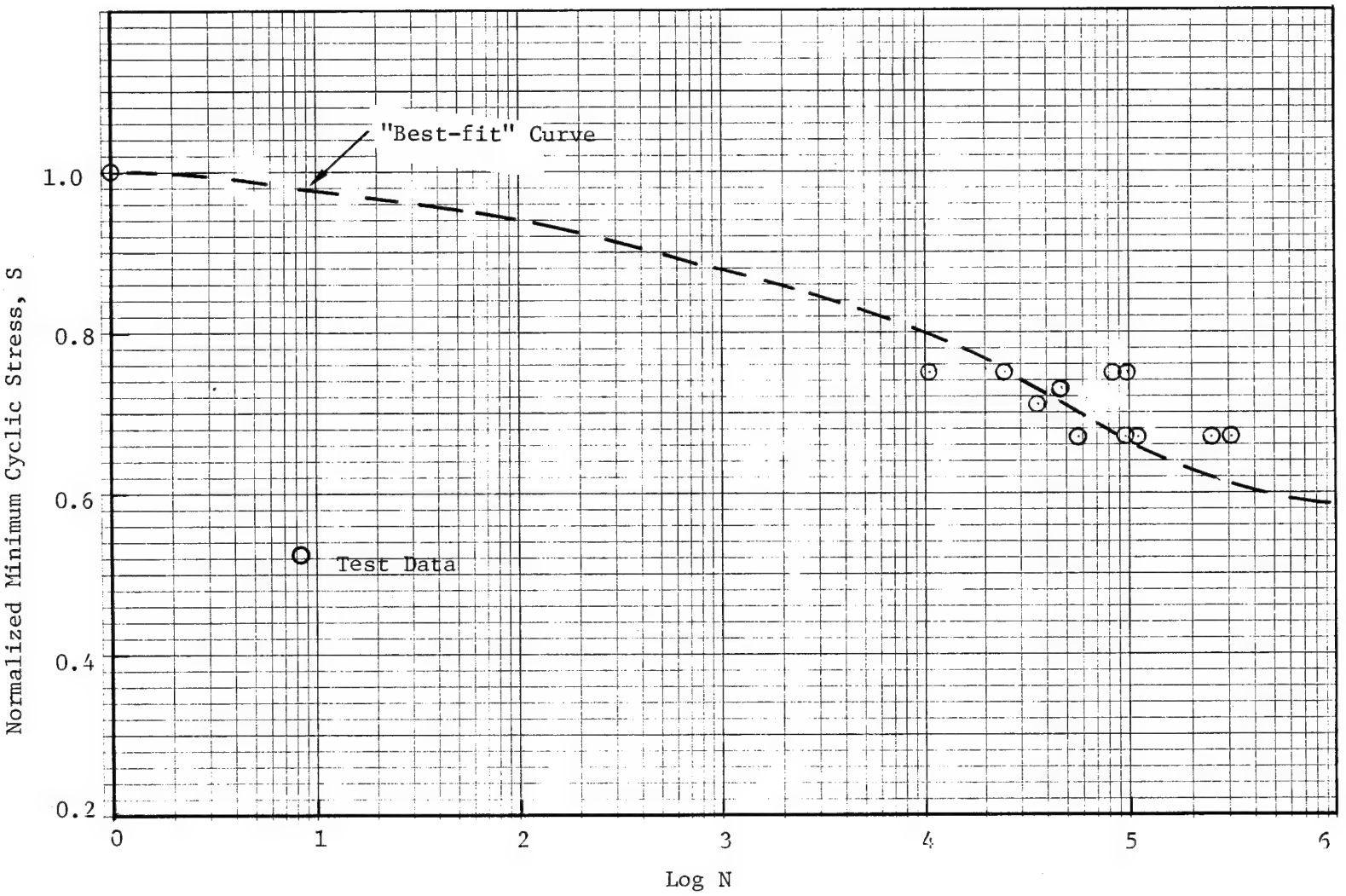

Figure 51. S-N Data for Laminate C Specimens with 1.27 cm Diameter Delamination (2-D) Between Plies 4 and 5.

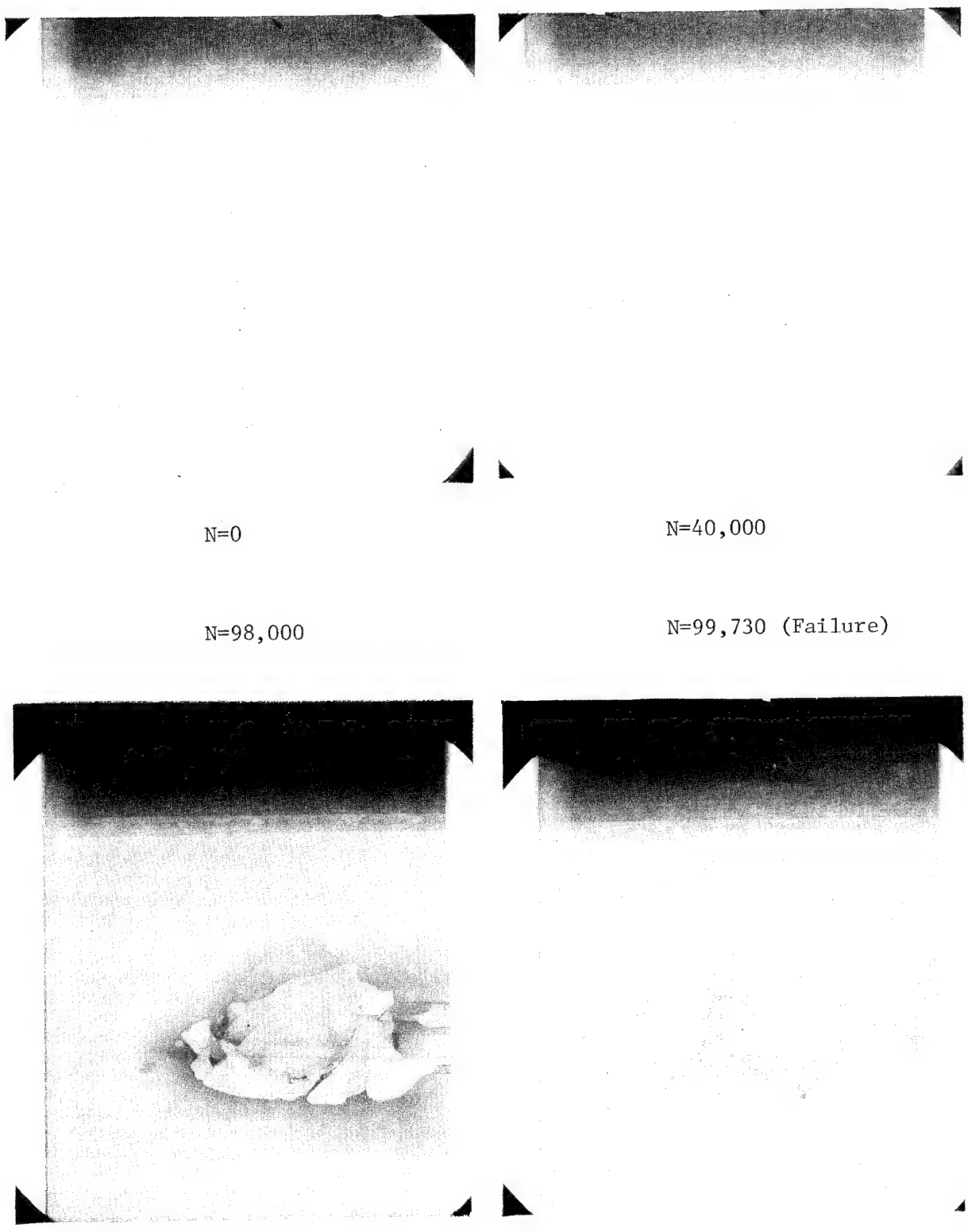

Figure 52. Delamination Growth in Specimen 4282-29: Laminate C; Test Series 14; S=0.75

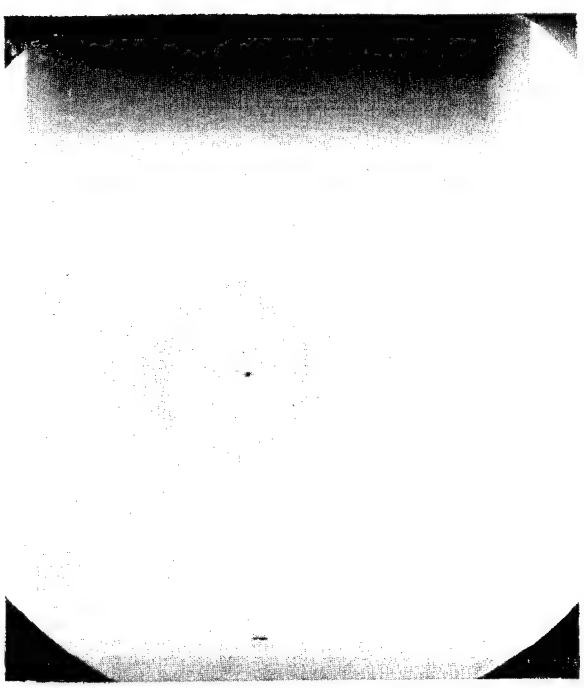

N=0

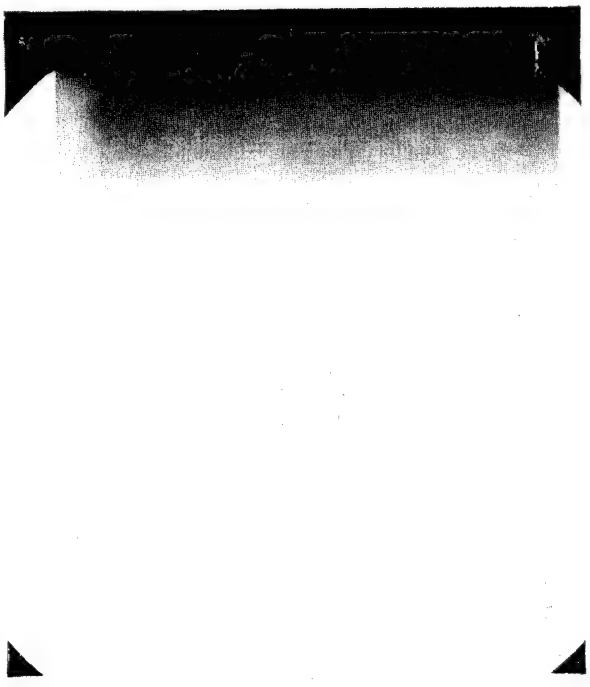

N=50,000

N=222,000

N=257,080 (Failure)
Delamination near tab on the flaw side but did not "merge" with the flaw.

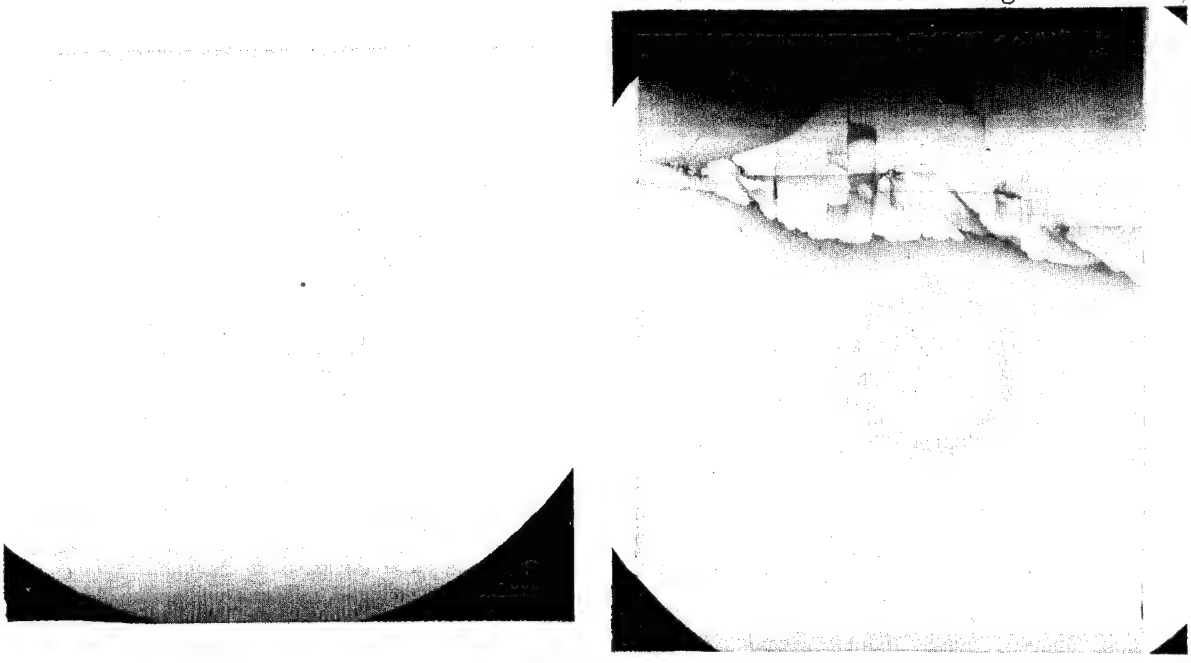

Figure 53. Delamination Growth in Specimen 4282-38; Laminate C; Test Series 15; S=0.67; Radiographs Taken with a 8.01 kN Load

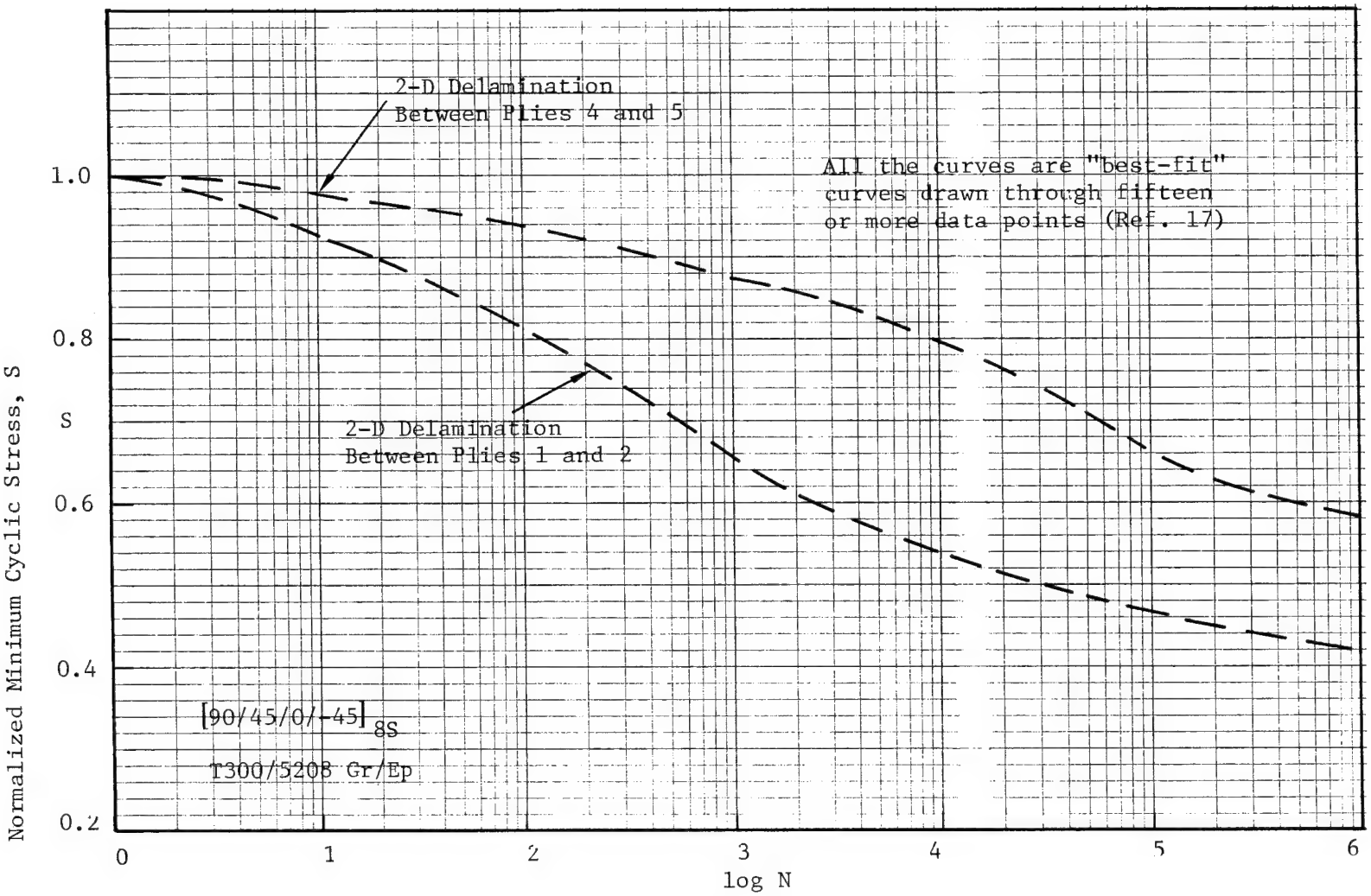

Figure 54. S-N Curves For Laminate C With 2-D Delaminations At Two Locations

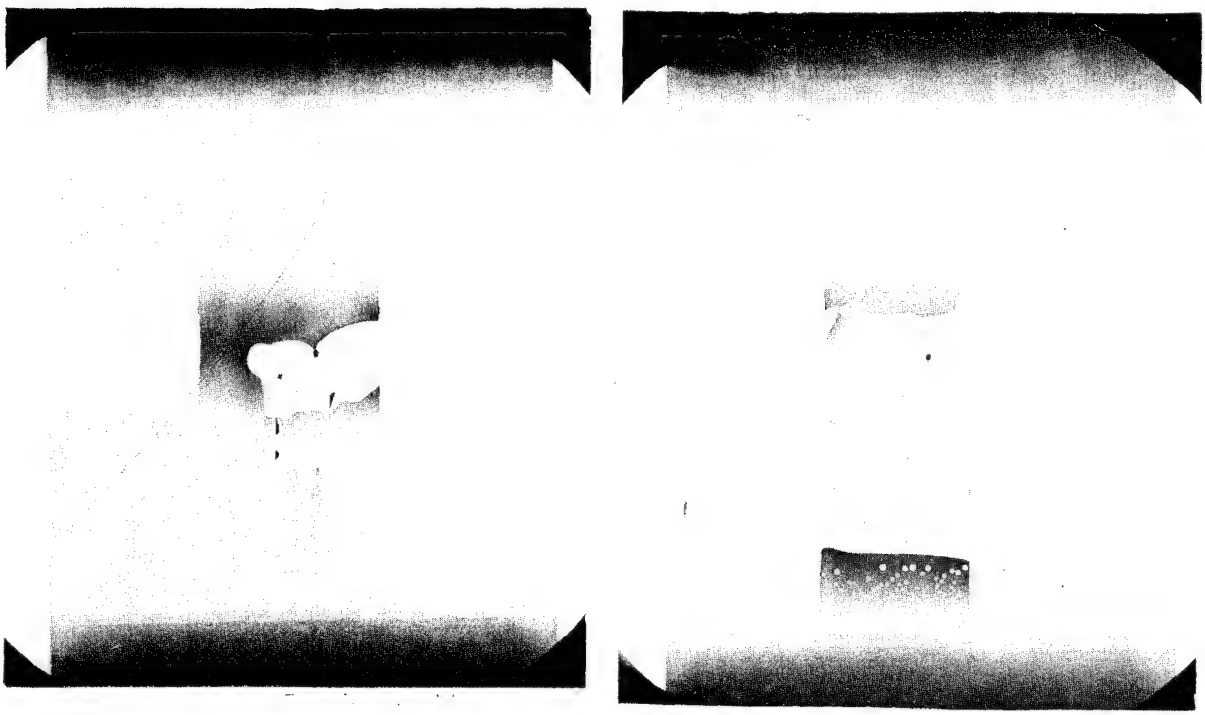

Specimen 4284-33; N=1000

Specimen 4284-53; N=680

Specimen 4284-59; N=1000

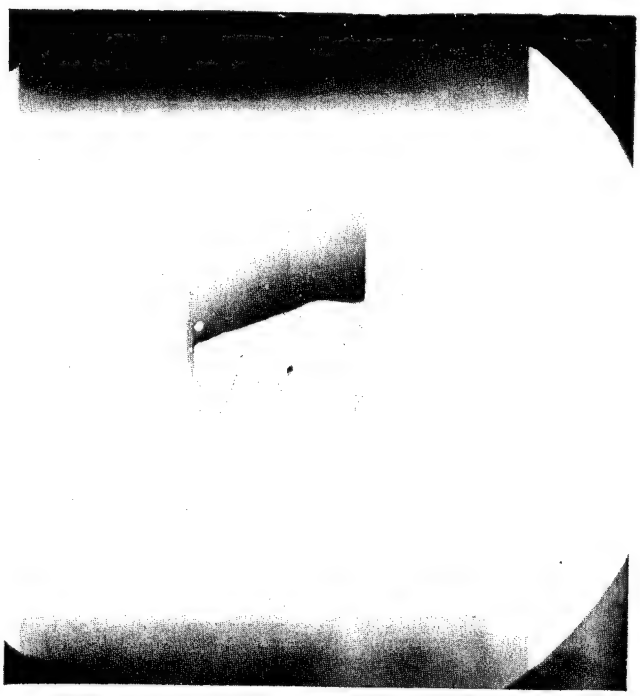

Figure 55. Radiographs of Residual Strength Test Specimens After Completing Approximately Half Their Lifetimes; Laminate A; Test Series 8; S=0.66

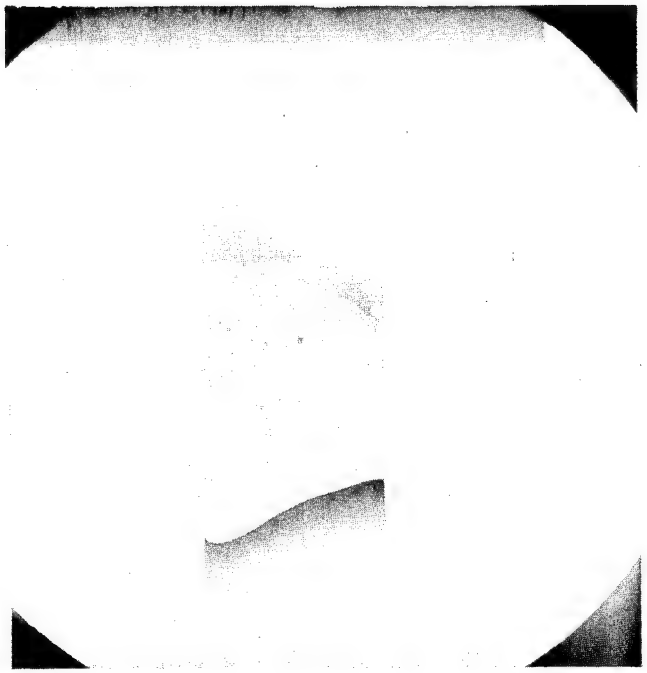

Specimen 4284-60; N=700

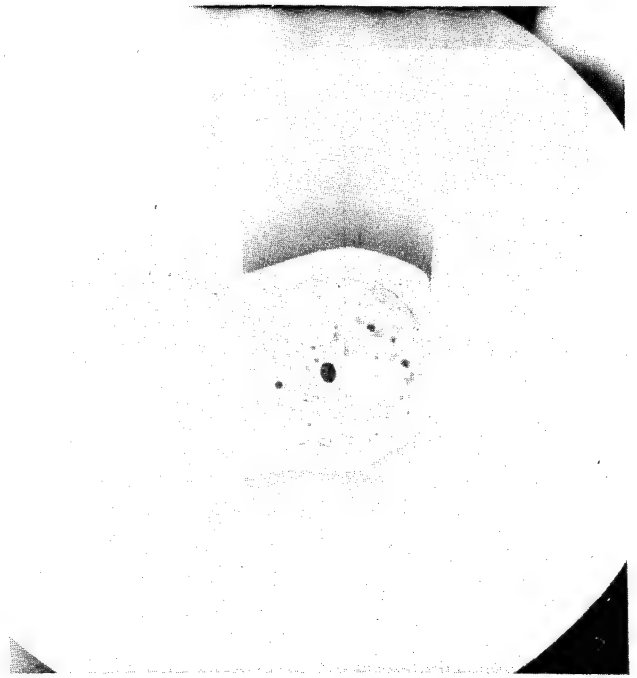

Specimen 4284-61; N=5000

Figure 56. Radiographs of Residual Strength Test Specimens After Completing Approximately Half Their Lifetimes; Laminate A; Test Series 10; S=0.58

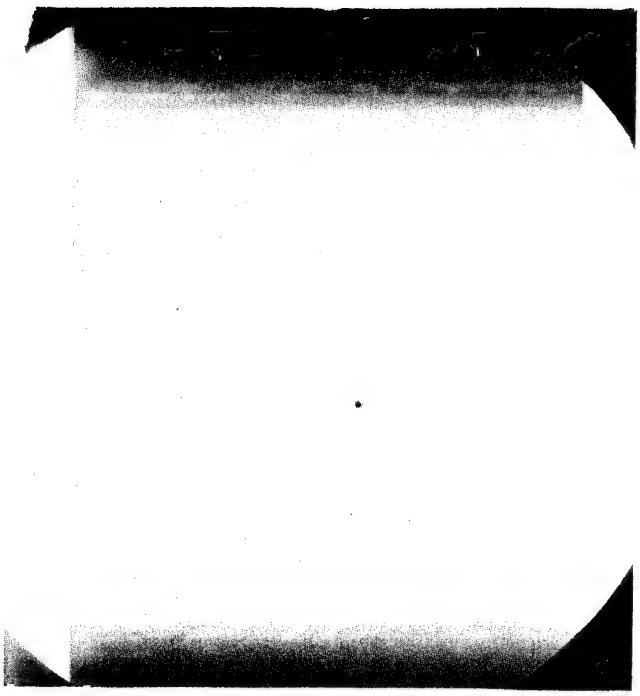

Specimen 4284-68; N=10,000

Figure 57. Radiograph of a Residual Strength Test Specimen After Completing Approximately Half its Lifetime Laminate A; Test Series 12; S=0.55

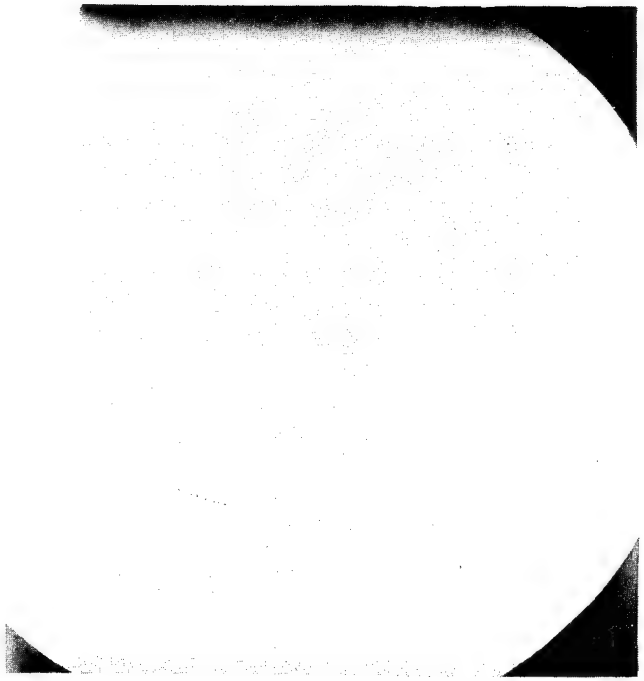

Specimen 4284-97; N=1000

Specimen 4284-98; N=550
(Failed)

Figure 58. Radiographs of Residual Strength Test Specimens After Completing Approximately Half Their Lifetimes; Laminate A ; Test Series 15; S=0.77

Specimen 4284-86; N=7500

Specimen 4284-101; N=7500

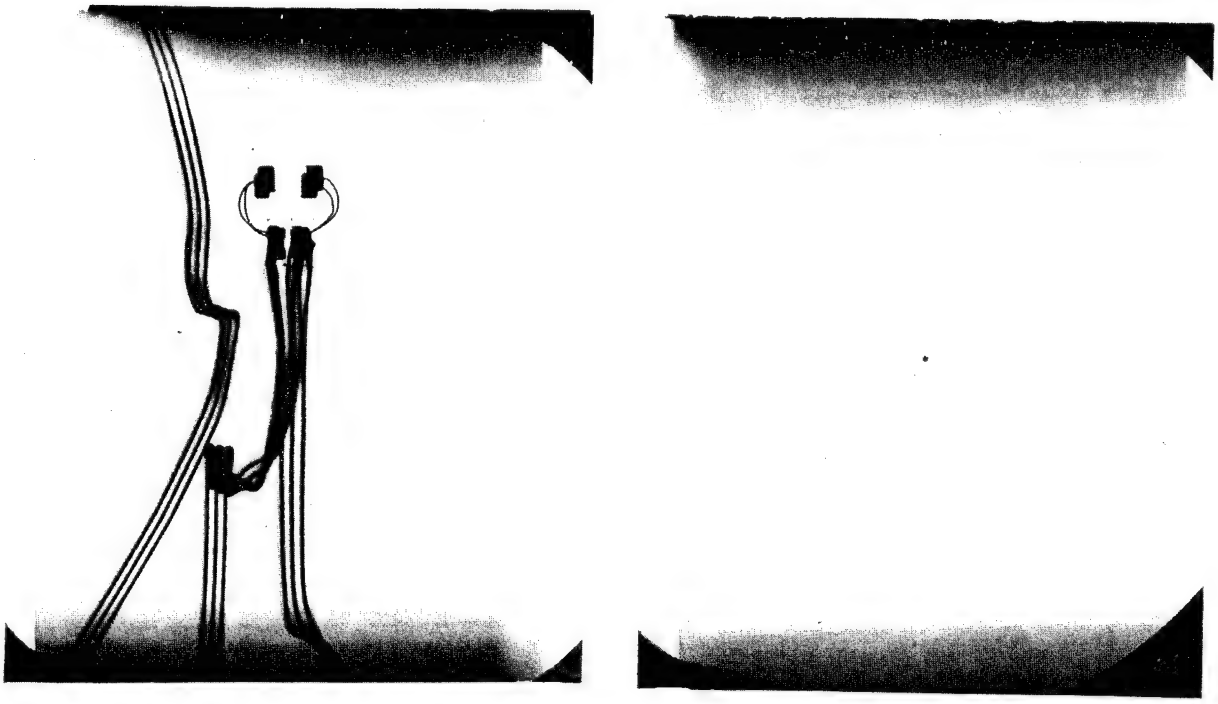

Specimen 4284-102; N=7500

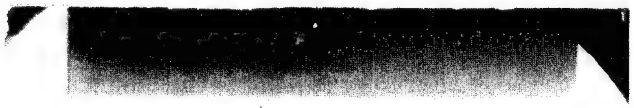

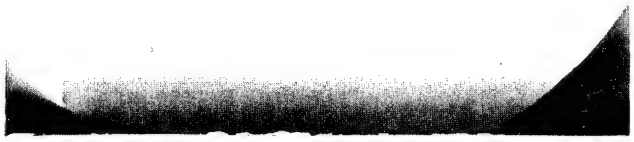

Figure 59. Radiographs of Residual Strength Test Specimens After Completing Approximately Half Their Lifetimes; Laminate A; Test Series 17; S=0.72

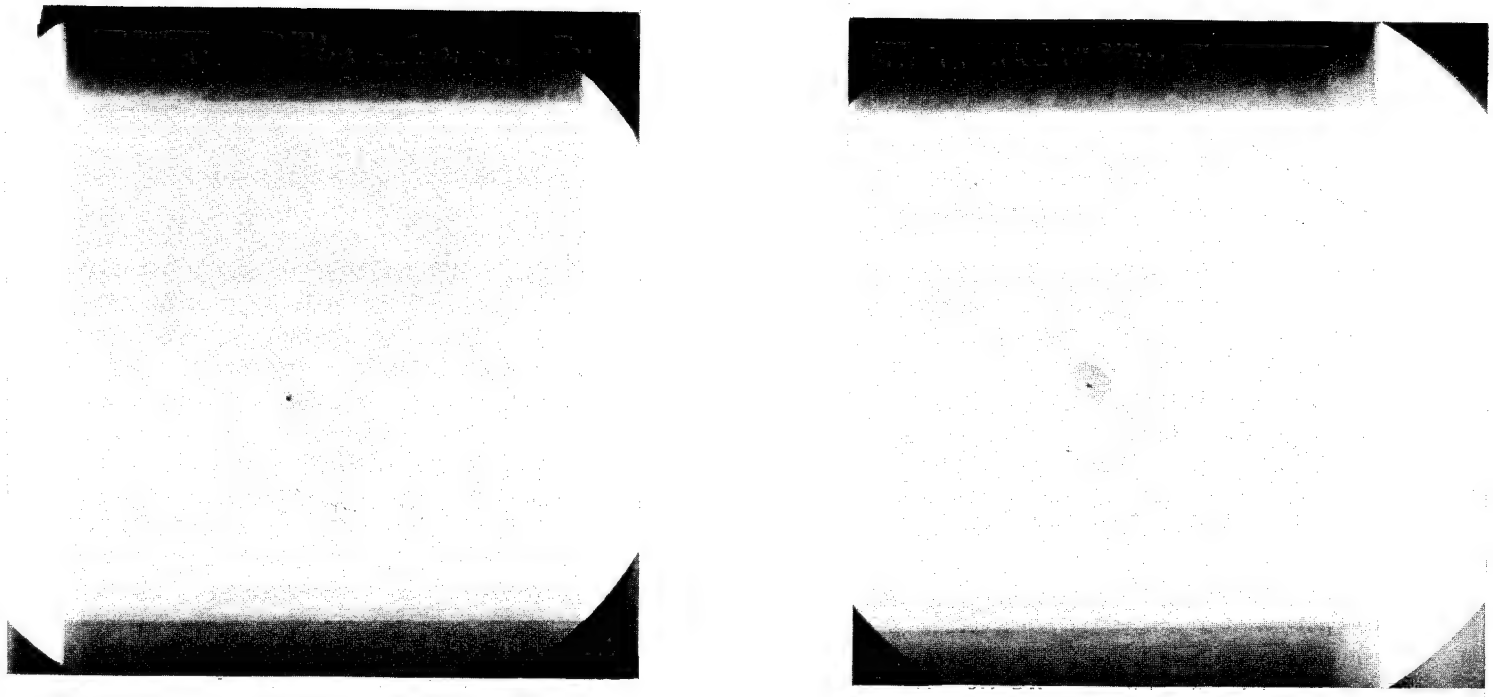

Specimen 4284-106; N=100,000

Specimen 4284-105; N=100,000

Figure 60. Radiographs of Residual Strength Test Specimens After Completing Approximately Half Their Lifetimes; Laminate A; Test Series 19; S=0.66

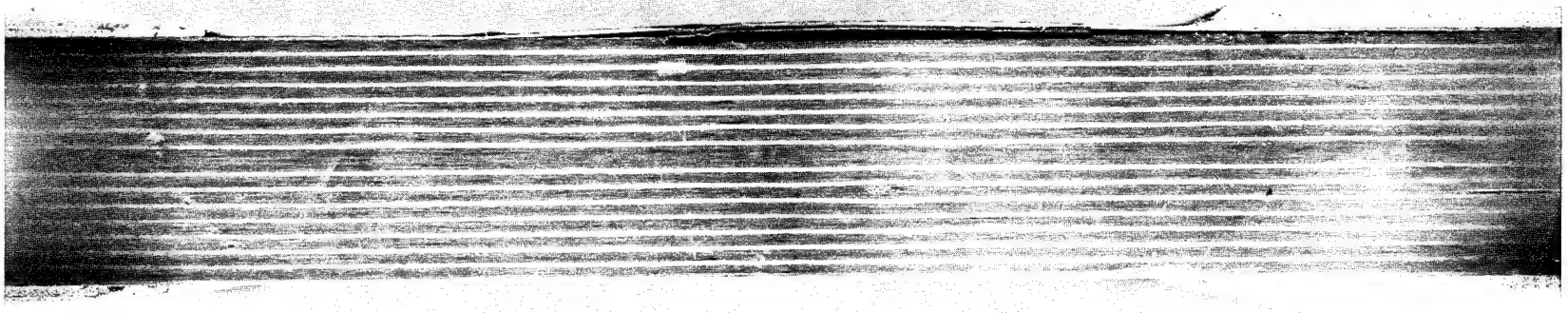

Figure 61. Photograph of a Laminate A Specimen (4284-70) after Fatigue Failure; Test Series 14

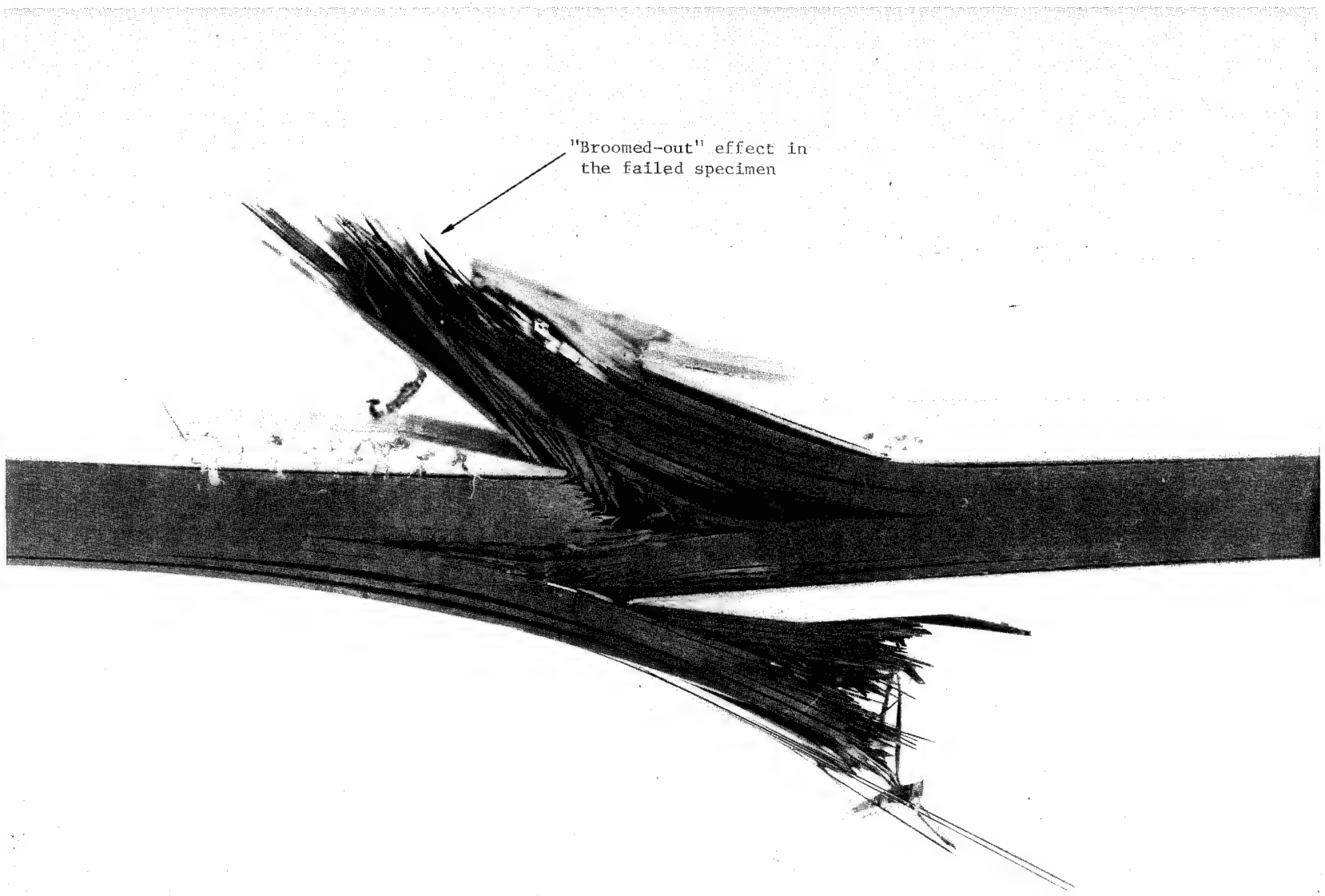

Figure 62. Photograph of a Laminate A Specimen (4284-60) after Residual Strength Testing; Test Series 10

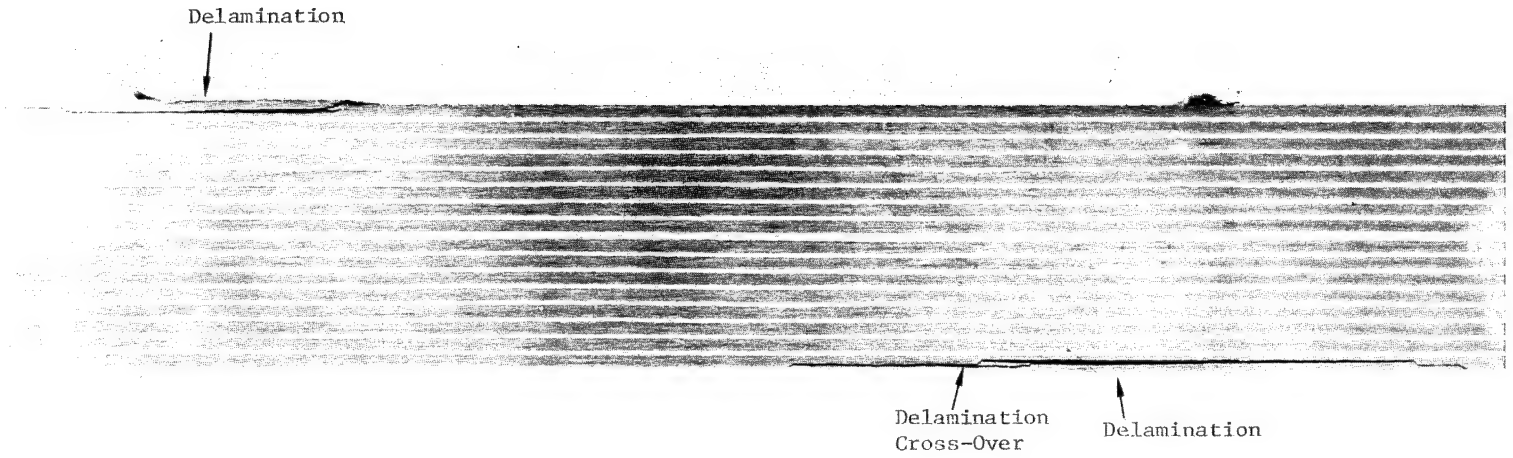

Figure 63. Photograph of a Laminate B Specimen (4256-36) After Fatigue Failure; Test Series 15

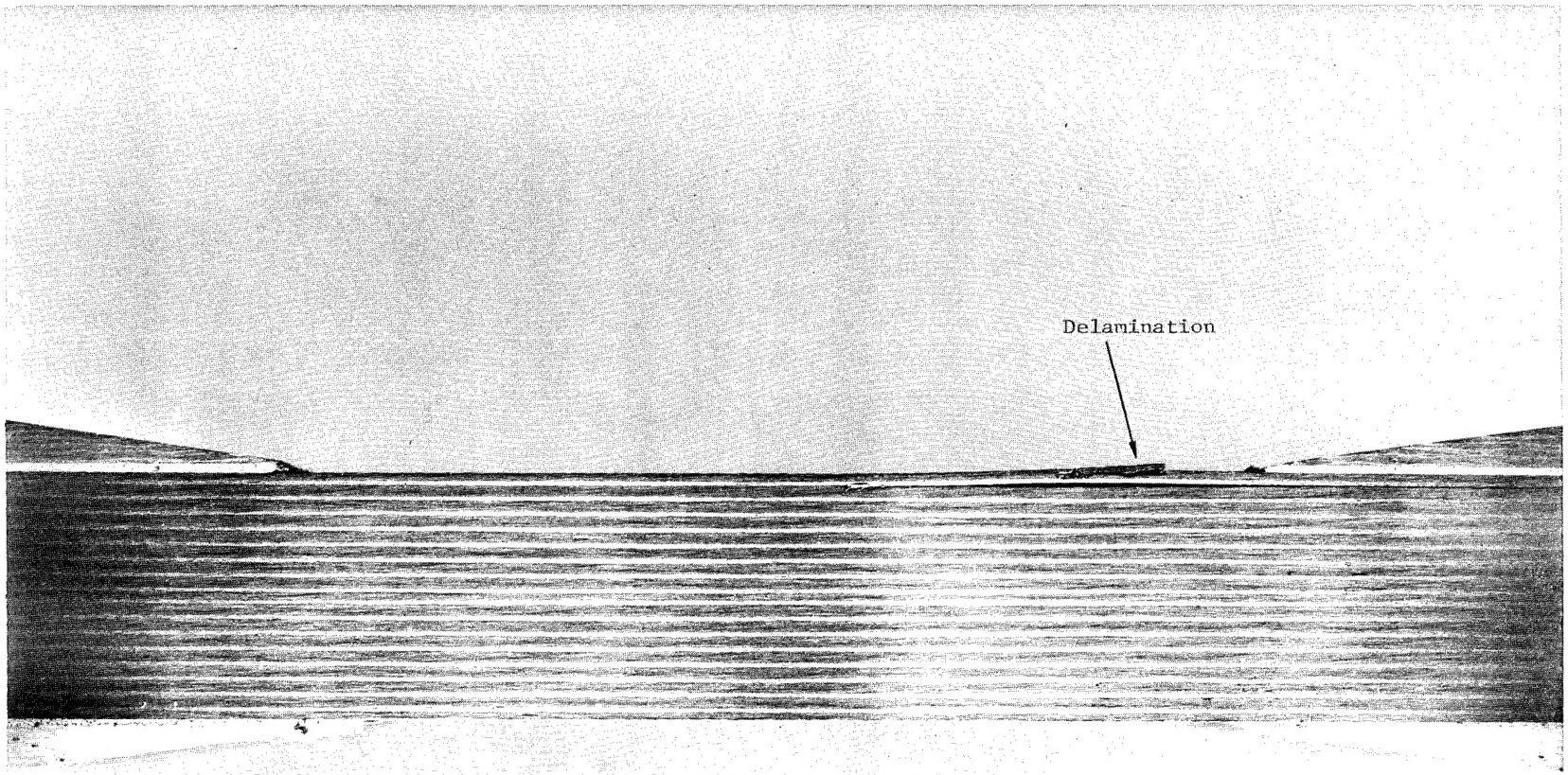

Figure 64 Photograph of a Laminate C Specimen (4282-26) After Fatigue Failure; Test Series 8

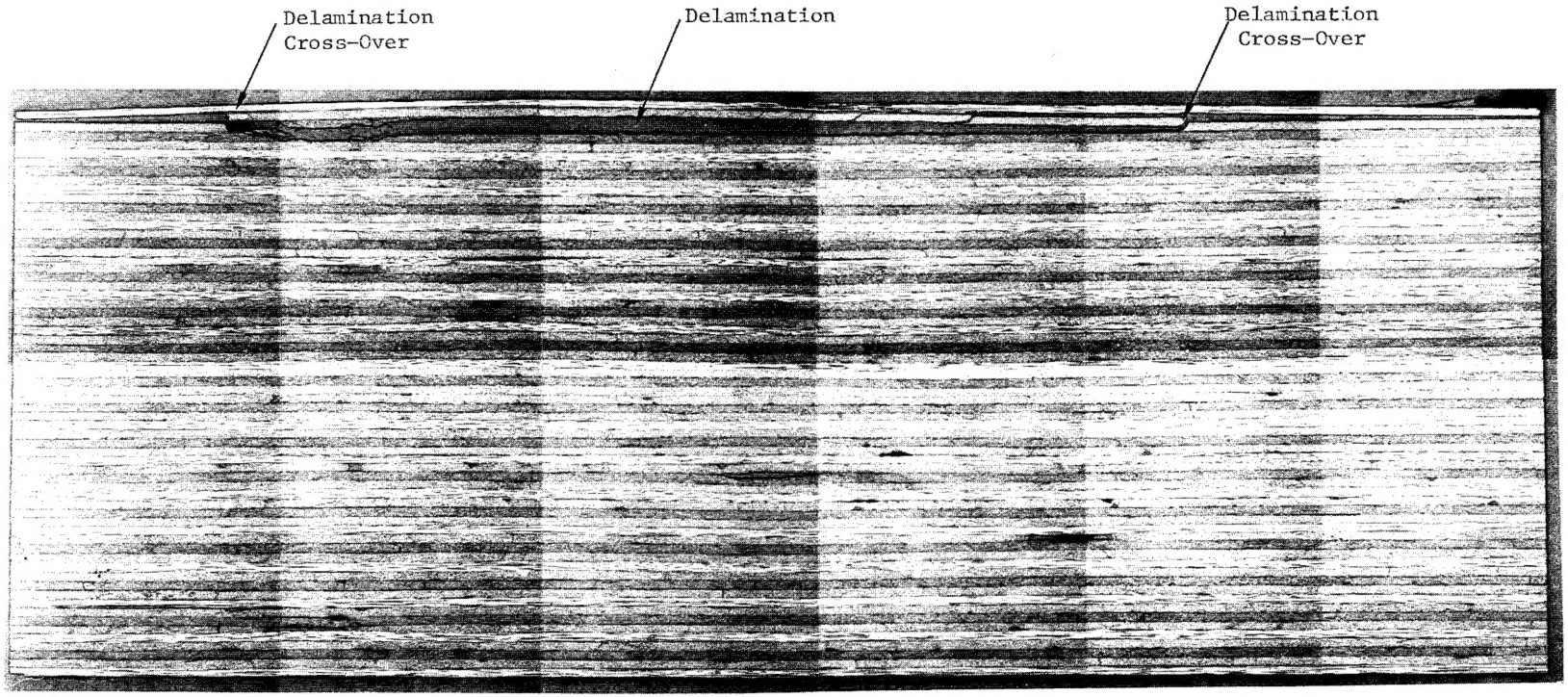

Figure 65 A Photomicrograph of an XZ Cross-Section of Specimen 4284-70; Laminate A; Test Series 14 (See Figure 61).

No failure visible; Section is away from imbedded delamination location

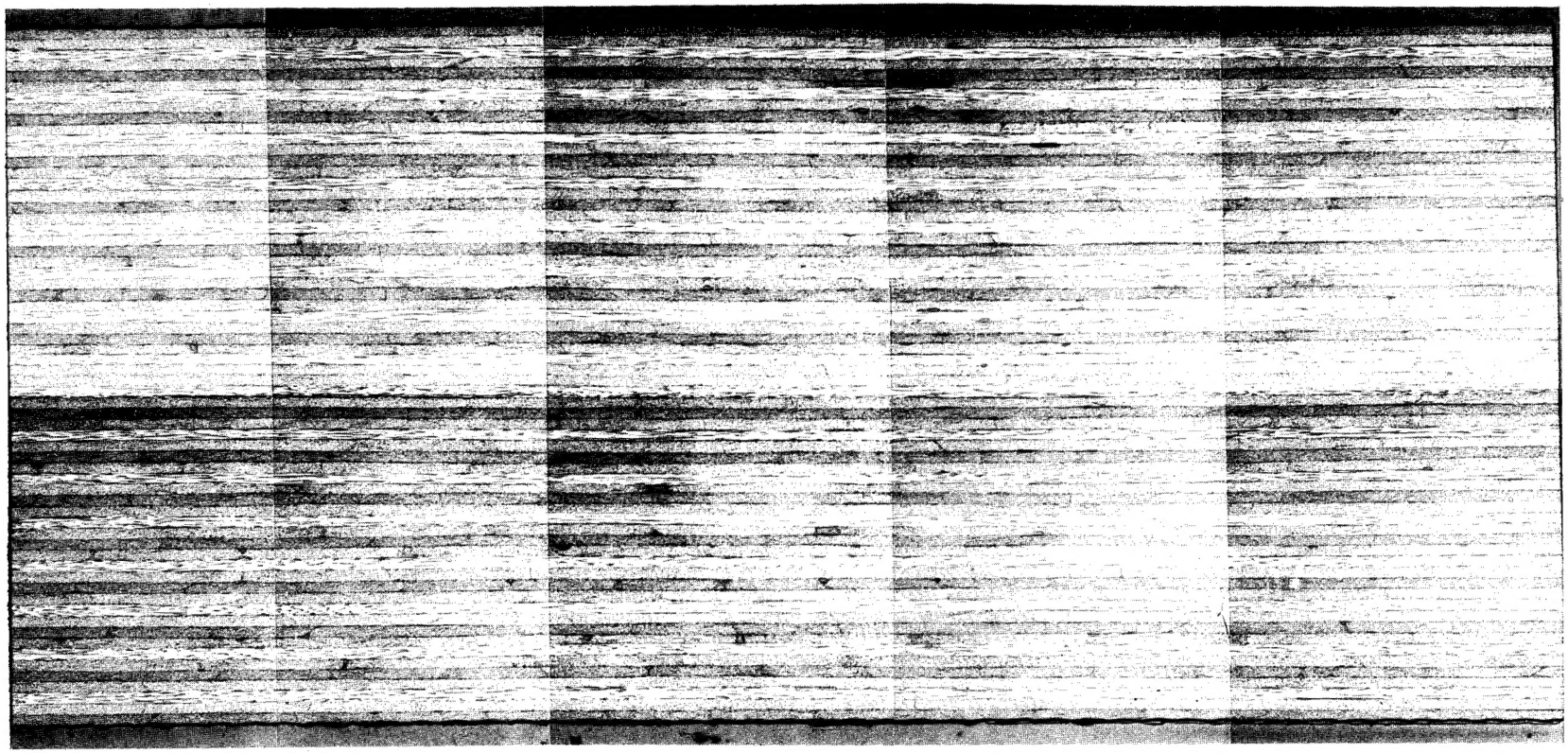

Figure 66. A Photomicrograph of a YZ Cross-Section, Corresponding to Figure 65, of Specimen 4284-70; Laminate A; Test Series 14 (see Figure 61).

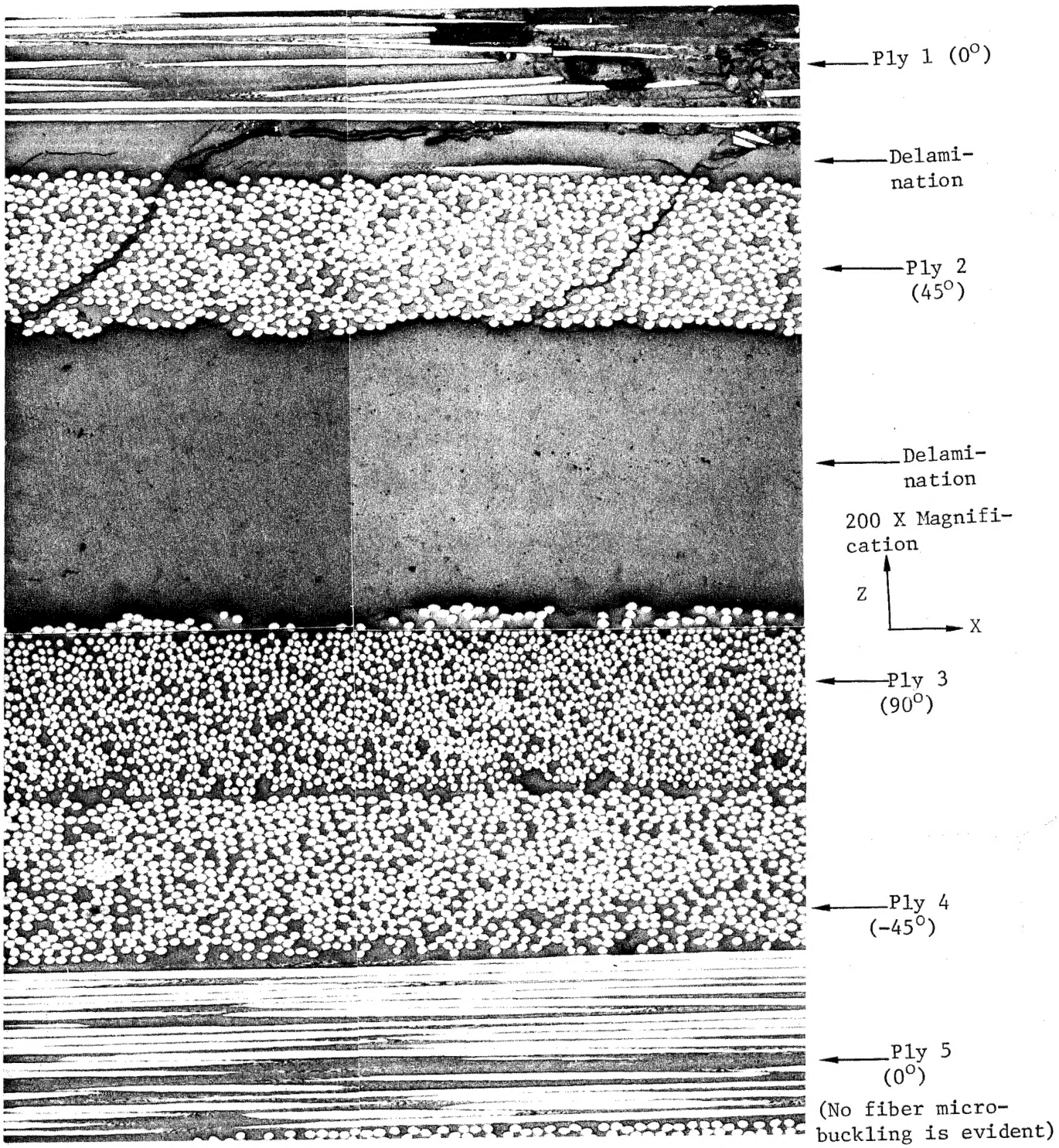

Figure 67. Photomicrograph of a Section of the XZ Cross-Section of Specimen 4284-70 (see Fig. 65) Laminate A; Test Series 14